University of Sussex

Hybrid Galaxy Evolution Modelling

Monte Carlo Markov Chain Parameter Estimation in Semi-Analytic Models of Galaxy Formation

Bruno Miguel Barreiro Henriques

Submitted for the degree of Doctor of Philosophy

University of Sussex

June 2009

Declaration

I hereby declare that this thesis has not been and will not be submitted in whole or in part to another University for the award of any other degree.

Signature:

Bruno Henriques

UNIVERSITY OF SUSSEX

Bruno Miguel Barreiro Henriques, Doctor of Philosophy

Hybrid Galaxy Evolution Modelling
Monte Carlo Markov Chain Parameter Estimation in Semi-Analytic Models of Galaxy Formation

Summary

We introduce a statistical exploration of the parameter space of the Munich semi-analytic model built upon the Millennium dark matter simulation. This is achieved by applying a Monte Carlo Markov Chain (MCMC) method to constrain the 6 free parameters that define the stellar mass function at redshift zero. The model is tested against three different observational data sets, including the galaxy K-band luminosity function, $B-V$ colours, and the black hole-bulge mass relation, to obtain mean values, confidence limits and likelihood contours for the best fit model. We discuss how the model parameters affect each galaxy property and find that there are strong correlations between them. We analyze to what extent these are simply reflections of the observational constraints, or whether they can lead to improved understanding of the physics of galaxy formation.

When all the observations are combined, the need to suppress dwarf galaxies requires the strength of the supernova feedback to be significantly higher in our best-fit solution than in previous work. We interpret this fact as an indication of the need to improve the treatment of low mass objects. As a possible solution, we introduce the process of satellite disruption, caused by tidal forces exerted by central galaxies on their merging companions.

We apply similar MCMC sampling techniques to the new model, which allows us to discuss the impact of disruption on the basic physics of the model. The new best fit model has a likelihood four times better than before, reproducing reasonably all the observational constraints, as well as the metallicity of galaxies and predicting intra-cluster light. We interpret this as an indication of the need to include the new recipe.

We point out the remaining limitations of the semi-analytic model and discuss possible improvements that might increase its predictive power in the future.

To Maria, my world, life and soul...

Acknowledgements

This thesis is dedicated to Maria, my love. Once somebody told me that one day I would find the love of my life and give up on my dream of becoming a scientist. Luckily I found the greatest of loves, who made that dream the dream of both. I thank you for all the nights you waited for me, during the years of my PhD. I thank you, because despite the distance, you were always so close and gave me the strength and motivation to live everyday.

I also express my gratitude to my family. More than 50 years ago, my grandfather left the countryside and went alone to the city chasing a better life. Apparently there is this need running through my blood...of never giving up on the life you dreamed, even if that means going to a new world. I would like to thank my grandfather, grandmother and aunt, but particularly to my mother and father, who gave me everything I ever asked for. It is only because I had the best education and opportunities that I am where I am now. I also thank my brother, who visited me so often and that is now an engineer, finishing his degree against all odds.

My next words necessarily go to what is for me, a second family: the great friends I left in Portugal that supported me throughout my life and which dreams I carry every day. I know you will always be there. A specially thanks to Rui, my brother in arms. One day the world will be our dream. Then to Andre, Branco, Carlos, Coito, Daniel, Diogo, Marinhas, Miguel, Paulo and Sev. Omnes pro uno...

The support in life the people above gave me is one of the main reasons that made me fulfill my goals and accomplish a thesis that I am really proud of. However, speaking of my PhD work directly, words cannot say how thankful I am for having Peter Thomas as my supervisor. He is responsible for more than half of the work presented in here (the good part), which couldn't have been without his wisdom and guidance. His almost disturbing habit of always pointing me in the right direction is all a student can ask for. I also leave a special word for Seb Oliver, since the work presented in this thesis was his idea. Many people are good scientists, only a few have vision.

In terms of the work directly relevant for this thesis, I also thank Jon Loveday who supervised in my first year and have always been extremely helpful ever since. In addition, I thank the other two faculty members that have been in Sussex since I started, Andrew Liddle and Kathy Romer, all together make this department an amazing working group. I couldn't have chosen a better place.

A crucial part in every scientific work is funding. I am thankful to the Portuguese Science and Technology Foundation for my fellowship, without which none of this work would have been possible. On a larger scale, I recognize the effort done by the Portuguese Science Minister and by every tax payer in Portugal to keep the science dream alive in trouble times.

I am immensely grateful to the people at the Max Planck Institute in Garching, Gabriela De Lucia, Simon White, Guinever Kauffmann and Volker Springel, for letting me use their model to perform my work and for being so supportive. Hopefully, much more will follow. I thank, Richard Bower and Ivan Baldry, for directing me in the beginning through the relevant areas of galaxy formation and the anonymous referees that helped improving the quality of my published work. I also leave a word to Carlton Baugh, my external examiner, for his thoughtful comments about the work presented in this thesis.

Despite the distance of the last years, I couldn't forget my friends from scouts, Ana Isabel, Ana Santos, Andreia, Guida, Joana and Ticha, we had great times out there. Also my friends from College, Alves, Ana Margarida, Babalita, Cordeiro, Gelly, Ines Borreicho, Ines Lima, Rita and Tome, our latest re-encounters mean the world to me.

I left a lot of friends in Portugal but made many new in UK, who helped me forgetting that in this country the sun sets at 4pm during the winter. From the Astronomy Centre, Alex, Mark F., Mark H., Mike and Nic were the first, Bon Jovi and Top Gun tunes on a summer night are definitely gonna be missed. More recently, Albert, Anthony, David, Duncan, Ed, Ippocratis, Leon, Leonidas, Mafalda, Matt, Owain, Chris and specially Isaac, helped establishing the falmer research group.

Somewhat unexpectedly, during these first years in a new country, I also made another group of friends, who always remind me of the sun at home. Mostly Brazilian, they have a way of looking at life that mimics my own, friendly, relaxed and more important human. Andre, Bruno, Daniel, Duda, Juliano, Leticia, Marcela, Marcelo G., Marcelo, Michel, Mary, Paulo (the only Portuguese), Rafa, Reinaldo, Ricardo, you made me almost feel at home.

In the year I was born one of my greatest idols was arriving at the UK, crossing

the ocean in the pursuit of his lifetime dream. For his determination, competence and character Ayrton Senna was, and still is an example for millions, and for me as well. I thank him, since his life model played a major role in what I am today and during my PhD helped me being focused and always try to perform the best I could.

I do astronomy because I believe it is my duty to help mankind better understanding the origins and fate of the Universe. For me, this only makes sense seeing mankind as a whole and not as individuals. For making me believe that one day this will be possible, I thank Ernesto Guevara (El Che), the people of Cuba and of Latin America in general. If it wasn't for them, I would have given up on the world a long time ago and would be living in the woods by now (or maybe underneath the bridge in front of Brighton station). With the work of Isaac Newton, it became apparent that the laws governing the events on earth and on the skies were identical. A day will come, when the perfection I see in the skies will surround me.

I finish as I started: thank you my love...The wait is over...

Contents

List of Tables

List of Figures

"Speak only if you can improve upon silence..."

Chapter 1

Introduction

"Nos esse quasi nanos, gigantium humeris insidentes, ut possimus plura eis et remotiora videre, non utique proprii visus acumine, aut eminentia corporis, sed quia in altum subvenimur et extollimur magnitudine gigantea."

John of Salisbury

1.1 State of the Art

In recent years the advent of technology as unveiled a new world of opportunities to astronomy. This means that previously unreachable environments can now be revealed, and what were before only theoretical hypothesis can now be tested against robust experimental data. For this reason, extra-galactic astronomy has seen unprecedented developments being now one of the most active fields of science.

As described by Baugh (2006), two main factors made possible by these technological advances shifted the main astronomical goals into galaxy formation. Firstly, the establishment of a cosmological model, the Lambda Cold Dark Matter (ΛCDM) model. Secondly, the possibility to have statistical knowledge of galaxy properties from the local universe to high redshift.

1.1.1 The ΛCDM Cosmology

The Λ CDM model stands for Cold Dark Matter with a cosmological constant. The Cold Dark Matter is a model where the dark matter is assumed to be non-relativistic at the epoch of matter-radiation equality. In addition it is assumed to be dissipationless and

collisionless, meaning respectively that dark matter cannot cool by radiative processes and can only interact through gravity and weak interactions.

From the predictions of inflation, the model also assumes that the primordial perturbations have a nearly-scale-invariant power spectrum, meaning that the amplitude of these primordial fluctuations is approximately constant as a function of wave number. In addition the Universe is assumed to be flat, homogeneous and isotropic in concordance with the cosmological principle.

The model predicts that structure grows hierarchically, as gravity accumulates the dark matter content of the Universe in the regions of over-density generated by the primordial fluctuations. The baryons fall into these potential wells after decoupling, leaving a trace of their previous acoustic oscillations as a serious of low amplitude peaks in the matter power spectrum.

Over the last decade the predictions from this model have been confirmed by a range of observations, making it a reliable framework. One of the most convincing tests comes from the measurement of the temperature anisotropies in the cosmic microwave background (CMB). These temperature variations trace the density fluctuations present in the Universe just after the Big Bang. At the epoch of recombination, baryons stopped interacting with radiation, leaving photons free to travel and carry information about their previous interactions until the present day. These anisotropies were initially detected on large scales using the COBE satellite (Smoot et al., 1992) and since then, their power spectrum has been uncovered. Presently, three Doppler peaks have been clearly detected in the CMB power spectrum (e.g. Spergel et al., 2003), which are caused by the baryon acoustic oscillations just before recombination, as predicted by the CDM model (Fig. 1.1).

Additional evidence favouring the CDM model has come from the power spectrum of galaxy clustering (Percival et al., 2001; Tegmark et al., 2004). In recent years, galaxy surveys such as the two-degree Field Galaxy Redshift Survey (Colless et al., 2001) and the Sloan Digital Sky Survey (York et al., 2000), obtained properties for millions of galaxies over a cosmological volume, which allowed robust determinations of the large scale structure of galaxies. The quality of the data means that the imprint of acoustic oscillations on the matter power spectrum can now also be detected (Cole et al., 2005; Eisenstein et al., 2005).

The different observations can be combined in order to increase their constraining power on theoretical models, meaning that currently the values for the parameters in the CDM model are known with high accuracy (e.g. Spergel et al., 2007; Seljak et al., 2005).

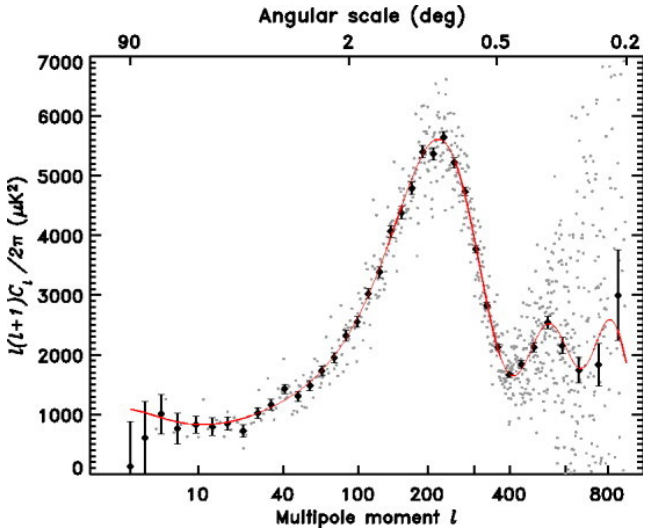

Figure 1.1: Comparison between the best fit power law ΛCDM model to the first year WMAP temperature angular power spectrum from Spergel et al. (2003)

The current best fit model for the CDM cosmology predicts an almost spatially flat Universe. However, the different forms of matter (dark and baryonic) can only account for 30% of the density required. This, together with the fact that the Hubble diagram of type-Ia supernovae (SNs) reveals a Universe that is now undergoing an accelerated expansion (Perlmutter et al., 1999), led cosmologists to propose a form of dark energy (of which the cosmological constant is the most accepted). However, the dark energy density required by cosmological arguments is many orders of magnitude smaller than what is expected from particle physics and a large amount of work remains to be done in order to reconcile predictions from the two fields.

Nevertheless, independently of the specific form of dark energy required, the CDM model is now well established with small uncertainties on its parameters. This provides a framework on which models of galaxy formation can be based and observational galaxy properties explained, making the study of galaxy evolution processes presently one of the most active areas of physics.

1.1.2 Galaxy Observations

At the same time that the technological advances allowed observations to confirm the predictions from the CDM model, they were used to study galaxy formation and evolution. This field has experienced an unprecedented development with properties determined for millions of galaxies, from the local Universe to high redshift and over different environments.

At low redshift, the stellar mass function is now determined with significant statistics for galaxies that range from the most massive objects at the centre of clusters to galaxies as small as 10^6 $M_\odot$(Baldry et al., 2008). This property is derived from the luminosity function of galaxies, which have been obtained with similar accuracy for a range of optical and near infra-red bands (Cole et al., 2001; Norberg et al., 2002b; Bell et al., 2003; Blanton et al., 2005; Jones et al., 2006).

Other highlights, include for example, the establishment that the galaxy population is bimodal in colour, with red objects with no star formation clearly separated from blue active galaxies (Strateva et al., 2001; Baldry et al., 2004; Weinmann et al., 2006a). In addition, further studies revealed that galaxies from the different populations are preferably found in distinct environments, with red galaxies being predominately in groups and clusters and blue galaxies being isolated (e.g. Baldry et al., 2006).

Together with their intrinsic properties, the spatial distribution of galaxies was characterized, with the clustering of galaxies at low (Zehavi et al., 2002; Norberg et al., 2002a; Budavári et al., 2003) and high z (Coil et al., 2006; Pollo et al., 2006; McCracken et al., 2007) measured as a function of luminosity, colour and spectral type. These studies showed that redder/early type and brighter galaxies tend to be more clustered.

The properties of nearby super-massive black holes (BHs) at the centre of galaxies can now be determined, with a strong correlation between the black hole and bulge masses emerging (Häring & Rix, 2004). At the same time compelling evidence is being found for the fact that black holes strongly affect the properties of their host galaxies, by emitting large amounts of energy in the radio (Fabian et al., 2003; McNamara et al., 2005).

Perhaps an even more important development in observations is the ability to study galaxy properties at high redshift. This allows galaxies to be traced over time and the physics that determine their evolution to be analyzed. One of the most important measurements obtained was the cosmic star formation history (Madau et al., 1996), showing that the most active period of star formation in the Universe occurred around redshift 2. It has also been shown that only the smallest galaxies have significant episodes of star formation until low redshift (Thomas et al., 2005). Another crucial aspect was the possibility to detect sub-millimetre/infra-red emission from galaxies, revealing the light from galaxies absorbed and re-emitted by dust (Smail et al., 1997). Since star formation occurs in dust dominated environments, this represents almost half of the total radiation in Universe.

1.1.3 Cosmological Simulations

The establishment of a cosmological paradigm with great predictive power and the recent improvement in observations allow for studies of galaxy formation and evolution to be performed. However, in order to understand the physics behind the complex processes that determine galaxy properties and for the large data sets to be meaningful, we need to construct an equally robust theory of galaxy formation. This means being able to produce simulations that start from the initial conditions and follow the properties of dark matter and baryons as they form structures that grow hierarchically.

The geometrical growth of computer power in recent years, has allowed direct N-body simulations to give us a comprehensive picture of the formation and evolution of the dark matter structure, from the primordial gravitational instabilities to the formation of massive super-clusters today (The Millennium Run, Springel et al., 2005a).

This progress is not yet reflected in our theoretical understanding of the behaviour of the baryons, with much of the physics governing galaxy formation and evolution still poorly understood. However, for the reasons described in the two previous sections, we now have a unique opportunity to increase our knowledge on the subject.

1.2 The Semi-Analytic Approach

A combined simulation of gas and dark matter, resolving small-scale galaxy evolution processes (such as gas cooling, star formation and feedback) over a cosmologically interesting volume, is still years away. For this reason, semi-analytic models are currently the best method to generate accurate predictions of galaxy properties for comparison with observed large-scale surveys.

Originally introduced by White & Rees (1978), this formalism treats galaxy formation as a two stage process. Dark matter halos form in a dissipationless collapse, evolving by means of gravitational instabilities, while galaxies grow embedded in these structures, through processes that are often dissipative and nonlinear. In this way, they can be treated separately and coupled together. The dark matter structures are studied using a Press-Schechter (Press & Schechter, 1974), Monte-Carlo or N-body techniques and on top of that, galaxy evolution is followed by parametrised equations governing the laws of sub-grid physics.

Using this approach, the formation and evolution of galaxies can be coherently followed at a relatively cheap computational cost. Theoretical predictions can then be produced,

ranging from the most massive objects at the centre of clusters to individual dwarf galaxies, from the local Universe to high redshift. For this reason, and considering present uncertainties, they can be crucial to improve our understanding of galaxy formation physics. The relative merit of different implementations of these physics can be easily tested, comparing the predicted galaxy properties with observations.

1.2.1 The Origins

The first self-consistent models based on this methodology were developed by Cole (1991), Lacey & Silk (1991) and White & Frenk (1991). At this early stage, a significant part of the physics in modern recipes were already present, despite the different parametrisations. These included: the collapse of gas into an hot phase and subsequent cooling into a cold disk, with the cooling rate determined by the dark matter halo density profile; the formation of stars from the cold disk and subsequent supernova feedback from the death of massive stars; chemical enrichment to account for the effect of these supernova explosions on the properties of the hot gas; and stellar population synthesis models to convert star formation histories into observed galaxy properties.

In the following years, Kauffmann et al. (1993), Lacey et al. (1993) and Cole et al. (1994) introduced newly-derived stellar population synthesis models and improved star formation and SN feedback laws into the original framework. In addition, Kauffmann et al. (1993) and Cole et al. (1994) also implemented recipes to follow merger events. The impact of these processes on the dark matter and stellar components of satellites is extremely different. The majority of the dark matter component (difuse outer parts of the halos) is stripped and dissolved on a relatively short time-scale, while galaxies can orbit around the central companion for much longer. For the first time, these models distinguished the two different interactions, by assuming that after a dark matter halo is disrupted galaxies continue in their orbit until dynamical friction drives them into their central companion. Finally, Kauffmann et al. (1993) differentiated galaxy types by assuming that whenever a major merger occurs the disks of both galaxies are destroyed and an elliptical galaxy is formed. This was the seed of modern day recipes, where disk and bulge components coexist (an elliptical galaxy can still cool gas and form a disk) and are followed through both minor and major mergers. The distinction between both components and the correct prediction of their properties is crucial for modern day recipes since observations have revealed clear differences between disk and bulge dominated galaxies.

1.2.2 Evolution

From these original recipes, two models started evolving separately, one mainly based in Munich and another in Durham. In the following years various physical processes were tested, from different star formation laws (Kauffmann, 1995a), to the impact of different cosmologies in semi-analytic predictions (Kauffmann, 1995b). In addition, models for the formation of disks were included (Mo et al., 1998), allowing semi-analytic recipes for the first time to follow the properties of these galaxy components (characteristic sizes, rotation velocities, etc.).

At the same time, the increasing predictive power of galaxy formation models allowed theoretical galaxy properties to match reasonably well a wide range of observational quantities. These included the B and K band luminosity functions (Kauffmann et al., 1994) and the properties of disks and bulges from the local Universe to high redshift (Kauffmann, 1996a,b; Baugh et al., 1996a,b).

By the end of the decade, most of the modern day prescriptions were already introduced (Kauffmann et al., 1999; Cole et al., 2000), including gas cooling, star formation, chemical enrichment and dust extinction, calculations of disks and bulge properties, stellar population synthesis models, merger follow up with dynamical friction and an early version of the SN feedback treatment. Kauffmann et al. (1999) also introduced the present technique to couple semi-analytic models into N-body simulations. Since the dark matter distribution on large scales is only weakly affected by baryons, simulations of this matter component can be run independently and used as a skeleton for semi-analytics.

A Black Hole Growth Model

Kauffmann & Haehnelt (2000) presented the first model for the evolution of black holes. This would prove to be crucial for modern recipes, allowing semi-analytics to follow the mass growth of these objects and to determine the amount of energy they release due to mechanical heating. In this first implementation a simple model was proposed solely to follow the build up of black hole mass. It assumed that, whenever a merger occurs, the two central black holes merge together without mass loss and a fraction of the cold gas is accreted by the newly formed object.

Supernova Feedback - The ejection Model

Since they were originally formulated semi-analytic models always included some form of supernova feedback. The halo mass function is much steeper at the low mass end than the

luminosity function and, without mechanisms to suppress star formation in these objects, their number density is much higher than observed. Originally, modellers assumed that the energy from supernova would simply reheat the cold gas back into the hot phase. However, galaxies in the relevant low mass range have short cooling time-scales and the reheated gas rapidly cools back into the disk, leading into a small reduction in the overall star formation rate.

Kauffmann et al. (1999) proposed a more efficient implementation, where this form of feedback can eject gas from the galaxy. Depending on the time-scale for reincorporation of the ejected gas, this approach can significantly delay the cooling of gas and considerably lower the faint end of the luminosity function. Benson et al. (2003) and De Lucia et al. (2004) studied different forms of this new approach and established the modern treatment, where energy from feedback initially reheats the gas from the cold disk with any excess being used to eject gas from the hot phase. The ejected gas can either be lost, or kept in an external reservoir and reincorporated at later times.

Reionization

Another form of energy feedback that is now believed to play a critical role in galaxy formation comes from reionization. At high redshift, the photo-ionizing background heats the intergalactic medium and can reduce the fraction of gas that collapses in low mass halos. Additionally, it can suppress cooling by reducing the abundance of collisionally excited atoms. In short, it has the effect of significantly decreasing the number of dwarf galaxies produced by semi-analytics. A self-consistent model of the evolution of the ionizing background was introduced into the Durham recipe by Benson et al. (2002a,b) and afterwards into the Munich model by Springel et al. (2005a).

Independent Studies

In parallel to Munich and Durham, a number of other groups began to develop independent models to study different aspects of galaxy formation (Somerville & Primack, 1999; Bullock et al., 2000; Menci et al., 2002; Hatton et al., 2003; Daigne et al., 2004; Monaco, 2004; Kang et al., 2005).

1.2.3 Present

The Coupling of Semi-Analytics to the Millennium Simulation

Most recently, the Munich and Durham semi-analytics have been combined with the Millennium dark matter simulation, following the technique implemented by Kauffmann et al. (1999) and Springel et al. (2001). As described in section 2.1, this simulation represents a major advance in computational cosmology. For its resolution and volume, it allows the semi-analytic models built on it to predict the properties of galaxies that range from the most massive objects at the centre of clusters ($M_\star \approx 10^{15}\,M_\odot$), to the population of dwarf galaxies ($M_\star \approx 10^{9}\,M_\odot$). This means that for the first time semi-analytic recipes could be constructed on top of a N-body dark matter simulation and still be representative of a cosmological volume.

AGN Feedback - The Radio Mode

The last major development was the introduction of the BH radio mode. (Springel et al. 2005a; Croton et al. 2006; Bower et al. 2006; see also Granato et al. 2004; Cattaneo et al. 2006; Menci et al. 2006; Monaco et al. 2007; Lagos et al. 2008; Somerville et al. 2008). In recent years, observations have established that the most massive galaxies in the Universe (those at the centre of the most massive clusters and groups) have little ongoing star formation, containing the oldest populations of stars. These observations were in contradiction with semi-analytic predictions and were initially seen as a challenge for the hierarchical growth paradigm. In a hierarchically growing Universe massive objects form later. Consequently, one could naively expect them to look younger, particularly since they have enough gas and receive enough mergers to trigger significant star formation episodes. Another intriguing aspect, was the excessive number density of massive galaxies predicted by the models.

The introduction of the radio mode AGN feedback reconciled theory and observations. The mechanical heating from super-massive central black holes largely reduces cooling in the most massive galaxies, eliminating the previous excess. For the same reason, despite having significant fractions of gas and short cooling times, these objects have no star formation and appear to be old and red.

Fine Tuning

Finally, present day improvements to the Munich model include the refinement of dust models (De Lucia & Blaizot, 2007) and the study of alternative feedback processes such as

galactic winds (Bertone et al., 2007). In the Durham recipe, Font et al. (2008) changed the stripping of gas in merging satellite galaxies to a progressive process, instead of happening instantaneously after the disruption of the dark matter halo. This allows satellite galaxies (mostly dwarfs) to form stars and stay blue for longer, which helps reducing the excess of red dwarf galaxies present in most semi-analytic recipes. Additionally, Bower et al. (2008) investigated the ability of the energy released by AGN feedback to reproduce the X-ray properties of the intra-cluster medium.

1.3 Taking Semi-Analytic Modelling One Step Forward

Complexity - A Double-Edged Sword

The adopted parametrisations for the cooling processes, feedback from different sources and the inclusion of galaxy mergers and dust extinction on galaxy properties, make present day semi-analytic models a comprehensive tool to understand galaxy formation and evolution. With the improvements included over the years, they are capable of successfully predicting a vast range of observational properties.

However, the level of agreement with observations and the relative weight of different observations in the final choice of the parameters in the model have never been studied in a statistically-consistent way. Moreover, the large number of physical processes that the model aims to reproduce require a large number of parameters (some of which are strongly correlated), producing considerable difficulties in determining how to improve the agreement with new observations without destroying the match with existing data sets. In addition, it is hard to know whether the discrepancies between theory and data represent a failure in determining the right parameter configuration, whether there is a fundamental problem with the underlying model, or whether the model physics need adjustments.

These difficulties can be overcome by combining the constraining power of multiple observations with sophisticated techniques to sample high-dimensional parameter spaces. This approach has been applied with success in theoretical cosmology where techniques such as Monte Carlo Markov Chain (MCMC) parameter estimation are now extensively used (see Trotta, 2008, for a comprehensive review). The core of the research presented in this thesis is the introduction of MCMC techniques into semi-analytic models of galaxy formation. This allows us to understand how each physical process in the model affects each observational property, to quantify the level of agreement between theory and ob-

servations and to identify the need for extra ingredients to be added into semi-analytic models.

This quantitative method of testing model predictions takes galaxy formation modelling a step forward. However, we emphasize that it can only be implemented because the recent inclusion of physical processes, such as the black hole growth and energy feedback, made the model robust enough to predict a range of observational properties with the required level of accuracy.

The Munich Semi-Analytic Model

In the next chapter we fully describe the last version of the Munich semi-analytic model (De Lucia & Blaizot, 2007), which we will use to introduce the MCMC techniques. A detailed explanation of the physics in the model can also be found in De Lucia et al. (2004), Croton et al. (2006) and De Lucia & Blaizot (2007).

Implementation of MCMC sampling Techniques

In chapter 3 we describe the implementation of the MCMC parameter estimation and the way in which it allows us to understand how galaxy properties are affected by individual parameters. Using three different constraints (the K-band luminosity function, the fraction of red galaxies per stellar mass bin and the black hole-bulge mass relation), we quantify the agreement between the model and the observations in a statistically robust way. In addition, we obtain best fit values and confidence limits for the parameters in the model. From the predictions for this best fit model, we learn about the ability of the original model to match the data and identify possible ways to improve it.

The Excess of Dwarf Galaxies

In chapter 4 we analyze a problem in model predictions identified using the MCMC techniques: the excess of dwarf galaxies. From the study done in the previous chapter we propose a possible solution, introducing the concept of satellite galaxy disruption: the loss of stellar material from satellites caused by the tidal forces exerted by their central companions. In this chapter the process is studied *a posteriori*, simply by assuming that at redshift zero, all the galaxies that already lost their dark matter halo are totally disrupted, with their material forming the intra-cluster light. The qualitative improvement of model predictions motivates the inclusion of the process in the semi-analytic model in the following chapter.

A Semi-Analytic Model with Satellite Disruption

In chapter 5 we implement satellite disruption self-consistently into the Munich semi-analytic model. Using the sampling techniques introduced in chapter 3, we analyze the impact of satellite disruption on the physics of the original model and on the allowed likelihood regions for each observational constraint. Since no additional parameters were included with this new physical process, the maximum likelihood value obtained by the MCMC sampling and its comparison with the value for the original model will indicate if the new ingredient was required by observations.

Future Challenges

The improvements introduced in this thesis, considerably raise the likelihood of the model when compared to the wide range of observations selected. Nevertheless, the model is still far from exactly reproducing the data and its physics are in most cases just approximations of the processes ongoing in real galaxies. In the final chapter of this thesis (6) we discuss improvements that might help to make future semi-analytic models more realistic.

Chapter 2

The Munich Semi-Analytic Model

"Any intelligent fool can make things bigger and more complex. It takes a touch of genius, and a lot of courage, to move in the opposite direction."

Albert Einstein

The work presented in this thesis was developed using the most recent version of the Munich semi-analytic model (De Lucia & Blaizot, 2007). As described in the previous chapter, it encompasses more than 30 years of research. Over the last decades the recipes controlling the different processes that govern galaxy formation have been updated and new physics included, following the growing knowledge obtained from observational studies.

The predicted properties of simulated galaxies and the relative importance attributed to different galaxy evolution physics are ultimately dependent on the underlying dark matter distribution. It determines the initial mass of hot gas in each galaxy that can later cool and eventually form stars. For this reason, it is crucial to build the analytic equations on top of a N-body simulation of dark matter of a volume big enough to sample the most massive clusters of galaxies in the Universe but that, at the same time, resolves the population of dwarf galaxies.

2.1 The Millennium Dark Matter Simulation

In Springel et al. (2005a) , the Virgo Consortium presented the Millennium Simulation, a N-Body simulation covering a cosmological volume. For its size and resolution it is

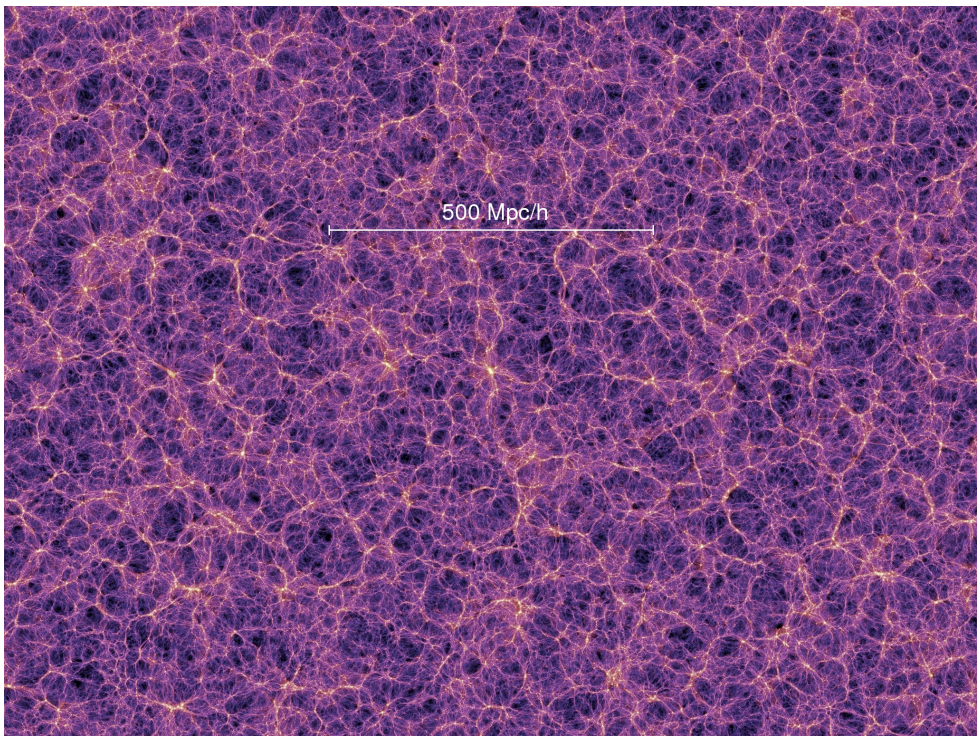

Figure 2.1: The dark matter distribution at redshift zero from the Millennium Simulation. The image represents the projected density field in a slab of thickness $15h^{-1}$Mpc, colour coded by local velocity dispersion.

still one of the highest quality dark matter simulations carried out to date [1]. The dark matter merger trees produced are the skeleton on which the semi-analytic model is built. The predicted cosmic web is illustrated in figure 2.1. The image shows the projected dark matter density field in a slab of thickness $15h^{-1}$Mpc, colour coded by local velocity dispersion.

The Millennium Simulation traces the evolution of dark matter halos in a cubic box of $500\,h^{-1}\,$Mpc on a side. This volume is large enough to sample the richest clusters of galaxies, the biggest of which have masses that exceed $10^{15}\,\mathrm{M}_{\odot}$. It assumes a ΛCDM cosmology with parameters $\Omega_{\mathrm{m}} = 0.25$, $\Omega_{\mathrm{b}} = 0.045$, $h = 0.73$, $\Omega_{\Lambda} = 0.75$, $n = 1$, and $\sigma_8 = 0.9$, where the Hubble parameter is $H_0 = 100\,h^{-1}\,\mathrm{km\,s^{-1}\,Mpc^{-1}}$. The simulation follows 2160^3 dark matter particles of mass $8.6 \times 10^8\,h^{-1}\,\mathrm{M}_{\odot}$. Since dark matter halos

[1] The Millennium 2 simulation was recently carried out by the Virgo Consortium. Despite having the same number of particles, the simulated region is 5 times smaller, meaning it has 125 times better mass resolution. This means that they are identical for intermediate mass objects but once the semi-analytic model is implemented into the new dark matter structure the properties of galaxies as small as $10^8\,\mathrm{M}_{\odot}$ can be predicted.

are required to contain at least 20 particles, the minimum halo mass is $1.7 \times 10^{10}\, h^{-1}\, \mathrm{M}_{\odot}$, with a corresponding baryonic mass of about $3.1 \times 10^{9}\, h^{-1}\, \mathrm{M}_{\odot}$.

The simulation was started at z=127, with initial conditions created by displacing particles from an homogeneous distribution, using a Gaussian random field with a ΛCDM linear power spectrum given by the Boltzmann code CMBFAST (Seljak & Zaldarriaga, 1996). The evolution of the dark mater particles is then recorded between z=20 and z=0 at 60 different output times, spaced according to the formula

$$\log(1 + z_n) = n(n + 35)/4200, \tag{2.1}$$

which assures a finer spacing towards redshift zero. Apart from the starting and additional 60 outputs, the dark matter distribution is also recorded at z=80, 50 and 30 producing a total of 64 snapshots.

In order to identify the groups of bounded dark matter particles the code includes an additional routine. The friend-of-friends (FOF) algorithm identifies the halos by joining together particles into groups with a mean over-density of about 200, approximately what is expected for a virialised group. This is achieved by isolating groups of particles assuming that in a bound system all neighbours have to be within a given inter-particle separation. Initially, each particle is assumed to be in its single group and then merge with other groups whenever a close enough pair is found. After the output containing the FOF group identifier is created, the SUBFIND routine (Springel et al., 2001) is applied. This procedure is necessary to identify substructures within the main FOF halos. It constructs the dark matter density field, storing the information about all the gravitationally bound substructures with more than 20 particles (sub-halos with a smaller number of particles are assumed to be disrupted). The distinction between halos, sub-halos and disrupted structures will be crucial for the treatment of galaxy evolution. They are a fundamental part of the semi-analytic model, since galaxies can only merge into their companion residing at the central halo and only these central galaxies retain their gas in the hot phase.

The properties of the FOF halos are derived by calculating their virial masses, using a spherical over-density approach. The radius of the halo is defined by the volume which encloses a mean over-density of 200 times the critical value. This value is an approximation to what is expected from the spherical top-hat collapse under the assumption that the cluster has just virialized, $18\pi^2$ (Peebles, 1980). The radius and virial mass of each halo are then related to its circular velocity at a given redshift by

$$M_{\mathrm{vir}} = \frac{100}{\mathrm{G}} H^2(z) R_{\mathrm{vir}}^3 = \frac{V_{\mathrm{vir}}^3}{10 \mathrm{G} H(z)}, \tag{2.2}$$

where $H(z)$ represents the Hubble constant at a given redshift.

After finding the dark matter structures and their properties at each snapshot their structural evolution is identified. This is achieved by identifying each halo's descendant, which defines the entire merger tree of each individual object (Springel et al., 2005b). In a hierarchically growing ΛCDM Universe the descendant of each halo is unique. However, the different algorithms used to identify dark matter structures and substructures have an impact on the construction of merger trees meaning that they are not always uniquely defined (Springel et al., 2005a). Since the halos contained in each tree are gravitationally isolated from other structures, the properties of galaxies within a tree are fully determined by the dark matter halos inside it. In this way the analytic properties of galaxies and their evolution over redshift can be computed separately for each tree.

2.2 Semi-Analytic Parametrisation

The coupling of the semi-analytic model with the high-resolution N-body simulation follows the technique implemented by Springel et al. (2001). The treatment of physical processes driving galaxy evolution in the model we use (De Lucia & Blaizot, 2007) builds on the methodology introduced by Kauffmann et al. (1999), Springel et al. (2001) and De Lucia et al. (2004), and is a slightly modified version of that used in Springel et al. (2005a) and Croton et al. (2006). The following description of the model is based on the works just mentioned.

The model treats the different physics involved in galaxy formation by parametrised equations. The processes modelled include the treatment of different gas phases, with the gas initially accreted into the hot phase and later cooling down to form a cold disk. Stars form from the disk and, in small objects, feedback of energy from supernovae can cause gas to be reheated from the cold disk to the hot halo. It is also possible to further heat the gas, ejecting it from the galaxy into an external reservoir from which it gradually leaks back into the hot halo. Massive systems grow a central super-massive black hole both during mergers and by quiescent accretion. These objects can also feedback energy into the surrounding medium and stop star formation. The cycle of metals is followed throughout the life of galaxies and spectroscopic evolution and dust models are included to produce observable luminosities for each object. Finally, mergers shape galaxies, with major mergers completely destroying disk components to form bulges.

The parameters controlling all these processes in the original model are shown in table 2.1.

Table 2.1: Values for the free parameters controlling the galaxy formation physics in De Lucia & Blaizot (2007).

parameter	description	value
f_b	baryon fraction	0.17
z_0, z_r	redshift of beginning and end of reionization	8, 7
$\alpha_{\rm SF}$	star formation efficiency	0.03
$\epsilon_{\rm disk}$	SN feedback gas reheating efficiency	3.5
$\epsilon_{\rm halo}$	SN feedback gas ejection efficiency	0.35
$\gamma_{\rm ej}$	ejected gas reincorporation efficiency	0.5
$f_{\rm BH}$	BH cold gas accretion fraction during mergers	0.03
$k_{\rm AGN}$	BH quiescent hot gas accretion fraction	7.5 x 10^{-6}
$T_{\rm merger}$	major merger mass ratio threshold	0.3
R	fraction of stellar mass instantaneously recycled to the cold disk	0.43
Y	yield of metals produced per unit of star formation	0.03

2.3 Gas Collapse and Cooling

2.3.1 Cooling Modes

At the formation time, each dark matter halo is assumed to have a fixed fraction of baryons. Following the adopted cosmology this corresponds to a mass fraction in baryons of $f_b = 17\%$, initialy in the form of diffuse gas with primordial composition, but that will later be distributed in different phases and fuel star formation.

Two different infalling processes are assumed depending on the redshift at which the halos form and on their mass (White & Rees, 1978). At early times and for low mass halos, the cooling radius can be larger then the virial radius. In this case, despite the infalling gas being shock heated to the virial temperature, it condenses within a halo dynamical time and a quasi-static atmosphere cannot form. For massive halos and at late times, the cooling radius lies within the virial radius and the infalling gas does form a quasi-static hot atmosphere that extends to the virial radius, after being shock heated to the virial temperature. This gas can cool at later times and its accretion into central regions is modelled through a cooling flow. In both cases the condensed gas settles into a central disk where star formation occurs.

2.3.2 Static Hot Halo Cooling Regime

Assuming that the shock-heated gas is in collisional ionization equilibrium, the cooling time-scale is defined as the ratio between the thermal energy density of the gas and the cooling rate per unit volume:

$$t_{\rm cool}(r) = \frac{3}{2}\frac{\tilde{\mu} m_p k T_{\rm gas}}{\rho_{\rm gas}(r)\Lambda(T_{\rm gas}, Z_{\rm gas})}, \tag{2.3}$$

where $\tilde{\mu} m_p$ is the mean particle mass, k is the Boltzmann constant, $\rho_{\rm gas}(r)$ is the hot gas density at radius r and $\Lambda(T_{\rm gas}, Z_{\rm gas})$ is the cooling function.

After being shock heated, the hot gas is assumed to follow an isothermal distribution identical to that of the dark matter halo. The temperature of the gas can then be obtained from the circular velocity of the halo using the hydrostatic equilibrium condition:

$$kT = \frac{1}{2}\mu m_p V_c^2, \tag{2.4}$$

from which $T_{\rm gas}$=35.9$(V_{\rm vir}/{\rm kms}^{-1})^2$K, assuming that $V_{\rm vir}$ is a good approximation to V_c. From the same isothermal distribution assumption, the hot gas density, $\rho_{\rm gas}$, is given by

$$\rho_{\rm gas}(r) = \frac{m_{\rm hot}}{4\pi R_{\rm vir} r^2}. \tag{2.5}$$

Following Springel et al. (2001) and De Lucia et al. (2004), the cooling rate is determined by the cooling radius, r_{cool}, defined to be the radius at which the local cooling time equals the halo dynamical time,

$$t_{\rm cool}(r) = \frac{R_{\rm vir}}{V_{\rm vir}} = 0.1 H(z)^{-1}. \tag{2.6}$$

Finally, combining eq. 2.3, 2.5 and 2.6, the cooling radius will be given by

$$r_{\rm cool} = \sqrt{\frac{2}{3}\frac{m_{\rm hot}\Lambda(T_{\rm gas}, Z_{\rm gas}) t_{\rm cool}(r)}{\tilde{\mu} m_p k T_{\rm gas} 4\pi R_{\rm vir}}}, \tag{2.7}$$

note the dependency on the gas temperature and metallicity in the overall cooling rate introduced by the cooling function. This reproduces the fact that the cooling is dominated by bremsstrahlung continuum at high temperatures, and by line cooling from heavy elements at low temperatures. The mass of gas that cools at each time step is then determined by a continuity equation,

$$\dot{m}_{\rm cool} = 4\pi \rho_{\rm gas}(r_{\rm cool}) r_{\rm cool}^2 \dot{r}_{\rm cool}, \tag{2.8}$$

which can be rewritten as

$$\dot{m}_{\rm cool} = 0.5\, m_{\rm hot}\frac{r_{\rm cool} V_{\rm vir}}{R_{\rm vir}^2}. \tag{2.9}$$

This last equation gives the cooling rate of hot gas into the disk, in halos where the cooling radius lies within the virial radius and a quasi-static atmosphere can be formed.

2.4 Let there be light - Star formation

Presently, our knowledge about the physics of star formation is still very limited. Therefore, it is not possible to construct a self consistent model, where the amount of stars formed is directly determined by the properties of the gas in the interstellar medium. Instead, semi-analytic models estimate the total rate of star formation by defining the fraction of cold gas that turns into stars via two different channels: either quiescently or in bursts during mergers.

2.4.1 Quiescent Star Formation

The quiescent mode is based on observations by Kennicutt (1998) and follows the implementation of Kauffmann (1996b), where there is a critical surface density above which gas can collapse and form stars. This threshold reproduces the observed gas fractions, since the gas density remains close to the value corresponding to the critical surface density. In this way, the model converts cold gas into stars at a rate given by

$$\dot{m}_\star = \alpha_{\rm SF} \frac{(m_{\rm cold} - m_{\rm crit})}{t_{\rm dyn,disk}}, \tag{2.10}$$

where $m_{\rm cold}$ is the mass of cold gas and $t_{\rm dyn,disk} = r_{\rm disk}/V_{\rm vir}$ is the dynamical time of the disk. The star formation efficiency, $\alpha_{\rm SF}$, is adjusted so that between 3% and 15% of cold gas is converted into stars per dynamical time. Note that the fraction of mass locked up in stars is $(1-{\rm R})\dot{m}_\star dt$, the rest being instantaneously returned to the disk (where R denotes the instantaneously recycled fraction determined by the adopted initial mass function). The critical gas mass above which star formation occurs, $m_{\rm crit}$, is derived from the critical surface density at a certain radius:

$$\Sigma_{\rm crit}(R) = 120 \left(\frac{V_{\rm vir}}{200\,{\rm kms}^{-1}}\right) \left(\frac{R}{\rm kpc}\right)^{-1} {\rm M}_\odot{\rm pc}^{-2}, \tag{2.11}$$

and is given by

$$m_{\rm crit} = 3.8 \times 10^9 \left(\frac{V_{\rm vir}}{200\,{\rm kms}^{-1}}\right) \left(\frac{r_{\rm disk}}{10\,{\rm kpc}}\right) {\rm M}_\odot, \tag{2.12}$$

where $r_{\rm disk}$ is calculated following Mo et al. (1998).

2.4.2 Merger Induced Bursts

The second star formation channel occurs violently through bursts when galaxies merge. Following the "collisional starburst" model of Somerville et al. (2001), based on the simulations by Mihos & Hernquist (1996), a fraction of the combined cold gas from the two

merging galaxies is turned into stars:

$$\dot{m}_{\star}^{\rm burst} = 0.56 \left(\frac{m_{\rm sat}}{m_{\rm central}} \right)^{0.7} m_{\rm gas}. \tag{2.13}$$

This formalism implies that in a major merger at least 14% of the cold gas is turned into stars (for a central/satellite mass ratio of 0.3), up to a maximum of 32% when $m_{\rm sat} = m_{\rm central}$.

2.5 Feedback

The fact that the halo mass function is much higher at both ends than the galaxy stellar mass function implies the existence of processes that suppress gas cooling in both dwarf and massive galaxies. The current model includes three of these processes: gas reheating by a photo-ionizing background, feedback from supernova when massive stars explode and energy released by super-massive central black holes. They are distinct in terms of their host galaxies. The first two are only effective in low mass galaxies and help explain the relatively low fraction of condensed baryons in dwarf galaxies, while AGN feedback is only effective for very massive objects with a substantial black hole at their centre.

2.5.1 Reionization

The impact of reionization on the formation and evolution of low mass systems in a ΛCDM Universe has been known since the theoretical work of Ikeuchi (1986) and Rees (1986), which pointed out that the photo-ionizing background might suppress the formation of galaxies below the Jeans Mass. In fact, the background heats the intergalactic medium to temperatures of around 10^4K, which can prevent the gravitational collapse of gas in low mass halos (reducing the number density of baryons in these objects), as well as decreasing its radiative cooling by reducing the abundance of collisionally excited atoms (Efstathiou, 1992; Thoul & Weinberg, 1996; Navarro & Steinmetz, 1997; Bullock et al., 2000; Gnedin, 2000; Benson et al., 2002b; Kravtsov et al., 2004). For this reason, it is now established that this phenomenon plays a critical role in reducing the number density of dwarfs in semi-analytic models.

In the current model, this effect is included using the results of the simulations by Gnedin (2000), which define a characteristic mass scale below which the baryonic fraction is reduced compared to the universal value:

$$f_b^{\rm halo}(z, M_{\rm vir}) = \frac{f_b^{\rm cosmic}}{(1 + 0.26 M_{\rm F}(z)/M_{\rm vir})^3}, \tag{2.14}$$

where $M_{\rm F}$ represents the filtering mass. This characteristic scale below which the density of baryons decreases, strongly depends on the assumed redshifts for the beginning and end of reionization and is determined using the results of Kravtsov et al. (2004) for the evolution of the IGM. This model distinguishes between three epochs: $z > z_0$, $z_0 < z < z_r$ and $z < z_r$, corresponding respectively to the epoch before HII regions form, epoch of overlap between multiple HII regions and the epoch after which the intergalactic medium is fully reionized (with the parameters describing the evolution of the IGM set to reproduce the numerical results of Gnedin (2000)). The value for $M_{\rm F}$ obtained from this model is then compared to the characteristic mass corresponding to a halo temperature $\approx 10^4$ K, with the biggest value used to reduce the baryon fraction. The chosen values for the beginning and end of reionization ($z_0 = 8$ and $z_r = 7$) imply a filtering mass of $4 \times 10^9\,{\rm M}_\odot$ at $z = z_r$ and $3 \times 10^{10}\,{\rm M}_\odot$ at redshift zero (just above the resolution limit of the dark matter simulation) and are in good agreement with the numerical results of Gnedin (2000).

2.5.2 Supernova Feedback

The supernova feedback treatment in the current semi-analytic recipe is based on the wind model first introduced by De Lucia et al. (2004). In this way, as massive stars complete their life cycle, SN events start injecting energy into the surrounding medium, reheating cold disk gas. If the available energy exceeds the necessary to reheat the gas into the hot phase, a fraction is ejected into an external reservoir, from which it will be reincorporated into the hot phase at latter times.

For each mass $\Delta m_\star$ turned into stars, the amount of gas reheated from the cold disk to the hot halo is given by

$$\Delta m_{\rm reheated} = \epsilon_{\rm disk} \Delta m_\star, \tag{2.15}$$

with the canonical efficiency of 3.5 being motivated by observations by Martin (1999).

This proves insufficient to prevent star-formation in dwarf galaxies as the cooling times are so short that the gas rapidly cools back down to rejoin the disk. For this reason, and motivated also by observations of galactic outflows (Martin, 1996), the models allow SN to expel gas completely from low-mass galaxies.

The amount of energy released by supernova during the formation of $\Delta m_\star$ stars is

$$\Delta E_{\rm SN} = 0.5\,\epsilon_{\rm halo}\,\Delta m_\star V_{\rm SN}^2, \tag{2.16}$$

where $V_{\rm SN} = 630\,{\rm km\,s^{-1}}$. Any *excess*[2] energy left over from reheating the cold gas is used

[2]Note that the reheated fraction is not reduced if this excess is negative.

to eject a mass of gas $\Delta m_{\rm ejected}$ from the galaxy

$$\Delta m_{\rm ejected} = \left(\epsilon_{\rm halo} \frac{V_{\rm SN}^2}{V_{\rm vir}^2} - \epsilon_{\rm disk} \right) \Delta m_\star, \tag{2.17}$$

where $V_{\rm vir}$ is the virial velocity of the dark matter halo.

This ejected gas is kept in an external reservoir and returned to the hot halo at a rate

$$\dot{m}_{\rm ejected} = -\gamma_{\rm ej} \frac{m_{\rm ejected}}{t_{\rm dyn}}, \tag{2.18}$$

where $m_{\rm ejected}$ is the mass of ejected gas and $t_{\rm dyn}$ is the dynamical time of the halo. The value of the reincorporation efficiency, γ_{ej}, is chosen so that the ejected gas returns to the hot phase in a few halo dynamical times.

In the original wind scheme introduced by De Lucia et al. (2004), the assumed reincorporation time scale was significantly larger, corresponding to the extreme case when most of the ejected gas is permanently lost from the halo. In the current model the ejected gas is assumed to return to the hot phase in a few halo dynamical times ($\gamma_{\rm ej}$ changed from 0.1 to 0.5).

This feedback implementation implies an exchange of material between different baryonic components. The metals produced in stars will follow these routes (section 2.8), with a fraction being retained in stars and the rest divided through the different gas phases (cold, hot and ejected).

2.5.3 AGN Feedback

SN feedback is ineffective in large galaxies, which requires another form of heating to be included. Without it, central cluster galaxies appear too massive and too blue, an aspect of the cooling flow problem, well-known to X-ray astronomers. The solution is thought to be mechanical heating by black holes accreting at well below the Eddington limit, with the amount of energy released depending on the mass accretion rate of the central supermassive black hole, which in turn depends on the black hole mass. To describe this process it is necessary to introduce two different modes of AGN activity: the quasar and radio modes.

Black Hole Growth - The Quasar Mode

The quasar mode regulates the growth of black holes during mergers, both by the accretion of cold gas and by the black holes merging themselves. It dominates the mass growth of these objects in comparison to the quiescent accretion of hot gas at late times. There is

a growing body of observational evidence indicating the importance of energy feedback from quasars (Crenshaw et al., 2003; Pounds et al., 2003). Moreover, recent semi-analytic works have also shown that it is required in order to explain the X-ray properties of Clusters (Bower et al., 2008; Short & Thomas, 2008). Nevertheless, feedback from this process is yet not included in the model.

The role of the quasar mode remains close to the one with which it was introduced by Kauffmann & Haehnelt (2000), to predict the mass of central black holes. However, since the black hole mass is now determinant for the amount of cooling suppressed by the radio mode its efficiency ends up having a great impact on galaxy properties.

Whenever two galaxies merge, their central black holes are instantaneously joined together and at the same time cold gas starts being driven into the merged black holes. The corresponding semi-analytic model parameter, $f_{\rm BH}$, regulates the black hole growth by cold gas accretion associated with galaxy mergers:

$$\Delta m_{\rm BH,Q} = \frac{f_{\rm BH}(m_{\rm sat}/m_{\rm central})\, m_{\rm cold}}{1 + (280\,{\rm km\,s^{-1}}/V_{\rm vir})^2}, \tag{2.19}$$

with the cold gas ($m_{\rm cold}$) being driven into the centre of the galaxy by any merger-induced instabilities. The parameter $f_{\rm BH}$ is set in order for the model to reproduce the local black hole-bulge mass relation (Häring & Rix, 2004).

AGN Feedback - The Radio Mode

The radio mode reflects black hole growth via quiescent accretion in a static hot halo. It may represent either Bondi accretion directly from the hot phase or the accretion of small quantities of cold gas. It is described by the phenomenological model

$$\dot{m}_{\rm BH,R} = k_{\rm AGN} \left(\frac{m_{\rm BH}}{10^8\ {\rm M_\odot}}\right) \left(\frac{f_{\rm hot}}{0.1}\right) \left(\frac{V_{\rm vir}}{200\,{\rm km\,s^{-1}}}\right)^3, \tag{2.20}$$

where $m_{\rm BH}$ is the black hole mass and $f_{\rm hot}$ is the mass fraction of hot gas in the halo. The efficiency parameter $k_{\rm AGN}$ is chosen to reproduce the turnover on the bright end side of the luminosity functions.

The radio mode makes a minor contribution to the growth in mass of the BH but is assumed to generate mechanical heating at a rate

$$L_{\rm BH} = \eta\, \dot{m}_{\rm BH,R}\, c^2, \tag{2.21}$$

where c is the speed of light and the efficiency parameter η is set to 0.1.[3] This heating is used to reduce the rate at which gas cools from the hot halo into the cold disk, creating

[3]Note that it is the combination $\eta\, k_{\rm AGN}$ that determines the heating rate so that the value of η is unimportant.

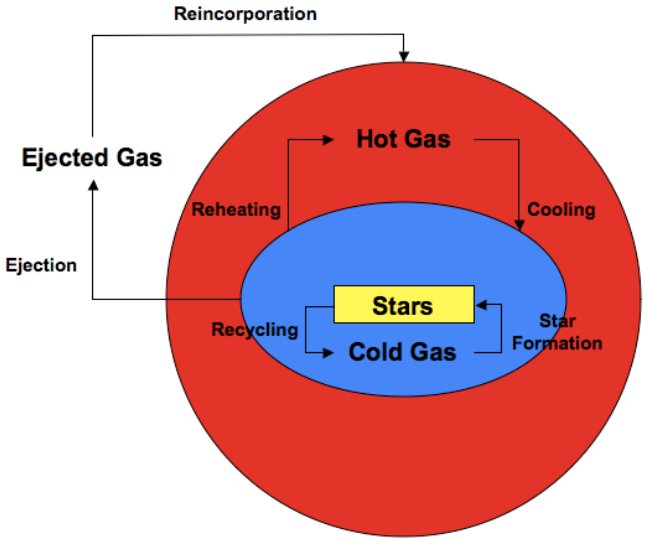

Figure 2.2: A schematic view of the basic galaxy formation processes in the De Lucia & Blaizot (2007) semi-analytic model. Gas cools from the hot into the cold phase, from which it can form stars. AGN reduces the cooling rate, while SN feedback can reheat the cold gas into the hot phase or even eject it into the external reservoir from where it will be reincorporated back into the hot phase at later times.

a modified cooling rate:

$$\dot{m}'_{\rm cool} = \dot{m}_{\rm cool} - \frac{L_{BH}}{\frac{1}{2}V_{\rm vir}^2}. \tag{2.22}$$

Only massive galaxies ($M_\star > 10^{10.5}\,M_\odot$) grow a black hole large enough to produce an amount of mechanical heating capable of reducing the cooling of gas. In this way, the effect of introducing AGN feedback is to decrease the cooling only in massive halos, decreasing their number density, suppressing their star formation and shifting them into the red population in the colour-magnitude relation as required by observations. This reconciles the models with the notion of "downsizing", since as time evolves, super-massive black holes grow in the most massive objects, shifting star formation towards smaller objects and making the biggest objects, which formed latter, contain the oldest populations.

A schematic picture of the galaxy formation processes described until now is presented in Fig. 2.2. Note that AGN feedback is present by means of decreasing the rate of gas cooling from the hot to the cold phase.

2.6 Mergers

In a hierarchically growing Universe mergers are a crucial phenomenon. They determine the mass evolution of galaxies, their morphology and also their star formation history (from merger induced starbursts and the effects of black hole growth). In the current semi-analytic model, mergers are treated following the information from the underlying dark matter substructure. Three different types are assigned to galaxies: central galaxies if they reside at the centre of a dark matter main halo (type 0), satellites with a sub-halo if they reside within a dark matter sub-halo (type 1), or satellites without a halo if their dark matter sub-halo has already been disrupted by the central halo into which they are merging (type 2).

A merger can accordingly be seen as a two stage process. Whenever two galaxies get within the gravitational potential of each other, the most massive is assumed to be the central galaxy. The satellite becomes a type 1, meaning that its dark matter halo is now a sub-halo and has started being stripped to become part of the central galaxy main halo. The hot gas of the satellite is instantaneously stripped and is added to the hot gas content of the central galaxy. The galaxy will be able to keep forming stars, but only for a short period until it consumes all its cold gas.

A second phase occurs when the sub-halo of this type 1 galaxy is stripped below the resolution limit of the dark matter simulation (20 particles, $1.7 \times 10^{10} h^{-1}\,\mathrm{M}_{\odot}$). At this point the galaxy loses its halo and becomes a type 2. Simultaneously, a merger time scale is calculated, dictating the time left until the galaxy merges with its companion at the centre of the main dark matter halo. The time is calculated assuming that the satellite galaxy is experiencing a force from the central halo due to dynamical friction. This force is estimated using Chandrasekhar's formula as in Binney & Tremaine (1987),

$$F_{\mathrm{df}} = -\frac{4\pi \mathrm{G}^2 m_{\mathrm{sat}}^2 \ln(\Lambda) \rho B(x)}{v_{\mathrm{rel}}^2}, \tag{2.23}$$

where m_{sat} represents the satellite mass, $\ln(\Lambda)$ is the Coulomb logarithm (assumed to be $\ln(1 + M/m_{\mathrm{sat}})$), ρ is the local density and v_{rel} represents the relative velocity of the satellite. $B(x)$ is given by

$$B(x) = \mathrm{erf(x)} - 2\mathrm{x} \exp \frac{-\mathrm{x}^2}{\sqrt{\pi}}, \tag{2.24}$$

where $x = |v_{\mathrm{rel}}|/\sqrt{2}\sigma$. The work done on the satellite by this force ($F.v$) will produce a change on its total energy over time:

$$\frac{d}{dt}\left(\Phi + \frac{1}{2} m_{\mathrm{sat}} v_{\mathrm{rel}}^2\right) = -\frac{4\pi \mathrm{G}^2 m_{\mathrm{sat}}^2 \rho \ln(\Lambda) B(x)}{v_{\mathrm{rel}}}, \tag{2.25}$$

where r represent the radius of the satellite's orbit and M the mass of the central halo. Considering this orbit to be circular, $v_{\rm rel}^2 = {\rm G}M/r$, and the equation can be rewritten as

$$\frac{d}{dt}\left(\Phi + \frac{{\rm G}M}{2r}\right) = -4\pi {\rm G}^2 m_{\rm sat}\rho \ln(\Lambda) B(x)\sqrt{\frac{r}{{\rm G}M}}, \tag{2.26}$$

from which follows

$$\frac{dr}{dt}\left(\frac{M}{r^2} - \frac{M}{2r^2} + \frac{2\pi\rho r^2}{r}\right) = -4\pi {\rm G}\, m_{\rm sat}\rho \ln(\Lambda) B(x)\sqrt{\frac{r}{{\rm G}M}}. \tag{2.27}$$

Assuming the distribution of mass in the host halo to be an isothermal sphere (only for this calculation), $M = 2\sigma^2 r/G$ and equation 2.27 can be rewritten as

$$\frac{dr}{dt}\frac{2\sigma^2}{{\rm G}r} = -4\pi {\rm G}\, m_{\rm sat}\rho \ln(\Lambda) B(x)\sqrt{\frac{r}{{\rm G}M}}, \tag{2.28}$$

where σ represents the velocity dispersion of the central halo.

Finally

$$dt = -\frac{\sqrt{2}\sigma r dr}{{\rm G}\, m_{\rm sat} \ln(\Lambda) B(x)}, \tag{2.29}$$

which integrated from the centre of the central galaxy to the initial position of the satellite, and for B(x=1), gives

$$t_{df} \approx 1.17 \frac{V_{\rm vir} r_{\rm sat}^2}{{\rm G}\, m_{\rm sat} \ln(\Lambda)}, \tag{2.30}$$

where $r_{\rm sat}$ is the satellite position at the time it lost the dark matter halo and became a type 2.

Whenever the two galaxies are finally joined together, the outcome will be determined by the baryonic mass ration between the objects. The threshold between a major and a minor merger is defined by a ratio between central and satellite mass of 0.3. Following Springel et al. (2001), if the two masses are comparable ($m_{\rm sat}/M > 0.3$) a major merger occurs. The disks of both galaxies are destroyed and all the stars added to the bulge of the central galaxy, after a major merger induced starburst has occurred (as described in section 2.4.2).

When the central galaxy is large compared to the satellite, the stars of the satellite are added to the bulge of the central galaxy, while its cold gas is added to the disk of the central object together with any stars formed during a minor merger induced starburst.

2.6.1 Disk Instabilities

Apart from mergers, another process that can shape galaxy morphologies is disk instabilities. In the model it is assumed that whenever the disk becomes unstable a fraction of its stars is transferred to the bulge until the stability criteria is met again. The cause is

assumed to be dynamical instabilities that will lead to the formation of bars and are likely to happen in galaxies where the self-gravity of the disk is dominant,

$$\frac{V_c}{(\mathrm{G}\, m_{\mathrm{disk}}/r_{\mathrm{disk}})^{1/2}} \leq 1, \tag{2.31}$$

where V_c is again assumed to be V_{vir}.

2.7 From Absolute Quantities to Observables

2.7.1 Spectroscopic Evolution

Theoretical models of galaxy formation and evolution predict intrinsic properties of galaxies such as masses, star formation rates, metallicities, bulge to disk ratios, gas contents in different phases and the amount of energy released by different feedback sources. In order to compare these predictions with observations it is necessary to convert these properties into observable fluxes. This is achieved in semi-analytic recipes by using stellar population synthesis (SPS) models. These models follow the properties of stars by means of evolutionary tracks and from the characteristics of each galaxy determine their mass to light (M/L) ratios.

The Initial Mass Function

One of the most important assumptions that needs to be included in SPS models is the initial mass function (IMF). This contains information about the mass distribution of a newly formed star population normalised by its total mass. Different forms for this probability distribution function taken over the years are plotted in figure 2.3 (from Baldry & Glazebrook (2003)). This function varied from the pioneering work of Salpeter (1955), which assumed a single power law, to the more recent results of Kroupa (2001); Chabrier (2003), which have converged into either the sum of two power laws, or the sum of a power law and a log-normal distribution. In the semi-analytic code we use, the Chabrier IMF is assumed, which corresponds to a power law with an exponent of 1.3 from 1 to 100 $\mathrm{M}_\odot$ and a log-normal distribution from 0.1 to 1 $\mathrm{M}_\odot$, centred at 0.08 $\mathrm{M}_\odot$ with dispersion 0.69. The recent IMFs predict a smaller fraction of low mass stars and a larger number of high mass stars compared to the original Salpeter. The excess of massive stars, origins higher M/L ratios, meaning that for the same galaxy mass the derived luminosities will be smaller.

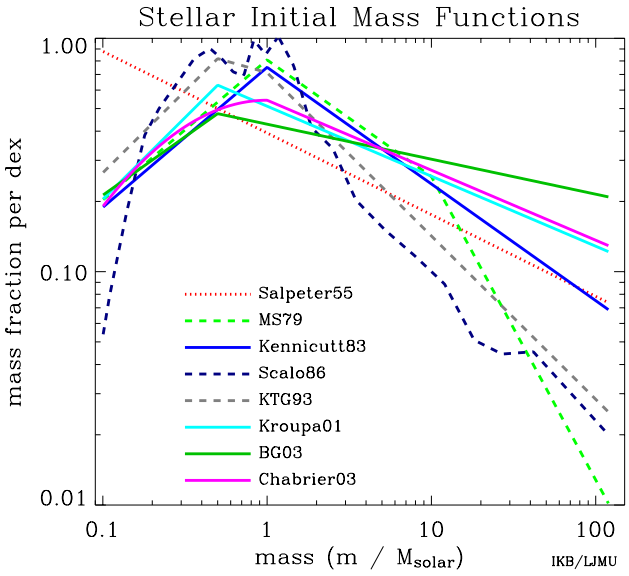

Figure 2.3: Comparison between different initial mass functions in the literature as in Baldry & Glazebrook (2003). The figure shows the original Salpeter (1955), later developments through more than 3 decades (Miller & Scalo, 1979; Scalo, 1986; Kroupa et al., 1993) and the recent results from Kroupa (2001); Baldry & Glazebrook (2003); Chabrier (2003), which together with Kennicutt (1983) have converged into a functional form that combines either two power laws, or a power law and a log-normal distribution.

Stellar Population Synthesis Model

In the semi-analytic model used in this work the SPS models of Bruzual & Charlot (2003) (with a Cabrier IMF) are used to derive photometric properties from the predicted masses of galaxies, taking into account the age and metallicity of their stellar populations. The star formation history of galaxies can be approximated by a series of bursts of different masses, which luminosities are given by the SPS look-up tables. To derive the fluxes of model galaxies, the semi-analytic code interpolates between these tables linearly in t and log Z, considering that stars form with a metallicity given by that of the cold gas. A crucial assumption that goes into these derivations are the evolutionary tracks followed by stars, assumed to be described by the Padova 1994 tracks. These contain information about the different phases of stellar evolution, from the main sequence to the post main sequence branches.

The chosen SPS model included in semi-analytic recipes plays a critical role on the final predictions of galaxy observables. Erroneous gas cooling, star formation and feedback strengths might be needed to compensate wrong assumptions made in these derivations. Over the past few years a growing body of work have exposed deficiencies in the

Bruzual & Charlot (2003) SPS code used in this work. Most noticeable the inadequate treatment of the thermally pulsating phase of stars when they reach the asymptotic giant branch (AGB). Stars on this phase dominate the near infra-red emission of young galaxies (within 0.2 to 2.0 Gyr) and models without it produce galaxies masses and ages that are too high. This leads to larger M/L ratios and generates semi-analytic predicted fluxes that are too small (Maraston, 2005; Conroy et al., 2008). This important aspect will be discussed throughout our results and conclusions, where we clarify in which way model galaxy properties might be affected and how the inclusion of updated SPS models might considerably improve the agreement between semi-analytic predictions and observations.

2.7.2 Dust Model

Star-forming galaxies are known to be rich in dust. This has a major effect on their observed properties, since the light emitted by these galaxies originally in the optical/UV part of the spectra, will be absorbed by the dust particles and re-emitted in the far-infrared/submillimetre. This effect, known as dust extinction, will reduce the overall emission of star-forming galaxies at short wavelengths. Detailed models of radiative transfer and dust reprocessing are complex and subject to high uncertainties. They need to take into account the dust creation by star formation, its destruction by energy sources within the galaxy and its distribution and geometry. Simpler approaches can be developed, which yield similar results for the optical properties of galaxies, by studying the observational relation between the optical depth of dust in galactic disks and the relative UV/optical and far-infrared/submillimetre emission.

The current semi-analytic model includes two different sources of dust attenuation. Extinction from a diffuse inter-stellar medium (ISM) component (following the work of Devriendt et al. (1999)) and from molecular clouds where stars are formed (from the work of Charlot & Fall (2000)). In order to compute the stellar flux absorbed by the different regions, first it is necessary to determine the optical depth of the dust in each and then make some assumptions about its geometry.

Optical Depth of the ISM Dust

To estimate the extinction of flux from the ISM, the optical depth of the dust in galactic disks for a given wavelength is assumed to be

$$\tau_{\lambda}^{ISM} = \left(\frac{A_{\lambda}}{A_{v}}\right)_{Z_{\odot}} \left(\frac{Z_{\rm gas}}{Z_{\odot}}\right)^{s} \left(\frac{\langle N_H \rangle}{2.1 \times 10^{21} \,{\rm atoms\,cm^{-2}}}\right), \tag{2.32}$$

where $\langle N_H \rangle$ represents the mean column density of hydrogen and its given by

$$\langle N_H \rangle = \frac{M_{\rm cold}}{1.4\, m_p \pi (a R_{\rm D})^2} {\rm atoms\,cm^{-2}}, \tag{2.33}$$

where $R_{\rm D}$ is the disk scale length (given by Mo et al. (1998)) and a=1.68 in order for $\langle N_H \rangle$ to represent the mass-weighted average column density of an exponential disk. Following the results from Guiderdoni & Rocca-Volmerange (1987) the extinction curve in Eq. 2.32 depends on the gas metallicity and based on an interpolation from the Solar Neighbourhood and the Large and Small Magellanic Clouds, s=1.35 for $\lambda < 2000$ Å and s=1.6 for $\lambda > 2000$ Å. The extinction curve for the solar metallicity, $(A_\lambda/A_v)_{Z_\odot}$, is taken from Mathis et al. (1983).

Optical Depth of Molecular Clouds Dust

Another source of extinction affects only young stars and comes from the molecular clouds where they are formed. Following Charlot & Fall (2000), the model assumes that the extinction occurs for stars younger than the lifetime of stellar birth clouds (taken to be 10^7 years). The dust from this source has an optical depth given by

$$\tau_\lambda^{BC} = \tau_\lambda^{\rm ISM} \left(\frac{1}{\mu} - 1 \right) \left(\frac{\lambda}{5500 {\rm Å}} \right)^{-0.7}, \tag{2.34}$$

where μ is given by a random Gaussian distribution with centre 0.3 and width 0.2, truncated at 0.1 and 1.

Extinction Rate

In order to get the final extinction from both sources a random inclination relative to the line of sight is assigned to the galaxy and a 'slab' geometry is assumed for the dust in the disk. Therefore, for each component the extinction is expressed as:

$$A_\lambda = -2.5 {\rm log} \left(\frac{1 - \exp^{-\tau_\lambda \sec\theta}}{\tau_\lambda \sec\theta} \right), \tag{2.35}$$

where θ is the angle of inclination of the galaxy relative to the line of sight and τ_λ corresponds to either τ_λ^{ISM} or τ_λ^{BC}.

2.8 Metals

The metals produced by the stars in the model follow routes which are identical to those of the gas. Accordingly, they can be found locked up in stars and in the cold, hot and ejected gas phases. For every solar mass of stars formed a yield (Y) of heavy metals is

produced by supernovae and instantaneously returned to the cold phase. The metals will then follow the gas routes, as it is reheated into the hot phase, ejected into the external reservoir, reincorporated and as it cools from the hot to the cold phase. Whenever a minor merger occurs the metals in the different satellite phases are added to the central galaxy, while in a major merger all the cold gas is consumed in a starburst and the metals are ejected to the external reservoir. The metal content on each component is determined by:

$$\dot{M}^{Z}_{\rm stars} = (1-R)\alpha_{\rm SF} Z_{\rm cold}, \tag{2.36}$$

$$\dot{M}^{Z}_{\rm cold} = \dot{M}_{\rm cool} Z_{\rm hot} - (1-R)\alpha_{\rm SF} Z_{\rm cold} + Y\alpha_{\rm SF} - \dot{M}_{\rm reheated} Z_{\rm cold}, \tag{2.37}$$

$$\dot{M}^{Z}_{\rm hot} = -\dot{M}_{\rm cool} Z_{\rm hot} + \dot{M}_{\rm reincorporated} Z_{\rm reservoir} + \dot{M}_{\rm reheated} Z_{\rm cold}, \tag{2.38}$$

$$\dot{M}^{Z}_{\rm reservoir} = \dot{M}_{\rm ejected} Z_{\rm cold} - \dot{M}_{\rm reincorporated} Z_{\rm reservoir} + \dot{M}^{\rm sat}_{\rm ejected} Z_{\rm cold}, \tag{2.39}$$

where M^z represents the amount of metals and $Z = M^Z/M$ the metallicity in each phase.

Chapter 3

Hybrid Galaxy Evolution Modelling

"Learn fast if possible, become the best, the most intrepid in every circumstance, but never stop improving..."

In "Ayrton Senna, Racing is in my blood."

The model described in the previous chapter (De Lucia & Blaizot, 2007) successfully reproduces a vast range of observational properties. The variety of simulated physical processes make it a comprehensive tool to understand galaxy formation and evolution physics.

Effective supernova feedback lowers the number density of dwarfs bringing the faint end of the luminosity function into better qualitative agreement with observations, while producing galaxies that agree with the observed Tully-Fisher relation and have the expected metallicity of stars (De Lucia et al., 2004). The inclusion of feedback from AGN decreases the fraction of massive galaxies while moving these objects, which are normally central galaxies of large groups and clusters, into the population of passive red galaxies. At the same time, the adopted star formation law, with a cold gas surface density threshold, reproduces the observational fraction of gas in star forming galaxies. These processes, together with the impact of mergers, give predicted objects that show a clear division between blue, star forming and passive, red galaxies in the colour-magnitude relation (Croton et al., 2006). Moreover, the black hole growth, mainly determined by galaxy mergers, produces galaxies and black holes with the observed black hole-bulge mass relation (Kauffmann & Haehnelt, 2000).

However, until now the level of agreement with observations and the relative weight of different observations in the final choice of the parameters in the model, have never been studied in a statistically-consistent way. Moreover, the large number of observational properties that the model aims to predict requires a large number of parameters (some of which are strongly correlated), producing considerable difficulties in determining how to improve the agreement with new observations without destroying the match with existing data sets. In addition, whenever reasonable agreement proves to be impossible, it is hard to know whether there is a failure in determining the right parameter configuration, whether there is a fundamental problem with the underlying model, or whether the introduction of new physics is required.

These difficulties can be overcome by combining multiple observations with proper sampling of high-dimensional parameter spaces. This has proved to be a fruitful approach in theoretical cosmology where techniques such as Monte Carlo Markov Chain (MCMC) parameter estimation have been extensively used. The core of the research presented in this thesis is the introduction of MCMC techniques into semi-analytic models of galaxy formation. In this chapter we describe the implementation of these techniques and the way in which they allow us to understand how galaxy properties are affected by individual parameters, obtain confidence limits for these parameters, and verify the agreement between the model and different observations in a statistically robust way.

This quantitative method of testing model predictions takes galaxy formation modelling a step forward. However, we emphasize that it can only be implemented since the recent inclusion of physical processes, such as the black hole growth and energy feedback, made the model robust enough to predict a range of observational properties with the required level of accuracy. In this chapter we describe how we implement MCMC parameter estimation in the semi-analytic model of De Lucia & Blaizot (2007) using a range of observational constraints (Henriques et al., 2009). In chapter 5, we show how this innovative technique allows us to verify the significance of including new physics whenever a discrepancy is identified between the model and observations (chapter 4).

While the work presented in this thesis was being developed a similar approach was proposed by Kampakoglou et al. (2008). These authors have introduced these tools into their own semi-analytic recipe, an extension of Daigne et al. (2004), which uses a statistical method to generate halos. This model differs from theirs in that it uses a semi-analytic model built upon a direct dark matter simulation of a cosmological size (the Millennium Run).

3.1 Monte Carlo Markov Chain Parameter Estimation

Monte Carlo Markov Chain (MCMC) methods are a class of algorithms for sampling a multidimensional space with a probability proportional to the likelihood with which the model describes the observational constraints. The following brief description follows that in Press et al. (2007). A typical application of this method is when it is possible to calculate the probability, $P(D|x)$, of a given data set, D, given the values of some model parameters, x. Bayes' theorem says that, given a prior $P(x)$, the (posterior) probability of the model is $\pi(x) \propto P(D|x)\,P(x)$ with an unknown normalising constant. MCMC uses this relation to sample points with a probability proportional to the posterior distribution function and does it preferentially where $\pi(x)$ is large. This property is the reason why MCMC methods are extremely efficient at sampling high-dimensional probability distributions, since the computational time needed scales linearly with the number of parameters, rather than exponentially as it would be the case in a random sampling through the parameter space. Moreover, from the principles described, we can see that the posterior distribution can be easily recovered from the unnormalized probability, knowing the density of sampled points in a given volume dx.

The MCMC method uses a Markov Chain to sample the parameter space, meaning that every point of interest x is visited in proportion to the underlying probability distribution $\pi(x)$. In order to generate the required sampling, each point in the chain should be chosen from a distribution that depends only on the preceding point (at each step, the chain only contains information about the current point x_i and the previous x_{i-1}). Another requirement is that the proposal distribution, $p(x_2|x_1)$, which gives the probability of choosing x_2 after x_1, is symmetric,

$$\pi(x_1)\,p(x_2|x_1) = \pi(x_2)\,p(x_1|x_2), \tag{3.1}$$

meaning that the probability of stepping from x_1 to x_2 is the same as the probability of stepping from x_2 to x_1.

3.1.1 Metropolis-Hastings Algorithm

There are several algorithms that can produce a chain with the required properties, the most commonly used being the Metropolis-Hastings algorithm (Metropolis et al., 1953; Hastings, 1970). This method requires a proposal distribution $q(x_2|x_1)$ that can assume various shapes, as long as the chain can reach every point in the region of interest.

The chain is then started at a randomly selected point in parameter space x_1. A

new candidate point x_{2c} is selected by drawing from the proposal distribution, and the acceptance probability $\alpha(x_1, x_{2c})$ calculated using the formula,

$$\alpha(x_1, x_{2c}) = \min\left(1, \frac{\pi(x_{2c})q(x_1|x_{2c})}{\pi(x_1)q(x_{2c}|x_1)}\right). \tag{3.2}$$

The candidate point is accepted with probability $\alpha(x_1, x_{2c})$ and x_2 is set equal to x_{2c}, or rejected and the point left unchanged ($x_2 = x_1$). The ratio $q(x_1|x_{2c})/q(x_{2c}|x_1)$ in equation (3.2) represents the prior, which we assume to be log-normal. Since the prior has the same functional form as the proposal distribution, it is in fact flat. This is the least constraining option that ensures maximum freedom to the MCMC to sample the parameter space. It also means that at any given step, we are assigning equal probabilities to equal states of knowledge, with the acceptance probability only depending on the likelihood of the model for the given set of parameters.

This method does indeed satisfy the balance equation, since equation (3.2) can be rewritten as:

$$\begin{aligned} \pi(x_1)q(x_2|x_1)\alpha(x_1, x_2) &= \min[\pi(x_1)q(x_2|x_1), \pi(x_2)q(x_1|x_2)] \\ &= \pi(x_2)q(x_1|x_2)\alpha(x_2, x_1), \end{aligned} \tag{3.3}$$

that resembles the symmetry equation, since the transitional probability is given by $p(x_2|x_1) = q(x_2|x_1)\alpha(x_1, x_2)$.

3.1.2 Convergence

The objective of the MCMC parameters estimation is to produce a distribution of samples that resembles the underlying likelihood distribution. This happens when the process has converged, meaning that the chain has reached a stationary state. For this reason, it is of major importance to have convergence diagnosis, indicating if all the chains reached a point where their distributions stay unchanged. This can be inferred by comparing the variance of different chains, when more than two are used to explore the same parameter space. In order to verify the convergence of our sampling method we use this principle, as proposed by Gelman & Rubin (1992).

For a given parameter x we have m parallel chains, with length n. Letting x_{ij} denote the i^{th} of the n iterations of x in chain j, we calculate the between-sequence variance B:

$$B = \frac{n}{m-1}\sum_{i=1}^{m}(\bar{x_i} - \bar{x})^2, \text{ where } \bar{x_i} = \frac{1}{n}\sum_{j=1}^{n} x_{ij} \text{ and } \bar{x} = \frac{1}{m}\sum_{i=1}^{m}\bar{x_i}, \tag{3.4}$$

and the within-sequence variance W:

$$W = \frac{1}{m\,(n-1)}\sum_{i=1}^{m}\sum_{j=1}^{n}(x_{ij} - \bar{x_i})^2. \tag{3.5}$$

From these two quantities we can estimate the variance σ^2 by a weighted average of B and W:

$$\hat{\sigma}_x^2 = \frac{n-1}{n}W + \frac{1}{n}B, \tag{3.6}$$

which would be an unbiased estimate of the true variance if the starting points of the sequence were drawn from the target distribution, but overestimates it if the starting points are properly over-dispersed. In order to verify the convergence of the sampling one would like to calculate the quantity $R = \frac{\hat{\sigma}^2}{\sigma^2}$. However, since σ^2 is not known it needs to be estimated from the data. For this reason, we use the Gelman-Rubin statistic R, defined as

$$\hat{R} = \frac{\hat{\sigma}_x^2}{W}, \tag{3.7}$$

which makes use of the fact that $\hat{\sigma}_x^2$ is an over-estimate of the true variance and that W is itself an under-estimate, since the sample has not yet reached all the points in the target distribution. In this way, as $n \to \infty$, $\hat{R} \to 1$, since $\hat{\sigma}_x^2$ decreases and W increases both becoming closer to the true σ^2.

3.1.3 Burn-In

The selection of the starting point for the chains is not crucial for the MCMC sampling. However, if this happens to be a region of low likelihood, it would take a considerable number of steps until the chain works its way into the high likelihood region. In this case, the steps taken while the chain is slowing moving upwards in likelihood space might bias the final calculation of the posterior probability distribution. To avoid this bias, the initial part of the chain, designated burn-in, should be discarded. Another good practice to avoid these effects is to run multiple chains with starting points randomly selected (preferably within regions of high likelihood).

3.2 MCMC Sampling in a Simulation Covering a Cosmological Volume

Implementing the MCMC sampling approach on the semi-analytic model parameter space raises considerable issues related not only to the copious amount of I/O (the original recipe reads in the full Millennium dark matter trees), but also to the volume of calculations required to follow the evolution of over 20 million galaxies in a cosmological volume, through more than sixty redshift slices. At each MCMC step the semi-analytic model needs to be run with the proposed set of parameters to compute the acceptance probability, by

comparing the outputted galaxy properties with the observational constraints. The size of the calculation and the number of steps required for convergence makes it unfeasible to perform our analysis using the full Millennium volume.

The structure of the Millennium Simulation provides a way to circumvent this difficulty. The output is divided into 512 files which have self-contained trees, with the galaxies on each treated independently. We choose to perform our analysis in a single file with a mean density and luminosity function analogous to those of the full Millennium box. This assures that the parameter study done on it is representative of the full data set [1]. For our best fit parameters, we rerun the SA model on the full simulation: these results are presented in section 3.4 below.

Using one file representative of the total volume significantly reduces the computational time required for our study. Nevertheless, the size of the calculations involved, even in that smaller volume, still make it a challenging task. Each run of the semi-analytic model takes around 2 minutes in order to compute galaxy properties from redshift 127 to redshift 0. Consequently the 30 000 steps needed take approximately 1000 hours of CPU time. In order to perform the sampling, the Cosmology Machine (COSMA) supercomputer supplied by Sun Microsystems was used, a machine based in the Durham University that is part of the Virgo Consortium facilities. The different runs with different observational constraints were run using 100 processors at a time, allowing for the same number of MCMC chains to be obtained. Due to the properties of MCMC methods these different chains can then be combined to perform the analysis.

3.3 Individual Observational Constraints

3.3.1 Overview

The traditional semi-analytic approach is to adjust parameters only considering observations at redshift zero. Following this philosophy we select 3 independent and local observational data sets: the K-band luminosity function, the colour-stellar mass relation and the black hole-bulge mass relation, to fully constrain the 6 parameters defining galaxy masses and formation rates of stars and AGN.

From the original 12 parameters in the model, we choose to freeze 6 of them at the

[1] Only the largest galaxies with stellar masses greater than $\approx 10^{11}\, h^{-1}\ \mathrm{M}_{\odot}$ are not properly sampled in this way. This would make our method inappropriate to compare theoretical predictions with observations of large scale structure. However, for the properties chosen to constrain the model and for the selected range of galaxy masses, it holds similar results to a MCMC sampling using the full millennium volume.

Table 3.1: Semi-analytic model parameters from De Lucia & Blaizot (2007). The first 6 parameters are frozen in our analysis at the values shown here. A detailed description of the parameters is given in the text.

$f_{\rm b}$	z_0	$z_{\rm r}$	$T_{\rm merger}$	R	Y
0.17	8	7	0.3	0.43	0.03
$\alpha_{\rm SF}$	$k_{\rm AGN}$	$f_{\rm BH}$	$\epsilon_{\rm disk}$	$\epsilon_{\rm halo}$	$\gamma_{\rm ej}$
0.03	7.5×10^{-6}	0.03	3.5	0.35	0.5

values chosen by De Lucia & Blaizot (2007), as shown in the top row of table 3.1. The cosmic baryon fraction, f_b, is fixed by the cosmology[2], while the redshifts of the beginning and end of reionization (z_0, $z_{\rm r}$) are used to modify the baryon fraction in small halos, accounting for the effects of photo-ionizing heating (Kravtsov et al., 2004; Croton et al., 2006). $T_{\rm merger}$ is the threshold mass ratio that defines the distinction between major and minor mergers. R is the recycled fraction and Y the yield, both of which depend upon the details of the stellar initial mass function. The observational data sets that we use in this work do not allow us to strongly constrain any of these values.

That leaves 6 free parameters in our study. These are the star formation efficiency, $\alpha_{\rm SF}$ (equation 2.10), the fraction of cold gas accreted by the central black hole during mergers, $f_{\rm BH}$ (equation 2.19), the quiescent hot gas black hole accretion rate, $k_{\rm AGN}$ (equation 2.20), the SN feedback disk reheating efficiency, $\epsilon_{\rm disk}$ (equation 2.15), the SN feedback halo ejection efficiency, $\epsilon_{\rm halo}$ (equation 2.16), and the ejected gas reincorporation efficiency, $\gamma_{\rm ej}$ (equation 2.18).

In this section we present the observations used in our analysis and we show how each individual property constrains the different parameters by running the MCMC sampling with one observational data set at a time over approximately 30 000 steps, excluding an initial burn-in to ensure the independence of the final results from the starting point of the chains. To further ensure this property, multiple chains are run at the same time, starting in different regions of the parameter space. Considering the underlying probability distribution of our parameters we choose a log-normal proposal distribution. Its width is selected to ensure that the final acceptance of the chain is between 10% and 40%. This

[2]Note that, as in De Lucia & Blaizot (2007), we use the value of 0.17 suggested by WMAP rather than the value of 0.18 used to generate the power spectrum for the Millennium Simulation.

acceptance rate ensures that the sampling is not too static or too erratic.

The output is analyzed using GETDIST, which is part of the COSMOMC software package (Lewis & Bridle, 2002), adapted to produce 1d and 2d maximum likelihood (profile) and MCMC marginalised (posterior) distributions. For the independent observational properties we use different statistical tests to compute the likelihood of the model, reflecting the observational uncertainties and the nature of the relation under study.

Running our sampling technique with separate observational data sets, one at a time, allows us to gain insight into which degeneracies between the different parameters are broken by each additional observation. We start by studying the influence of varying the parameters on the final K-band luminosity function.

3.3.2 The K-band Luminosity Function

Despite being one of the most fundamental properties of a galaxy, stellar mass is not easily derived from observations. To get estimates for this quantity from the observed luminosities it is necessary to assume mass-to-light (M/L) ratios based on stellar population synthesis models that include still poorly-understood dust corrections, initial mass functions (IMFs) and metallicity evolution. On the other hand, semi-analytic models directly predict mass, but to produce observable luminosities the same crudely-established process must be taken in the reverse direction. In any case the mass to light conversion (or vice-versa) requires a knowledge of the galaxy age and metallicity. In theoretical models these quantities are directly predicted, while in observations they are normally derived from other properties and subjected to significant uncertainties.

This difficulty leads us to use the K-band luminosity function. The K-band is known as a good mass indicator as it is relatively unaffected by dust and represents a fair sample of the stellar population. We combine three observational studies (Cole et al., 2001; Bell et al., 2003; Jones et al., 2006), respectively from 2DFGRS, 2MASS and 6DFGRS, from which we build a final luminosity function. The final data points are given by the average of the maximum and minimum number-density estimates in each magnitude bin, with errors σ_i equal to half the difference between them.

The comparison between the K-band luminosity function from the original model of De Lucia & Blaizot (2007) (using the published parameter values) with the observations is shown in Fig. 3.1. The original model already shows good agreement with the combined data except for the faint end, over predicting the number of dwarf galaxies with magnitudes fainter than $K \approx -22$.

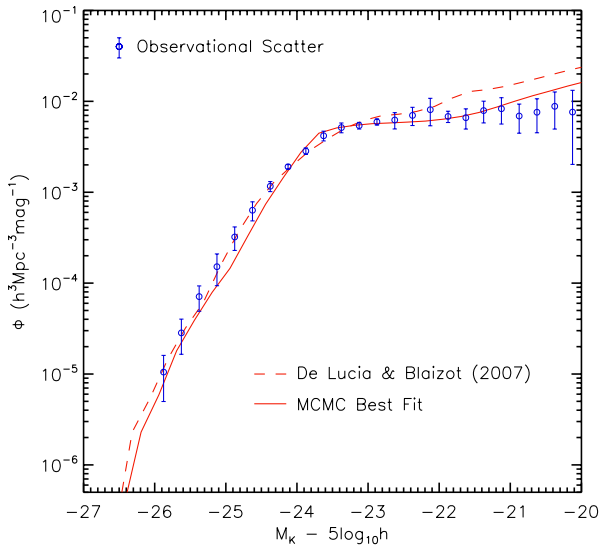

Figure 3.1: The galaxy K-band luminosity function at z=0 for the De Lucia & Blaizot (2007) model (dashed red line) and our best fit model (solid red line). The model predictions are compared with observations from (Cole et al., 2001; Bell et al., 2003; Jones et al., 2006) combined to produce a new luminosity function reflecting the scatter between them.

To compute the likelihood of the model for the K-band luminosity function we use the chi-square probability function where

$$\chi^2 = \sum_i \frac{(N_i - n_i)^2}{\sigma_i^2 + n_i}, \tag{3.8}$$

is summed over the observational bin range plotted in Fig. 3.1, and N_i and n_i represent the number of observational and simulated galaxies in each bin, respectively. We note that due to the limited volume used, the sampling is not constrained by the two brightest bins of the K-band luminosity function.

In Fig. 3.2 we plot the 1σ and 2σ preferred values from the MCMC (solid lines) and the maximum likelihood value sampled in each bin (colour contours), for the subset of the original parameters (with values plotted in log space) constrained only by the observational K-band luminosity function.

In interpreting this and future plots, one should bear in mind that the contours follow the MCMC sampling in parameter space, which should trace out the relative likelihoods of different regions (the posterior distribution). The colours represent the maximum likelihood projected along all the hidden dimensions in the plot (profile distribution). Usually, as in this case, the two match fairly well. The exceptions arise when there is a high-likelihood region that only occupies a small volume of parameter space.

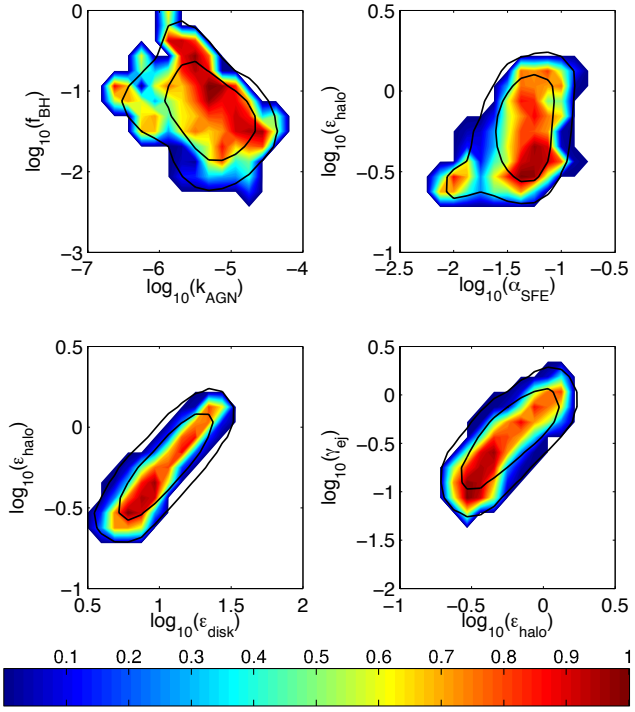

Figure 3.2: Correlations between the 6 parameters analysed in our study only constrained by the χ^2 test on the K-band luminosity function. For the values of the parameters plotted in log space, the solid contours represent the 68% and 95% preferred regions from the MCMC (the posterior distribution) and the colours the maximum likelihood value sampled in each bin (the profile distribution). The colour scale is normalized by the maximum likelihood value of 0.87. White regions in the plot represent regions either with very low likelihood, less than 0.1 per cent of the peak, or regions that have not been visited by the MCMC chain.

The two lower panels of Fig. 3.2 show that the three parameters controlling the SN feedback are all positively correlated with each other, in a way that allows us to learn how the K-band luminosity function constrains the feedback model. To do this, we rewrite equation 2.17 as

$$\frac{\Delta m_{\rm ejected}}{\Delta m_\star} = \epsilon_{\rm halo} \frac{V_{\rm SN}^2}{V_{\rm vir}^2} \left(1 - \frac{\epsilon_{\rm disk}}{\epsilon_{\rm halo}} \frac{V_{\rm vir}^2}{V_{\rm SN}^2}\right), \tag{3.9}$$

from which we see that the amount of ejected gas per unit mass of star formation drops to zero for halos with virial speed greater than

$$V_{\rm vir,0} = \left(\frac{\epsilon_{\rm halo}}{\epsilon_{\rm disk}}\right)^{\frac{1}{2}} V_{\rm SN}. \tag{3.10}$$

In our analysis this cutoff is represented by the line of maximum likelihood in the lower left panel of Fig. 3.2 and corresponds to $v_{\rm vir} \approx 140\,{\rm km\,s^{-1}}$, which translates into $\mathrm{M}_\star \approx 10^{10.0}\,\mathrm{M}_\odot$ and $M_K \approx -22$. This cutoff virial velocity is lower than in De Lucia & Blaizot (2007), which means that our SN feedback stops being effective at fainter magnitudes, allowing more stars to form in $\mathrm{L}_\star$ galaxies. Since we need to assume a stronger SN feedback to decrease the faint end of the luminosity function, this is the only way to ensure that this form of feedback will not be effective in galaxies with intermediate brightness and enough stars will form in these galaxies.

For a given value of $V_{\rm vir,0}$ the amount of ejected gas is proportional to $\epsilon_{\rm halo}$, with the maximum likelihood solutions showing a linear relation $\gamma_{\rm ej} \propto \epsilon_{\rm halo}$. This corresponds to a roughly constant amount of gas being held in the external reservoir: in a steady state the external gas content is proportional to the ratio of the influx and outflux rates. Our regions of high likelihood represent a considerably higher amount of gas being held in the external reservoir than in De Lucia & Blaizot (2007), with a corresponding reduction in star formation in faint galaxies.

The value of $\epsilon_{\rm disk}$, controlling the reheating of cold to hot gas, has a minor impact except as a way of controlling the critical magnitude limit above which feedback is ineffective. Presumably cooling times are so short in dwarf galaxies that any gas that is reheated will quickly cool down again. One might have expected that it could be used to control the stellar mass fraction in large galaxies where the cooling time is relatively long, however this does not seem to be the case.

The AGN feedback parameters, shown in the top-left panel of Fig. 3.2, have a broader acceptable region but also show a high-likelihood spine that runs diagonally down from top-left to bottom right. This can be explained by combining equations 2.19, 2.20 and

2.21 to obtain the mechanical heating rate produced by this process,

$$L_{\rm BH} \propto f_{\rm BH}\, k_{\rm AGN}\, m_{\rm cold}\, f_{\rm hot}. \tag{3.11}$$

Thus, for given cold and hot gas fractions in the galaxies, the line represents a single heating rate. This degeneracy is broken if the black hole masses are used as a constraint (section 3.3.4), since their growth is mainly dominated by the quasar mode.

The maximum likelihood channels described above all have star-formation efficiencies of $\epsilon_{\rm SF} \approx 0.04$, similar to that of De Lucia & Blaizot (2007). This reinforces the conclusion that the SN and AGN feedback parameters act to maintain a constant mass of cold gas available for star-formation.

Apart from the main band discussed above, the two upper panels in Fig. 3.2 show alternative regions with acceptable likelihood. These have lower star-formation efficiencies, requiring a greater mass of cold gas. This, in turn, leads to a smaller product of $f_{\rm BH}$ and $k_{\rm AGN}$. We do not dwell on these solutions here as they seem to be ruled out by other observations: in particular they result in excessive black hole-bulge mass ratios.

3.3.3 The Colour-Stellar Mass Relation

The star formation rate is another essential quantity in characterising the galaxy population. Although this property can be directly extracted from the models, it is not easily comparable with observations. While in the models, the mass transformed into stars at each time step is computed, only indirect observational estimators are available.

Galaxy colours are one such indirect measure of the recent star-formation history of galaxies, with a clear bimodality between an old, passively evolving red population, and a young star forming blue sequence (e.g. Kauffmann et al., 2003; Brinchmann et al., 2004; Baldry et al., 2004).

The top panel of Fig. 3.3 shows the colour-stellar mass relation for the original De Lucia & Blaizot (2007) model. Although it has some problems in correctly predicting the slope and fraction of each population in some mass ranges (see Baldry et al., 2006; Weinmann et al., 2006a), it clearly reproduces the bimodality.

To test the correctness of model colours, we divide the galaxies into the two populations using the selection criteria in Weinmann et al. (2006a), $(g-r) = 0.7 - 0.032\,(M_r - 5\log h + 16.5)$, converted into a cut on the colour-stellar mass relation at redshift zero, $(B-V) = 0.065\,\log(\mathrm{M}_\star h^2/\,\mathrm{M}_\odot) + 0.09$, shown as the solid line in the upper panel of Fig. 3.3. The conversion from the $g-r$ to the $B-V$ colour was done following Fukugita et al. (1996), $g - r = 1.05(B-V) - 0.23$. The fraction of red galaxies for different mass bins is then

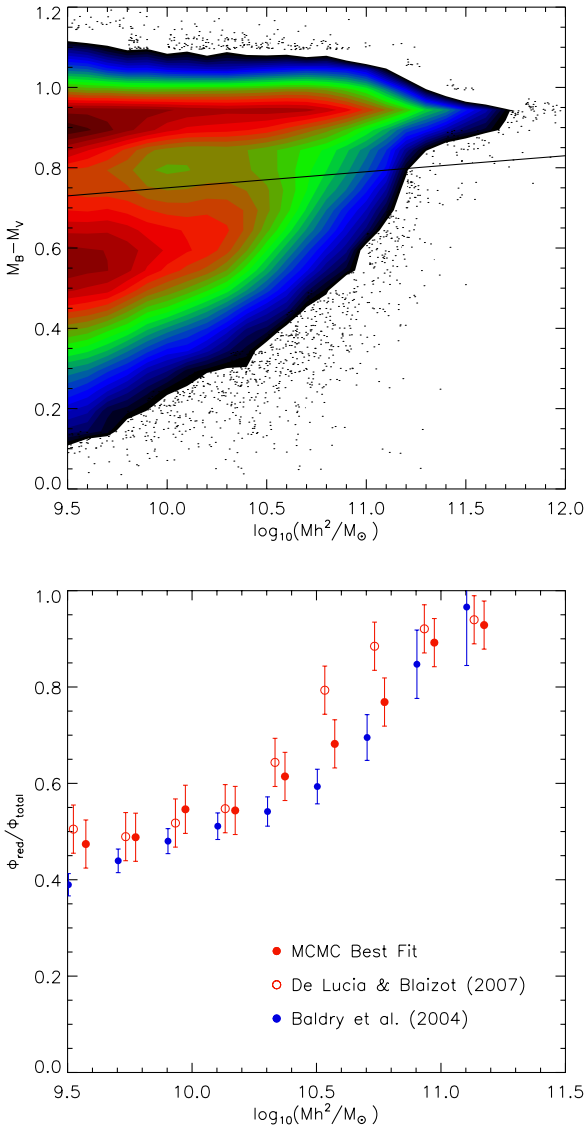

Figure 3.3: Comparison between model and observational colours. The upper panel shows the De Lucia & Blaizot (2007) B-V colour-stellar mass relation, with the solid line representing the observational division between populations from Weinmann et al. (2006a) (dots represent regions with a number density of galaxies below the lowest contour value). In the bottom panel the fraction of red galaxies as a function of stellar mass from De Lucia & Blaizot (2007) (red open circles) and our best fit model (red filled circles) is compared with observations from Baldry et al. (2004) (filled blue circles).

compared with observations from Baldry et al. (2004) as shown in the lower panel. The observational masses based on the 'diet' Salpeter IMF (Bell et al., 2003) were reduced by 0.15 dex to agree with the IMF assumed in our semi-analytic model (Chabrier, 2003). The fact that a different blue band was used in the observational colour cut ($u-r$ instead of our converted $g-r$) could potentially lead to discrepancies in the number of objects identified in each population if the two gaussian distributions defining each population significantly overlap. However, as Fig. 3.3 shows, there is a clear division between red and blue galaxies in the $B-V$ colour-stellar mass diagram for model galaxies. For this reason, any small differences in the number of red galaxies caused by the different colour cut used, should be well within the 0.05 error assumed for the model fraction.

Following Croton et al. (2006) we take the resolution limit for model colours to be at a stellar mass of approximately $10^{9.5}\,h^{-2}\,M_{\odot}$, above which the model reproduces the red fraction reasonably well, with some minor excess for galaxies near $\mathrm{L}_{\star}$.

The agreement between model and observational colours is calculated using a maximum likelihood method with a constant value for the errors in the model ($\sigma_{model} = 0.05$) given by the variation in the fraction of red galaxies in a sample of 20 sub-volumes of the Millennium Simulation, similar to the one used in our analysis.

We assume that both model and observational values are Gaussian distributed around the true fraction F, with a likelihood

$$\mathcal{L}_{(\mathrm{Colour})} = \exp\left\{-\frac{(f_{\mathrm{model}}-F)^2}{2\sigma^2_{\mathrm{model}}} - \frac{(f_{\mathrm{obs}}-F)^2}{2\sigma^2_{\mathrm{obs}}}\right\} \tag{3.12}$$

that has a maximum value

$$\mathcal{L}_{(\mathrm{Colour})} = \exp\left\{-\frac{(f_{\mathrm{model}}-f_{\mathrm{obs}})^2}{2(\sigma^2_{\mathrm{model}}+\sigma^2_{\mathrm{obs}})}\right\}. \tag{3.13}$$

The De Lucia & Blaizot (2007) model, tuned to reproduce a different set of observational colours (the red and blue luminosity functions from 2DFGRS), correctly predicts the fraction of red galaxies at low and high masses but makes the transition from moderate to high red fractions at a stellar mass which is too low.

In Fig. 3.4 we plot the allowed regions in likelihood and posterior space. Perhaps surprisingly, the colour constraint picks out a similar relationship between ϵ_{halo} and ϵ_{disk} as does the K-band. This is because it also requires a cessation of SN heating in galaxies with virial speeds above $140\,\mathrm{km\,s^{-1}}$ which would otherwise have an excessive red fraction.

The observational constraint again requires a constant mechanical heating from AGN feedback (as shown by the line of maximum likelihood in the upper-left panel of the figure) which is responsible for the elimination of blue galaxies at high masses. The line of

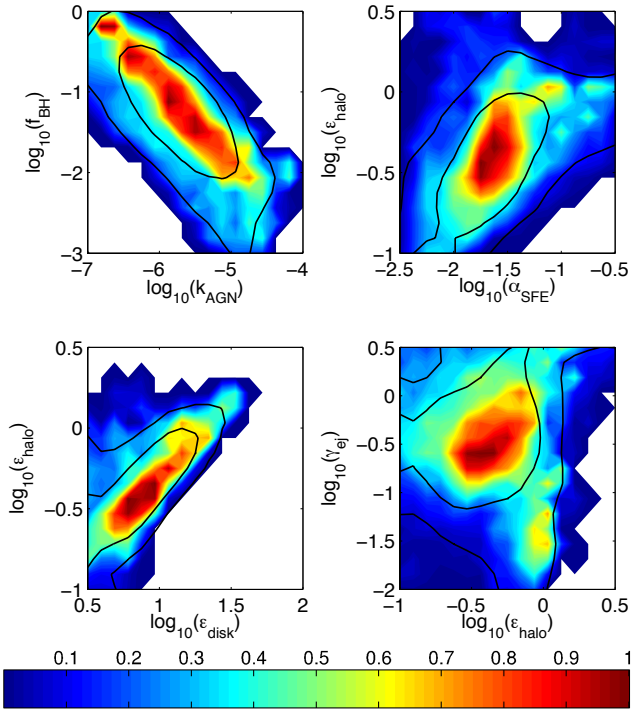

Figure 3.4: As for Fig. 3.2, but constrained only by the maximum likelihood test on the fraction of red galaxies. The colour scale is normalized by the maximum likelihood value of 0.89.

highest likelihood lies slightly below that seen for the K-band constraint. Along with this, the upper-right panel of the figure shows a preference for a slightly lower star-formation efficiency. However, in each case there is an acceptable region where the allowed parameter spaces overlap. This changes when we move to our third constraint.

3.3.4 The Black Hole-Bulge Mass Relation

We have seen in the previous section that the power of the radio-mode AGN feedback depends upon the product of the quasar and radio-mode growth factors. However, the mass growth of the black holes is dominated by the quasar mode alone. We can therefore use the black hole-bulge mass relation to break this degeneracy.

If we require semi-analytic galaxies to be constrained solely by this relation, then the other parameters in the model will be free to shift into implausible values allowing any point in parameter space to have a reasonable likelihood. For this reason, we require model galaxies to follow both the black hole-bulge mass relation and the K-band luminosity function of bright galaxies (i.e. the host galaxies of these black holes).

The black hole and bulge masses for the original model are plotted in Fig. 3.5 and compared with local observations from Häring & Rix (2004). The model galaxies fall on

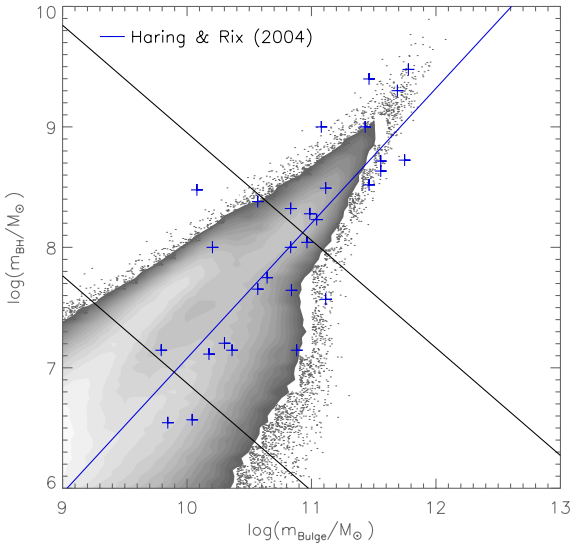

Figure 3.5: The black hole-bulge mass relation for De Lucia & Blaizot (2007) (solid contours) is compared with local observational data from Häring & Rix (2004) (blue crosses) (black dots represent regions with a number density of predicted galaxies bellow the lowest contour value). The best fit to the observational data points is given by the blue line running from bottom-left to top-right, while the two black lines perpendicular to this relation divide galaxies into the two mass bins used to compute the likelihood.

top of the observational best fit (given by the blue line), with the scatter in the relation also reproduced.

In order to test the semi-analytic results against observations, we divide the data into two bins (perpendicular to the observational best fit), represented by the solid black lines on Fig. 3.5, $15.2 < m_{\rm BH} + 0.90\, m_{\rm Bulge} \leq 17.75$ and $17.75 < m_{\rm BH} + 0.90\, m_{\rm Bulge}$. For each of the bins we compute the binomial probability for the observed distribution of mass ratios above and below the best fit line, given the fractional distribution from the model galaxies:

$$\mathcal{L}_{\rm (BH-Bulge)} = \begin{cases} 2I_p(k, n-k+1), & I_p \leq 0.5 \\ 2(1 - I_p(k, n-k+1)), & I_p > 0.5 \end{cases} \tag{3.14}$$

where k is the number of observed galaxies above the best fit in each bin, n the total number of observed galaxies in the same bin, and p is the equivalent fraction, k/n, for the model galaxies in the bin. $I_p(a, b)$ is the incomplete beta function as defined in Press et al. (2007). The two formulae are required since we need to exclude both extremes of the distribution, corresponding to an excess of points both above and below the best fit line.

The choice of the binomial test with only two bins, in order to compare the theoretical black hole-bulge mass relation with observations, is motivated both by the small number

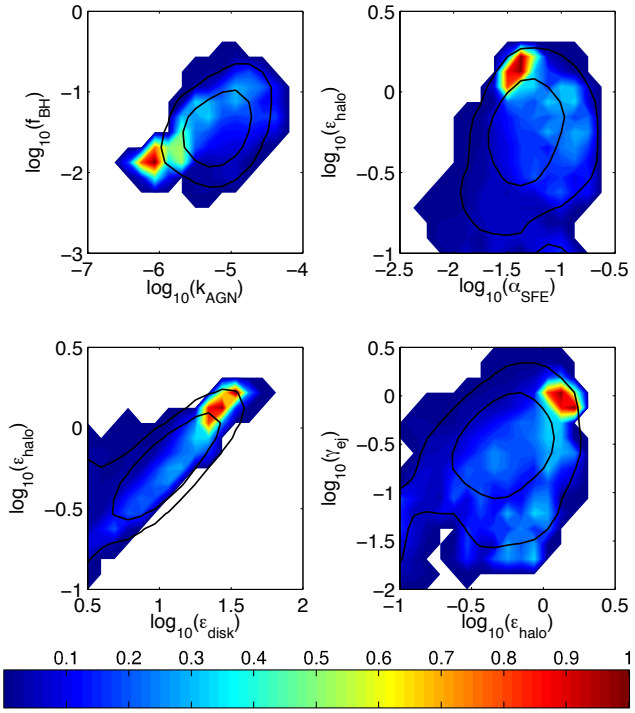

Figure 3.6: As for Fig. 3.2, but constrained only by the binomial test on the black hole-bulge mass relation and by the K-band luminosity function of galaxies above $M_k = -23$. The colour scale is normalized by the maximum likelihood value of 0.86. The mismatch between likelihood and MCMC contours is due to a region that despite having a very high likelihood covers a reduced volume in parameter space, meaning it is not highly favoured in a Bayesian sense.

of objects available in the latter and by the large uncertainties in the black hole growth model used by the former. The test requires both sets to lie on top of each other, but is not as demanding as the χ^2 or the maximum likelihood methods used for the other two properties. In practice, this means that we give a stronger weight to the ability or not of the model to reproduce the observational masses and colours of galaxies (which are more precisely determined by data).

In Fig. 3.6 we plot the posterior and profile likelihood distributions of the parameters constrained only by this binomial test and the K-band luminosity function of galaxies brighter than $M_k = -23$.

It is immediately apparent that the region of high likelihood is much smaller for this test than for the first two constraints. Moreover, this region corresponds to higher values for the SN feedback parameters, combined with a low AGN feedback efficiency. As such, it is incompatible with the acceptable regions in those previous tests.

However, there is a lower-likelihood, but still acceptable (likelihood > 0.1) region that

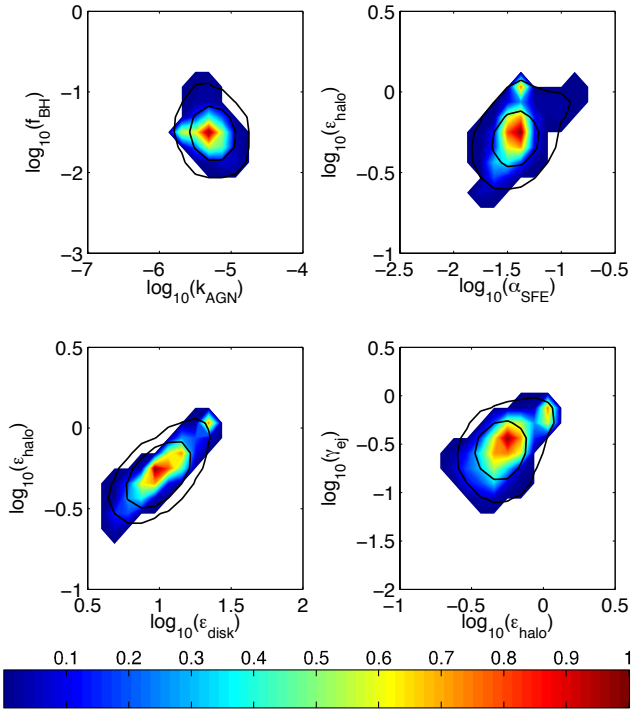

Figure 3.7: As for Fig. 3.2, but constrained by all three observational properties: the K-band luminosity function, the fraction of red galaxies, and the black hole-bulge mass relation. The colour scale is normalized by the maximum likelihood value of 0.037.

extends towards lower SN and higher AGN parameters. As the MCMC contours show, this occupies a much larger volume of parameter space than the high-likelihood peak (and so, in a Bayesian sense, the true solution is more likely to be found in the former than the latter).

Looking at the upper-left panel in the figure, we can see that the acceptable region runs from bottom-left to top-right, perpendicular to the lines seen in the previous two tests. The black hole-bulge mass ratio thus breaks the degeneracy in the AGN parameters.

3.4 Combined Observational Constraints

The likelihood of the model for a given point in parameter space is computed by taking the product of the three independent observational constraints described in the previous sections.

$$\pi(x_i) = \mathcal{L}_{(\mathrm{K-band})} \times \mathcal{L}_{(\mathrm{Colour})} \times \mathcal{L}_{(\mathrm{BH-Bulge})} \tag{3.15}$$

This quantity is calculated at each MCMC step and used to derive the acceptance probability (equation 3.2). As for the individual constraints, we run our sampling over approximately 30 000 steps, excluding an initial burn-in to ensure the independence of the

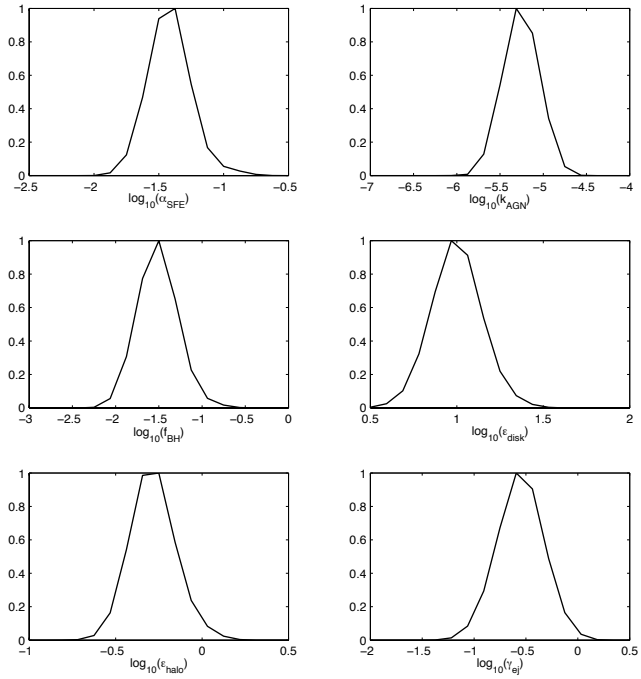

Figure 3.8: Likelihood distributions for the 6 parameters studied. The solid lines represent the maximum likelihood in each bin marginalised over the other dimensions in parameter space.

final results from the starting point of the chain.

Although, in our sampling we do not impose rigid limits on the parameters range, Fig. 3.7 shows that the preferred regions are well-constrained. Fig. 3.8 shows the profile distribution for each parameter, marginalised over all others. Unfortunately, the maximum likelihood is just 0.037, thus the best fit solution is incompatible with the three combined observations at the 2-σ level.

The principal cause of the low likelihood is an incompatibility between the black hole-bulge mass constraint and the K-band and $B-V$ colours. As discussed in section 3.5, this might be caused by observational uncertainties in the black hole and bulge masses or might reflect a deficiency in the black hole growth model, which is still very simplistic. Nevertheless, uncertainties associated with stellar population synthesis and dust modelling, make it premature to conclude that the De Lucia & Blaizot (2007) formalism is ruled out.

3.4.1 Best Fit Parameters and Confidence Limits

The best fit and confidence limits for the 6 free parameters, together with the published values from De Lucia & Blaizot (2007) are shown in table 3.2. All the parameter values

Table 3.2: Statistics from the MCMC parameter estimation for the 6 parameters selected from the original model. The best fit and confidence limits (derived from the colour contours in Fig. 3.7) are compared with the published values from De Lucia & Blaizot (2007).

	DLB07	Mean	-2σ	-1σ	+1σ	+2σ
$\alpha_{\rm SF}$ (SFE)	0.03	0.039	0.020	0.020	0.11	0.13
$k_{\rm AGN}$ (AGN Radio)	7.5×10^{-6}	5.0×10^{-6}	2.4×10^{-6}	2.4×10^{-6}	9.7×10^{-6}	1.1×10^{-5}
$f_{\rm BH}$ (AGN Quasar)	0.03	0.032	0.014	0.014	0.103	0.115
$\epsilon_{\rm disk}$ (SN Reheating)	3.5	10.28	4.43	4.52	24.37	24.37
$\epsilon_{\rm halo}$ (SN Ejection)	0.35	0.53	0.26	0.26	1.17	1.17
$\gamma_{\rm ej}$ (SN Reincorporation)	0.5	0.42	0.08	0.08	0.73	0.79

in the original model fall within our 2σ regions except for the SN disk reheating efficiency, which we require to be larger than before.

Both the star formation efficiency and the AGN quasar mode parameters from the original De Lucia & Blaizot (2007) recipe closely match our best fit values, while our AGN radio mode efficiency is slightly lower than before.

For the SN feedback parameters, the original halo ejection efficiency, $\epsilon_{\rm halo}$ is below our best fit, whereas the original gas reincorporation efficiency, $\gamma_{\rm ej}$, is slightly higher. This combination acts so as to produce a higher fraction of gas trapped in the external reservoir with the new parameters, and hence a smaller mass of cold gas available for star-formation in dwarf galaxies.

The De Lucia & Blaizot (2007) SN reheating efficiency ϵ_{disk}, is considerably lower than our best fit. As discussed earlier, the main effect of this is to lower the ratio $\epsilon_{\rm halo}/\epsilon_{\rm disk}$ with the new parameters and hence, from equation 3.10, to lower the critical virial speed above which feedback is ineffective.

3.4.2 Galaxy Properties in our Best Fit Model

The MCMC parameter estimation was carried out using only one data-file representing 1/512 of the Millennium volume. In this section we present results using our best fit parameters in the full volume.

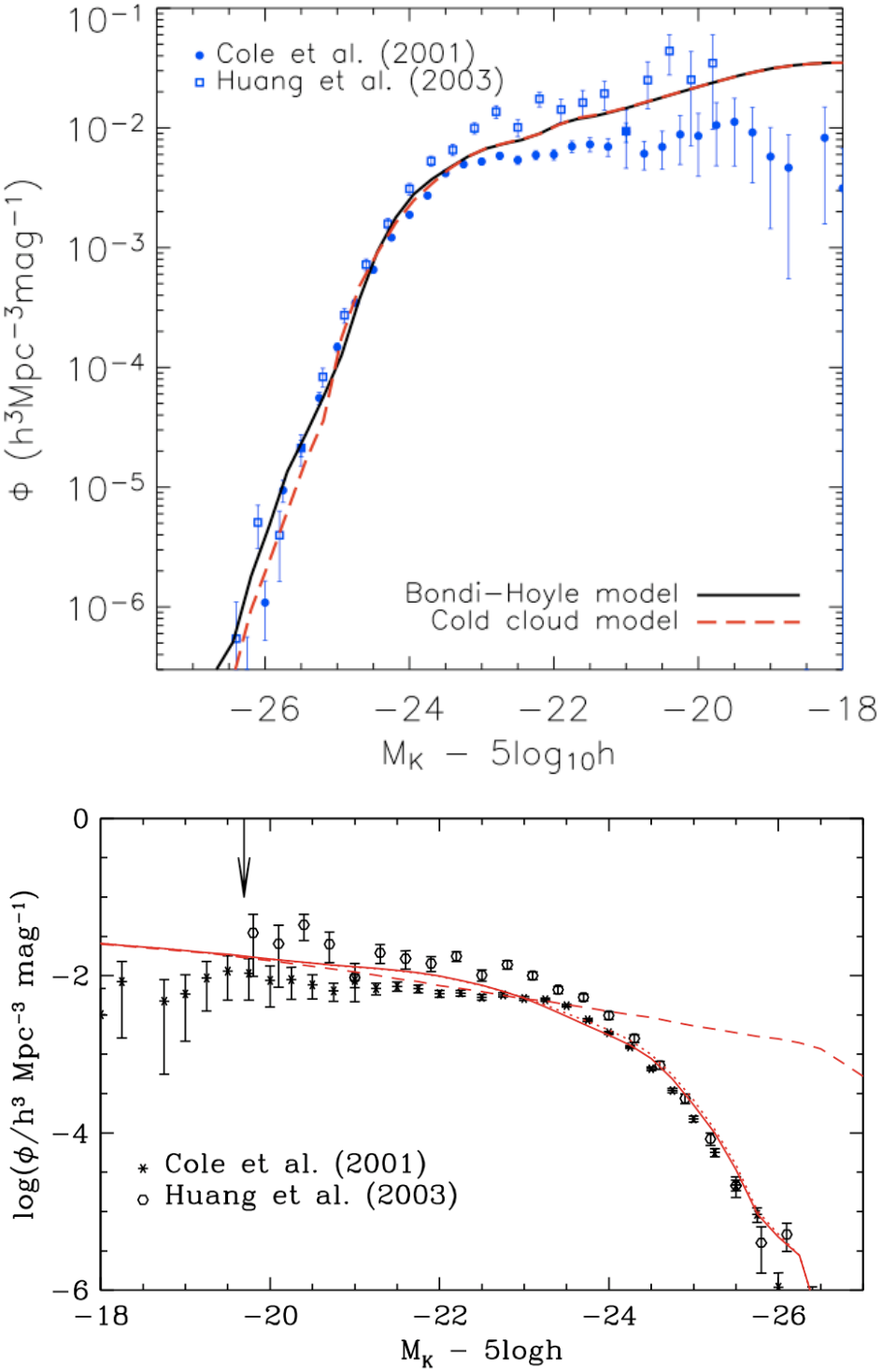

Figure 3.9: The K-band Luminosity Function from two semi-analytic models built on top of the Millennium Simulation. Croton et al. (2006) is shown on the top panel with two different AGN feedback models that leave the dwarf population unchanged and Bower et al. (2006) with and without AGN feedback on the bottom panel. If the observational data set from Huang et al. (2003) is not considered, both models show an excess of dwarf galaxies (this data set covers a smaller volume than other surveys, being subjected to larger systematic uncertainties).

Galaxy Luminosity Functions

The requirement for star formation to be inefficient in low-mass galaxies is a common problem to both sets of semi-analytic models built upon the Millennium Simulation. There is an apparent excess of dwarf galaxies that can be seen in the K-band luminosity function in both Croton et al. (2006) and Bower et al. (2006). This is clear from Fig. 3.9, if the observations of a very narrow region of the sky (and thus more subjected to systematic uncertainties) from Huang et al. (2003) are not considered.

In the top panel of Fig. 3.10 the K-band luminosity functions from De Lucia & Blaizot (2007) and our best fit model are plotted against the observational data set used to constrain the sampling. As discussed in section 3.3.2, to get a good agreement with observations, the model needs to form considerably fewer stars in low mass galaxies. This is achieved by reducing the amount of cold gas available for star-formation, by increasing the SN heating efficiency and decreasing the amount of gas reincorporated at each time step. To ensure that enough $L_\star$ galaxies are produced, the virial velocity cutoff above which SN feedback is ineffective is lowered, by raising $\epsilon_{\rm disk}$ relative to $\epsilon_{\rm halo}$ (equation 3.10).

In the bottom panel of Fig. 3.10, the best fit model seems to show poorer agreement with the $b_{\rm J}$-band than the original De Lucia & Blaizot (2007). The new fit does reproduce the number-density of dwarf galaxies accurately, but shows a large excess around $L_\star$. This is partly a reflection of the excess seen in the K-band in the same region, but has a larger magnitude. Given the good match to the colour fraction, this seems surprising and points to inconsistencies and/or uncertainties in the conversion of mass to luminosity via stellar population synthesis (see section 3.4.3) or in the different observational data sets.

Galaxy Colours

In Fig. 3.11 we show the predicted galaxy colours in our best fit model, the B-V colour-stellar mass relation in the top panel and the fraction of red over the total number of galaxies as a function of stellar mass in the bottom panel. Our best fit correctly reproduces the fraction of red galaxies by slightly increasing the number of blue galaxies around $L_\star$ compared to De Lucia & Blaizot (2007).

The colour-stellar mass relation also shows improvements, keeping the bimodality between the red and the blue galaxies, but increasing the slope of each population as suggested by observations Fig. 3.12. Nevertheless, near the lower-mass limit we impose in our study a population of red dwarfs starts to emerge, representing the highest number density peak in the red population. This is in disagreement with observations, where the

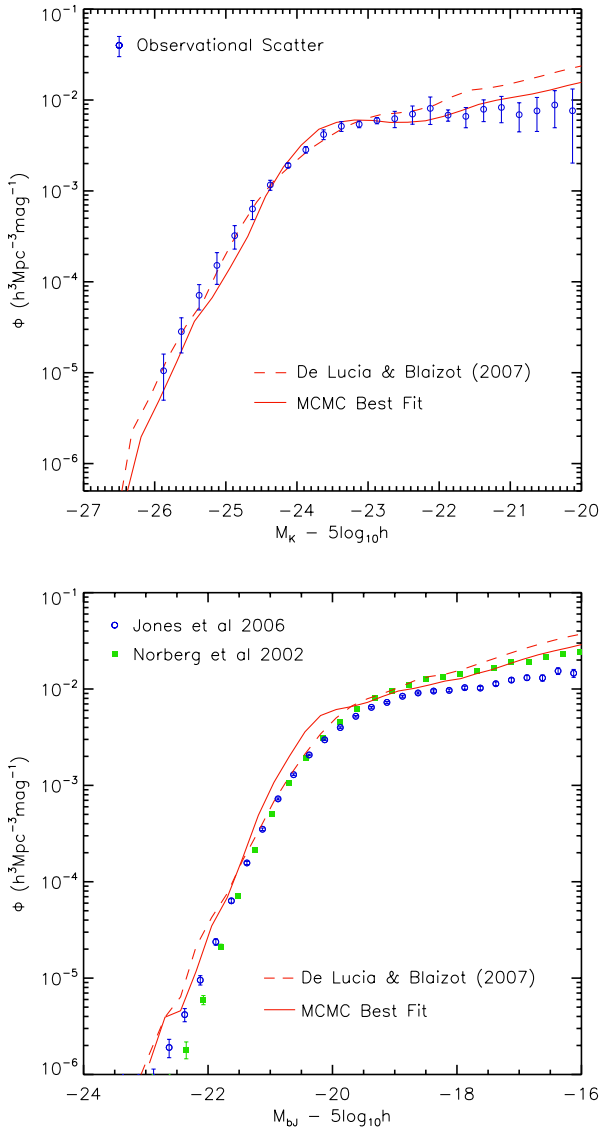

Figure 3.10: Comparison of the predicted K-band (top panel) and b_J-band (bottom panel) luminosity functions at $z = 0$ from De Lucia & Blaizot (2007) (dashed red line) and our best fit model (solid red line). On the top panel, the data points represent the observations used to constrain the luminosities of galaxies in our MCMC parameter estimation (Cole et al., 2001; Bell et al., 2003; Jones et al., 2006). In the bottom panel, the b_J-band luminosity function is compared with observations from 2DFGRS (green filled squares) and 6DFGS (blue open circles), respectively Norberg et al. (2002b) and Jones et al. (2006).

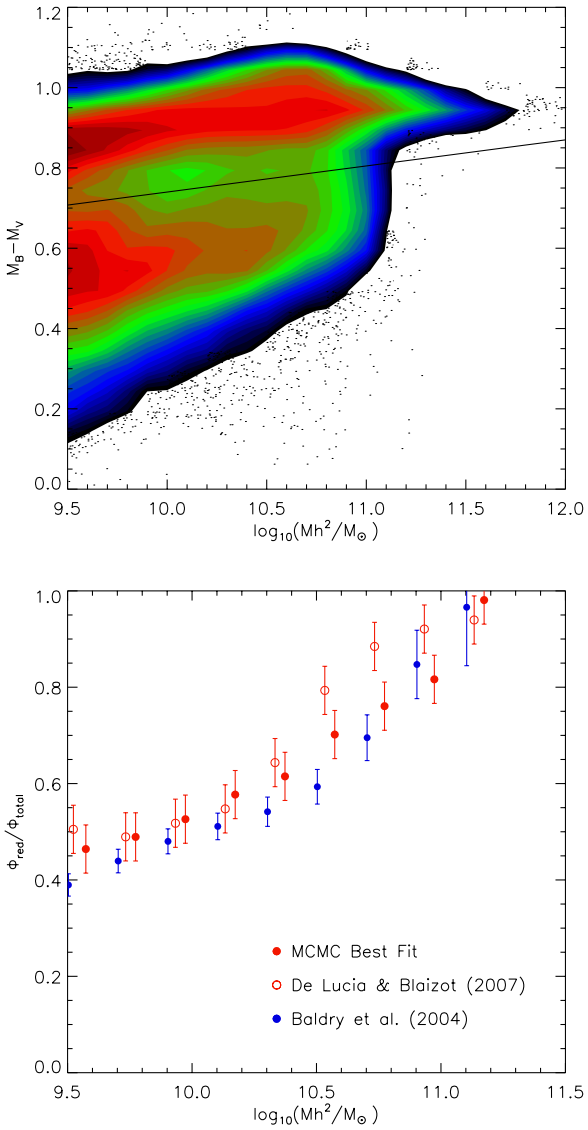

Figure 3.11: The top panel shows the B-V colour-stellar mass relation for the galaxies in our best fit model. The solid line represents the division between the red and blue populations in Weinmann et al. (2006a). The predicted fraction of red galaxies as a function of stellar mass is showed in the bottom panel. The original De Lucia & Blaizot (2007) model (open red circles) is compared with our best fit model (filled red circles) and observational data from Baldry et al. (2004) (filled blue circles).

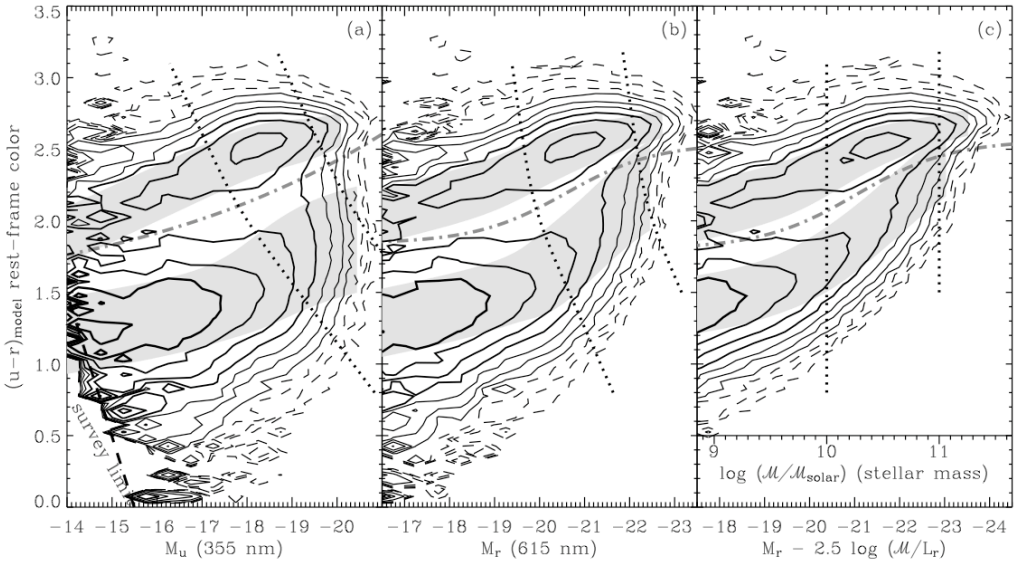

Figure 3.12: The observational colour-magnitude and colour-stellar mass relation from Baldry et al. (2006). The u-r colour is plotted versus the u-band magnitude (left panel), the r-band magnitude (middle panel) and the stellar mass (right panel). The dashed and solid lines represent density contours, while the grey regions represent the colour means and 1-sigma regions of the red and blue sequence.

majority of the red galaxies are massive, and the dwarfs are predominately blue. We address this problem, and explore possible solutions in section 3.5.

The Black Hole-Bulge Mass Relation

In Fig. 3.13 we show the black hole-bulge mass relation for our best fit model. This relation is almost unchanged from that shown in Fig. 3.5 for the original De Lucia & Blaizot (2007) parameters. There is enough freedom in the model to allow the AGN parameters to adjust themselves to recover the correct black hole masses, despite the differences in the SN parameters between De Lucia & Blaizot (2007) and our best fit.

3.4.3 The Galaxy Stellar Mass Function

As discussed in section 3.3.2, the stellar mass function is one of the most fundamental properties of a galaxy population, but it is difficult to derive accurately from observations. In Fig. 3.14 we show how our best fit model and De Lucia & Blaizot (2007) masses compare with observationally-derived stellar mass functions from Bell et al. (2003) and Baldry et al. (2008). The latter is one of the most robust mass derivations, using the

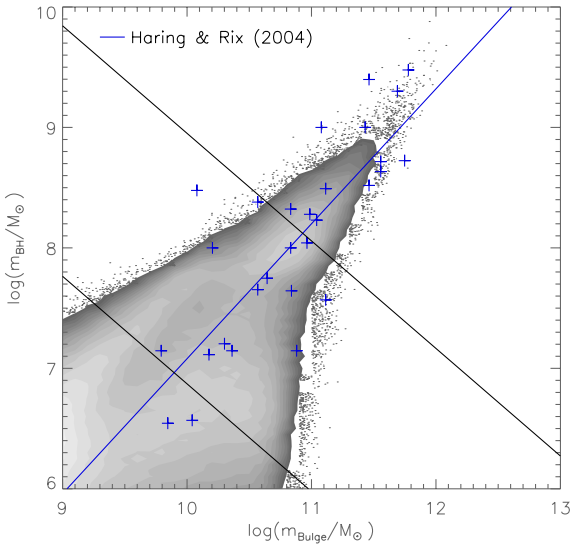

Figure 3.13: The black hole-bulge mass relation for our best fit model (solid contours). The blue crosses represent observations from Häring & Rix (2004) with the best fit to the data points given by the blue line.

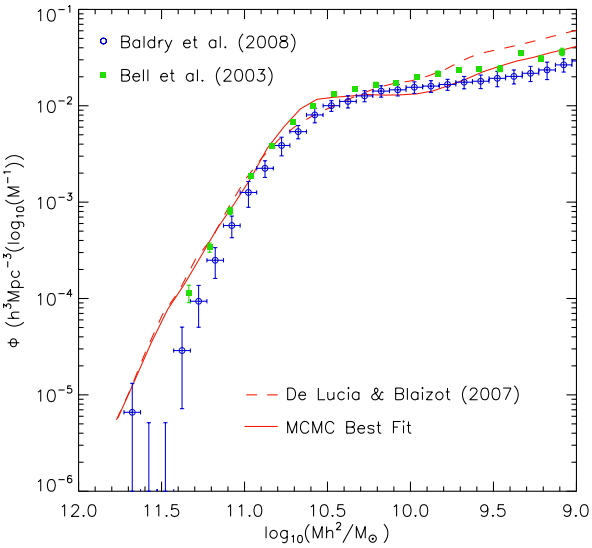

Figure 3.14: Comparison for the predicted stellar mass function at z=0 from De Lucia & Blaizot (2007) (dashed red line) and our best fit model (solid red line) with observations from Baldry et al. (2008) (blue open circles) and Bell et al. (2003)(green filled squares).

New York University Value-Added Galaxy Catalogue that combines 4 different methods for determining galaxy masses from SDSS data. The error bars in the figure span the maximum and minimum mass estimates from that analysis.

After all the data sets are converted into the same IMF (that of Chabrier, 2003), the comparison between our best fit model and the masses derived from Bell et al. (2003) in Fig. 3.14 shows the same behaviour as the K-band luminosity function. With our more effective supernova feedback the excess of dwarf galaxies largely disappears, but there is a slight excess of $L_\star$ galaxies. Small differences might arise when comparing both the k-band and stellar mass functions from the model and a specific observational data set, even though similar stellar population synthesis models were used. This is because, to convert stellar mass into luminosity, one should have knowledge about the age and metallicity of the galaxy stellar population. These quantities are directly available in the model, but in observations they are difficult to derive and are subject to large uncertainties. This is mainly due to the fact that age and metallicity are degenerate in some photometric properties, with for example high metallicities and older populations both producing redder colours (Worthey et al., 1994; Ferreras et al., 1999).

Also shown in Fig. 3.14 is a comparison of the predicted masses with data from Baldry et al. (2008). A systematic difference between the model and the data is evident, with the former predicting a much larger number of galaxies on and above $L_\star$. While the horizontal error bars plotted in Fig. 3.14 for Baldry et al. (2008) reflect only the bin size, the authors refer to differences as large as 0.15 dex in mass estimates from the different methods. Other recent works (Maraston, 2005; Conroy et al., 2008) point to even larger errors of up to 0.3 dex that may result from imprecise modelling of key phases of stellar evolution. If these uncertainties are assumed to be symmetric in the x-axis ($M_\star \pm 0.15$) then our best fit and observations from Baldry et al. (2008) would be in extremely good agreement throughout the whole mass range.

In order to fully account for these uncertainties one could convolve the derived error bars from stellar population assumptions with the theoretical mass function. We postpone this method to future work, if this analysis of observational uncertainties becomes widely used, since now it would restrict the comparison to a single observational mass function (increasing the potential effects from systematic uncertainties).

The differences between data sets highlight the need for caution when galaxy formation models are compared with observations. In principle one should expect the properties and allowed parameter ranges to change if either the stellar population synthesis or the dust

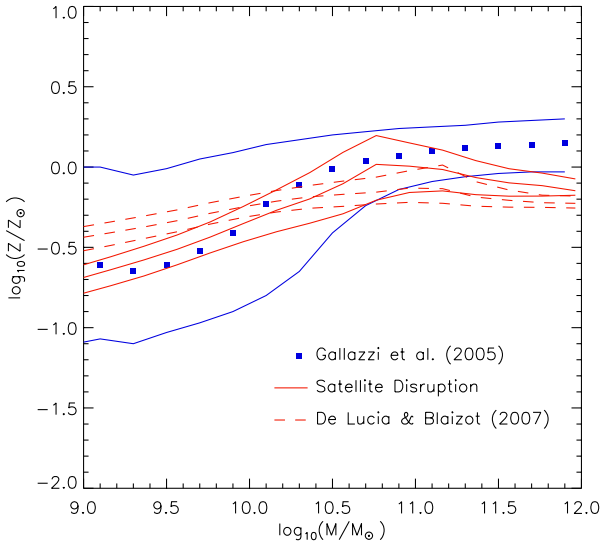

Figure 3.15: Comparison between the metallicity of stars in our best fit model (solid red lines), in De Lucia & Blaizot (2007) (dashed red lines) and in observations from Gallazzi et al. (2005) (blue squares and lines). For all the data sets, the central line represents the median value of metallicity in each mass bin (the blue squares for the observational data), while the upper and lower lines represent the 16th and 86th percentiles of the distribution.

model need to be readjusted. In this paper we have chosen to fix these so as to focus our study on the parameters controlling the most basic properties of the semi-analytic model: star formation and feedback.

3.4.4 The Metallicity of Stars

Considering the changes introduced in the treatment of SN feedback it is an important test to verify the new model predictions for the distribution of metals in stars. As explained in section 2.8, the metals follow the gas routes in the model and changes in the amount of gas being reheated, ejected and reincorporated will affect the relative metallicity of stars and of the the cold and hot gas phases.

As shown in Fig. 3.15, our model significantly improves the agreement between semi-analytic predictions and observations. Our increased SN feedback efficiency, takes more metals to the gas phases, decreasing the metallicity of stars for small galaxies (the ones affected by this form of energy).

An interesting difference between theory and data is the scatter of this relation, with observations covering a wider range of metallicities for all mass bins. This discrepancy

can be caused by two factors. On the one hand the observational scatter can be virtual, reflecting not an intrinsic scatter in the relation but observational uncertainties. On the other hand, more robust observations can prove the scatter to be real, requiring a change in the physics of the model. In that case, a time dependent cooling function would have the desired effect, producing a wider ratio of cold to hot gas fractions for a given stellar mass, and hence a wider range of metallicities.

3.5 Discussion

Since they were introduced as a technique to understand galaxy formation (White & Rees, 1978; White & Frenk, 1991; Lacey & Silk, 1991; Cole, 1991), semi-analytic models have always lacked a proper statistical analysis of the allowed range of their free parameters and a consistent way to test the goodness of the fits produced. Recent improvements introduced in these recipes have opened this possibility by significantly improving model predictions in comparison to the observables that define a galaxy population.

In this way, and in order to overcome the weakness just mentioned, we have implemented a Monte Carlo Markov Chain parameter estimation technique into the Munich semi-analytic model (De Lucia & Blaizot (2007)), to obtain the best values and confidence limits for the 6 free parameters in the model responsible for shaping the stellar mass function and the colours of galaxies. Comparing the model with three different observational constraints separately: the combined K-band luminosity function from Cole et al. (2001); Bell et al. (2003); Jones et al. (2006), galaxy colours from Baldry et al. (2004) and the black hole-bulge mass relation from Häring & Rix (2004), we are able to identify which particular parameters (and hence which galaxy formation processes) are responsible for each individual property and which show correlations and degeneracies.

Combining the three observational tests, we are able to fully constrain the model parameters, obtaining a best fit and confidence limits within the very limited region of acceptable likelihood. Our best fit model is given by: $\alpha_{\rm SF} = 0.039^{+0.091}_{-0.019}$, $k_{\rm AGN} = (5.0^{+6.0}_{-2.6}) \times 10^{-6}$, $f_{\rm BH} = 0.032^{+0.083}_{-0.018}$, $\epsilon_{\rm disk} = 10.28^{+14.09}_{-5.85}$, $\epsilon_{\rm halo} = 0.53^{+0.64}_{-0.27}$ and $\gamma_{\rm ej} = 0.42^{+0.37}_{-0.34}$). As shown in table 3.2, all the parameters in the original model, except the supernova reheating efficiency, fall within our 2-σ confidence limits. Our best fit maintains the values for the star formation efficiency and for the AGN quasar mode parameters, while increasing the SN gas reheating and ejection and decreasing the AGN radio mode and gas reincorporation efficiencies. For our preferred set of parameters the model has a likelihood of $\pi(x_i) = L_{\rm (Mass)} \times L_{\rm (Colour)} \times L_{\rm (BH-Bulge)} = 0.037$. This value means that the best fit

solution is incompatible with the three combined observations at the 2-σ level.

In the following chapters (4 and 5) we will investigate, using the statistical tools we have implemented in the semi-analytic recipe, if the introduction of new physics is justified and if it helps increasing the model likelihood against the same observational data sets. Moreover, the MCMC techniques will allow us to understand how new ingredients included in the model affect the already present physics of star formation, feedback, black hole growth, etc. This is possible since the correlations between the parameters, arising from the sampling, are a direct probe of the impact of the different semi-analytic physics on the predicted galaxy properties.

3.5.1 Future Improvements to Semi-Analytic Modelling

The ΛCDM Cosmology

In this work, we have used the Millennium Simulation which adopts a ΛCDM cosmology. It is possible that the Universe may be better described by an alternative cosmology with fewer low-mass halos. However, our purpose here is to try to find an astrophysical solution that is compatible with ΛCDM.

Black Hole Growth Model

As discussed in previous chapters, observational uncertainties, principally that associated with stellar population synthesis and dust modelling, make it premature to conclude that the De Lucia & Blaizot (2007) formalism is ruled out: shifting the observed black-hole/bulge mass ratio by 0.15 dex raises the best fit likelihood to 0.07, which is marginally acceptable. Nevertheless, the apparent incompatibility between the black hole-bulge mass relation and the other constraints indicates that the black hole growth treatment in the model might be too simplistic, in particular by assuming that there is no feedback from the quasar mode, when it seems to be required to reproduce the X-ray luminosity function of halos (Bower et al., 2008; Short & Thomas, 2008). As discussed below, some additional recipes might also need to be included for the model to better reproduce observational luminosities and colours, which could in principle increase the likelihood of the best fit model.

The Supernova Feedback Efficiency

We produce a K-band luminosity function for our best parameter values that improves the agreement with observations at the low-luminosity end. This is achieved by taking

a higher heating efficiency from SN and a lower reincorporation rate of gas ejected from the halo. This reduces the amount of cold gas available to form stars, avoiding the excess of faint galaxies in the original recipe. A more effective SN feedback has been proposed in the past. For example, Bertone et al. (2007) studied a wind model that improved model predictions for the number density of dwarfs for both the mass and luminosity function and also for the distribution of metals. However, the high value of ejection that is required by our model seems to be unrealistic when compared with observations (Martin, 1999). This indicates that additional processes such as the disruption of satellites through tidal effects might need to be included (Bullock et al., 2001; Taylor & Babul, 2001; Benson et al., 2002b; Monaco et al., 2006; Weinmann et al., 2006b; Murante et al., 2007; Henriques et al., 2008; Somerville et al., 2008).

For both the luminosity-function and colour constraints, the SN reheating and ejection parameters are strongly correlated, which we interpret as an upper virial velocity limit of $140\,\mathrm{km\,s^{-1}}$ for galaxies that can eject mass via SN heating. Since we need to assume a stronger SN feedback to decrease the faint end of the K-band luminosity function, this relatively low value assures that our SN feedback stops being effective for galaxies with masses above $\mathrm{M}_\star \approx 10^{10.0}\,\mathrm{M}_\odot$. This is the only way to ensure that enough stars will form in brighter galaxies and also produces more blue galaxies around $\mathrm{L}_\star$ than the original De Lucia & Blaizot (2007) parameters.

Significant correlations exist between the three parameters governing SN feedback, ϵ_{disk}, ϵ_{halo} and γ_{ej}, even in the combined analysis. This suggests that the model could be rewritten with one or two fewer free parameters.

The Population of Dwarf Galaxies

The model with the original De Lucia & Blaizot (2007) parameters correctly predicts the bimodality in the colour-stellar mass relation, however, it has difficulties in matching the exact number of blue and red sequence galaxies. Our best fit model correctly predicts the relative fraction of galaxies in each colour population, nevertheless, the early cutoff on SN feedback leads to an excess of galaxies with masses between $10^{10.5}$ and $10^{11.0}$ $\mathrm{M}_\odot$. Furthermore, as the original model, it shows a large population of small red galaxies in the $B-V$ colour-stellar mass plot in contradiction with observations.

The problems with low-mass galaxy colours in semi-analytic models have been identified in the past, particularly the excess of red dwarfs (Croton et al., 2006; Baldry et al., 2006). Possible solutions might include the delayed stripping of gas from satellites after

their dark matter halo is disrupted (allowing them to cool gas, form stars and stay blue for longer Font et al. 2008). Or again, tidal disruption of dwarfs, which would affect mostly red, satellite galaxies. This would move them to even lower masses, below $10^{9.0}\,M_{\odot}$ (where an upturn in the stellar mass function is seen) and produce intra-cluster light (ICL) (Weinmann et al., 2006b; Henriques et al., 2008; Somerville et al., 2008).

In chapter 4 we will investigate if the disruption of satellite galaxies might be part of the solution to the problems identified here. We will search for evidence supporting this phenomenon in observations and infer how it might affect model predictions. Finally in chapter 5 we will implement this new physical recipe in the semi-analytic model and by means of MCMC sampling verify if its introduction is justified. This is to say, if it improves the model likelihood significantly, when the predictions are compared with the chosen observational constraints.

The purpose of the work described in this chapter is to show that MCMC parameter estimation techniques, adapted from those used in cosmology, can be used to map out likelihood contours in the parameter space of semi-analytic models of galaxy formation. For this particular analysis we chose the formalism of De Lucia & Blaizot (2007), but the same method could equally be applied to other models.

Chapter 4

The Population of Dwarf Galaxies

"There are only two ways of always being right. Say nothing or change opinion."

Ancient Quote

In the previous chapter, we concluded that in current semi-analytic models of galaxy formation and evolution there is an excess of dwarf galaxies, a clear feature in both the stellar mass and the luminosity functions. With our MCMC sampling we are able to find a region in parameter space that brings the number density of these objects into agreement with observations, however this is achieved by assuming an extremely effective SN feedback in order to quench star formation in the dwarf population. Observations of this phenomenon suggest that such a strong feedback might be implausible (Martin, 1999), pointing out that the model might be too simplistic and other physical processes might need to be included in order to correctly predict the formation and evolution of dwarf galaxies.

There is a growing body of evidence showing that this might indeed be the case. From observations, high resolution numerical simulations and other semi-analytic works, it seems that the disruption of stellar material in satellite galaxies merging with their central companion, plays a crucial role in determining the properties of dwarfs. If such a process is included, the dwarf galaxies will lose material in the merging process, reducing their overall mass and being shifted to even smaller mass bins (where an up-turn is seen in observations). This would decrease the slope of the faint end of the luminosity function, eliminating the need for such an effective SN feedback. In this chapter we look for evidence of this process and investigate the magnitude of the effects it might have in our semi-analytic model.

4.1 Disruption of Satellite Galaxies

The existence of a diffuse population of intra-cluster stars was first proposed by Zwicky (1951) and has since been detected unambiguously. Individual intra-cluster AGB stars (Durrell et al., 2002), planetary nebulae (Arnaboldi et al. 1996, Feldmeier et al. 2003, Arnaboldi et al. 2004, Feldmeier et al. 2004a), novae and supernovae (Gal-Yam et al. 2003, Neill et al. 2005) have been resolved in nearby clusters and trace an unbound population of red, old stars orbiting freely in the cluster potential (Krick et al., 2006).

The light associated with intra-cluster stars, or diffuse intra-cluster light, can contribute between 10 and 30 per cent of the optical emission of rich galaxy groups and clusters (Bernstein et al. 1995; Gonzalez et al. 2000; Feldmeier et al. 2002; Feldmeier et al. 2004b; Gonzalez et al. 2005; Zibetti et al. 2005). In the core of massive clusters like Coma, ICL emission not associated with the central giant elliptical galaxy can account for up to 50 per cent of the total optical light (Bernstein et al., 1995).

Rather than having formed in the intra-cluster medium, intra-cluster stars are believed to be the remnants of disrupted galaxies. Gas-dynamical simulations generally agree that the bulk of the ICL is emitted by stars that have been continually stripped from member galaxies throughout the lifetime of a cluster, or have been ejected into intergalactic space by merging galaxy groups (Moore et al. 1996; Napolitano et al. 2003; Murante et al. 2004; Willman et al. 2004; Sommer-Larsen et al. 2005; Monaco et al. 2006; Murante et al. 2007). Several mechanisms can contribute to disrupting galaxies, the most efficient ones being tidal stripping by the gravitational forces of the cluster halo (Merritt, 1984) and high-speed galaxy encounters (Richstone, 1976). Smoothed particle hydrodynamic simulations by Murante et al. (2007) show that 60 to 90 per cent of the population of intra-cluster stars has been generated at $z < 1$ by relaxation processes during galaxy mergers, with a minor fraction arising from tidal stripping. In groups, low speed galaxy encounters and dynamical heating by galaxy scattering with halo substructures may enhance the removal of stars by tidal stripping once a group merges with a larger cluster (Gnedin 2003; Mihos 2004; Rudick et al. 2006).

Low surface brightness features have been identified in the Coma and Centaurus clusters (Gregg & West 1998; Trentham & Mobasher 1998; Feldmeier et al. 2002), indicating the presence of dynamically-young tidal structures produced by the disruption of infalling galaxies. These features carry information about the orbit of the parent galaxy and can be used to trace the cluster accretion history and its past dynamical interactions (Calcáneo-Roldán et al., 2000). Another indication comes from the number density

of satellites in groups. Faltenbacher & Mathews (2005) show that the projected number density profile of dwarf galaxies in NGC 5044 can only be explained by assuming that a significant amount of mass in satellite galaxies is tidally disrupted.

Further compelling evidence for galaxy disruption comes from the population of ultra compact dwarf galaxies in clusters (UCDs, Hilker et al. 1999; Drinkwater et al. 2000; Hilker et al. 2007), which is believed to form when the low surface density disk component of a dwarf galaxy is tidally-stripped away. Indeed, UCDs might share a common origin with intra-cluster stars (Zibetti & White 2004).

High-resolution numerical simulations suggest that galaxies may disperse a non-negligible fraction of their stellar component into the intra-cluster medium during merging events (Monaco et al. 2006; Murante et al. 2007; Conroy et al. 2007). Monaco et al. (2006) find that the small degree of evolution seen at $z < 1$ for the high-mass end of the stellar mass function can be accounted for if merging galaxies eject at least 20 per cent of their stars. The combined analysis of simulation-based models and observations of ICL by Conroy et al. (2007) favours models in which as much as 80 per cent of stars are stripped into the intra-cluster medium from satellite galaxies whose dark matter substructure has been disrupted.

If, as simulations suggest, intra-cluster stars have been stripped from galaxies from all mass ranges (Bullock et al. 2001; Taylor & Babul 2001; Monaco et al. 2006; Murante et al. 2007), it is likely that the faint end of the luminosity and stellar mass functions are affected as strongly as the bright end. However, while several works have investigated the effect of galaxy disruption on the evolution of massive galaxies, there are only a few suggestions in the literature that pinpoint the effect of disruption on the abundance of dwarfs (Benson et al., 2002b; Zibetti & White, 2004; Zibetti et al., 2005; Somerville et al., 2008).

4.2 The model

In this work, we use simulated galaxy catalogues, produced by the De Lucia & Blaizot (2007) semi-analytic model of galaxy formation to investigate how galaxy disruption affects the abundance of dwarf galaxies by considering its effects on the faint end of the stellar mass and luminosity functions. In particular, we focus on the abundance of dwarf red galaxies, which is considerably over-predicted by current galaxy formation models (Croton et al., 2006). For now, we will not implement the process directly into the semi-analytic recipe, instead, we study its potential impact by looking at some specific pop-

ulations of galaxies in the model. In the next chapter we will introduce this physical phenomenon into the model and by means of MCMC sampling verify its impact.

As explained in Section 2.6, the semi-analytic model of De Lucia & Blaizot (2007) makes a distinction between cluster galaxies associated with dark matter substructures and those whose substructure has completely merged with the parent halo. For this reason, it is an ideal instrument for investigating the origin of interstellar stars. The substructures of dark matter halos can be identified by the algorithm SUBFIND (Springel et al., 2001). As a consequence, galaxies in clusters can be of three different types: central galaxies, satellites of "type 1" and satellites of "type 2". Satellites of type 1 are associated with dark matter substructures, which usually are recently-merged halos. Satellites of type 2 are instead galaxies whose dark matter halo has completely merged with a bigger halo and are not associated with a substructure. In the model, only type 2 galaxies merge with the halo central galaxy.

In this work, presented in Henriques et al. (2008), we include galaxy disruption in the De Lucia & Blaizot (2007) model *a posteriori* and investigate its effects at $z = 0$. To do this, we assume that type 2 galaxies have been completely stripped of their stars and that these stars represent the population of intra-cluster stars that produces the ICL. Type 2 galaxies therefore do not contribute to galaxy counts at redshift zero. These assumptions are motivated by the fact that type 2 galaxies in the simulation usually fall into a larger structure at $z > 1$ and are not associated with a dark matter substructure. This implies that they have had enough time to experience a number of low and high speed encounters with other galaxies during their lifetime, and that most of their stars might have been stripped away when their associated dark matter substructure was disrupted.

Although this simple model allows us to investigate the effect of galaxy disruption on the abundance of dwarfs, it does not implement the disruption self-consistently within the semi-analytic model. Since we apply our assumption *a posteriori*, we do not modify the evolution of type 2 galaxies at $z > 0$. Instead, we consider as disrupted only type 2 galaxies that have not yet merged at $z = 0$.

Our assumption of complete galaxy disruption, if consistently implemented, would eliminate merging from the model, because in the Munich semi-analytic model only type 2 galaxies can merge with central galaxies. Moreover, the definition of galaxy type that we adopt is dependent on the resolution of the dark matter simulation. An increase in resolution would in principle mean that type 1 halos survive longer before being disrupted. In addition, disruption is a gradual process and one might expect most type 1 galaxies

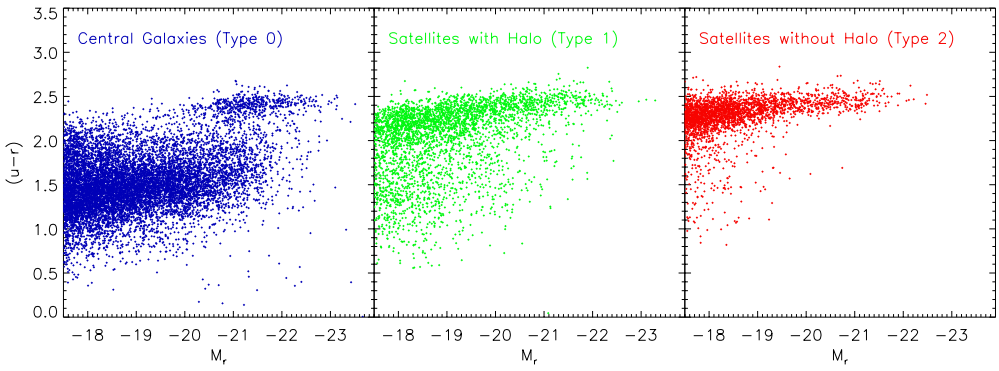

Figure 4.1: The $u-r$ colour distribution of galaxies as a function of $M_{\rm r}$ for the canonical model. Galaxies have been colour-coded by type: central galaxies (blue, left panel), type 1 galaxies (green, central panel) and type 2 galaxies (red, right panel).

to be partially stripped, while some type 2 galaxies retain a compact core. Finally, the softening length of the dark matter simulation is bigger than most galaxies, meaning that despite having the dark matter halo stripped some galaxies might remain intact.

Accordingly, this work represents a qualitative indication of the importance of disruption rather than a detailed physical model of these processes, which will be described in the next chapter. A self-consistent treatment of disruption should for example, include partial disruption of the merging galaxies, as assumed by Monaco et al. (2006), or follow the forces acting on satellites, to define a disruption radius outside which the galaxy mass will be lost (Bullock et al. 2001; Taylor & Babul 2001; Benson et al. 2002b).

4.3 Results

In this Section we present our results for the colour-magnitude diagram (Subsection 4.3.1) and for the galaxy stellar mass and $b_{\rm J}$-band luminosity functions (Subsection 4.3.2). Finally, Subsection 4.3.3 shows our predictions for the fraction of interstellar light produced by disrupted galaxies.

4.3.1 The colour-magnitude diagram

Colour-magnitude diagrams indicate the existence of two distinct populations of galaxies, namely a population of blue, star-forming galaxies and a population of red galaxies with no significant star formation activity.

Fig. 4.1 shows the $u-r$ colour distribution of galaxies of different types in the original model, as a function of $M_{\rm r}$. The faint reddest galaxies (in red, right panel) are predomin-

antly type 2 galaxies. Their colour and the amount of light produced by their stars agree well with the observed properties of the ICL. Type 1 galaxies have somewhat bluer colours than type 2 galaxies, because they might not have yet exhausted their reservoir of gas and may still be forming stars. However, as can be seen in the middle panel of Fig. 4.1, a large fraction of type 1 galaxies accumulates along the red sequence, once their reservoir of gas is extinguished. Most central galaxies are blue (in blue, left panel), because they can continually accrete gas and form stars. The exceptions are very massive galaxies, in which star formation is suppressed by AGN feedback (Croton et al. 2006; Bower et al. 2006) and a significant fraction of dwarf galaxies. These last ones mostly represent isolated galaxies which already consumed all their gas and accreted all their satellites.

In Fig. 4.2 we directly compare the colour-magnitude distribution for the original model (top panel) and for the disruption model (bottom panel) with the observed distribution in $u-r$ of Baldry et al. (2004). In the original model, the blue population is modelled with a sufficient degree of accuracy. On the other hand, the red population considerably differs from the observed one. Firstly, the colour of bright, red galaxies is underestimated by about 0.2 magnitudes. This is likely due to the underestimate of the metallicity of massive galaxies in the De Lucia & Blaizot (2007) model, as shown by Bertone et al. (2007). In fact, both the Bertone et al. (2007) model and that of Bower et al. (2006) do predict higher metallicities and redder colours for the brightest galaxies. This may also explain the flat distribution for the population of red galaxies in the top panel of Fig. 4.2, in contrast with the sloping behaviour seen in observations (Baldry et al. 2004; Baldry et al. 2006) and predicted by other models (Bower et al., 2006; Bertone et al., 2007).

A more serious problem, however, is that the original model vastly over-predicts the abundance of faint red galaxies. The disruption model, whilst not completely solving the problem, does produce a distribution of red galaxies with a distinct red peak at $M_{\rm r} \approx -21$ and a decreasing rather than flat distribution towards fainter magnitudes. This can be seen in Fig. 4.3, where the colour distribution of galaxies with absolute magnitudes in the range $M_{\rm r} = -18.25 \pm 0.5$, for the original and the disruption models, are compared to the observational data of Baldry et al. (2004). In this magnitude bin, the disruption model predicts a considerably smaller number of red galaxies, in better agreement with the observations. This is because the reddest dwarf galaxies are type 2 galaxies, which we assume become disrupted once their dark matter substructure has been lost. This clearly indicates that galaxy disruption might play a role in shaping the faint side of colour-magnitude distributions.

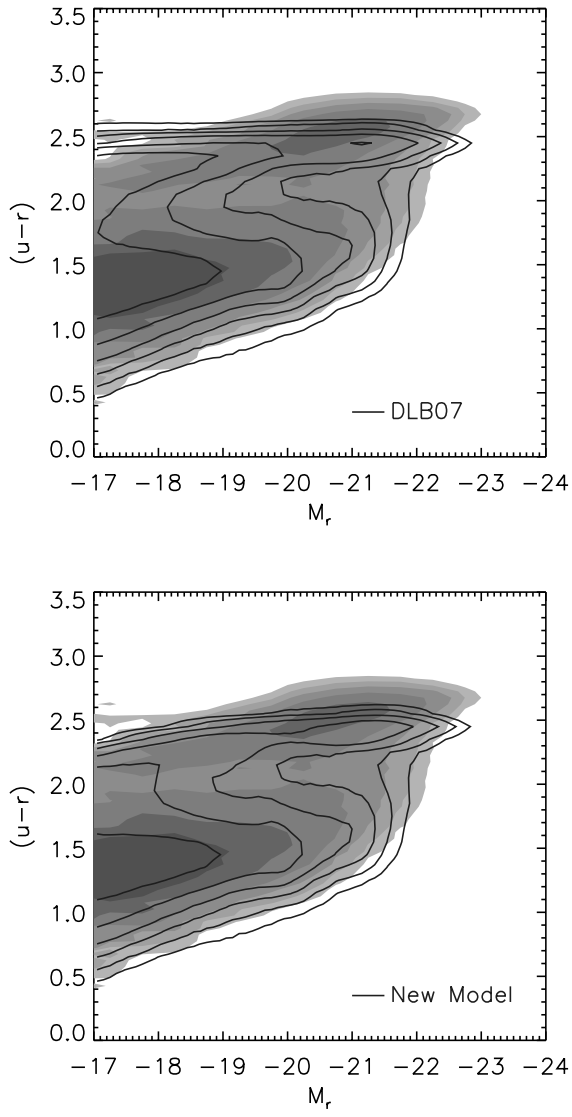

Figure 4.2: Comparison of the colour-magnitude relation for galaxies in the original model (upper panel) and in the disruption model (lower panel). The shaded contours are for the observed distribution of Baldry et al. (2004). The contour scale is logarithmic, with 4 divisions per dex.

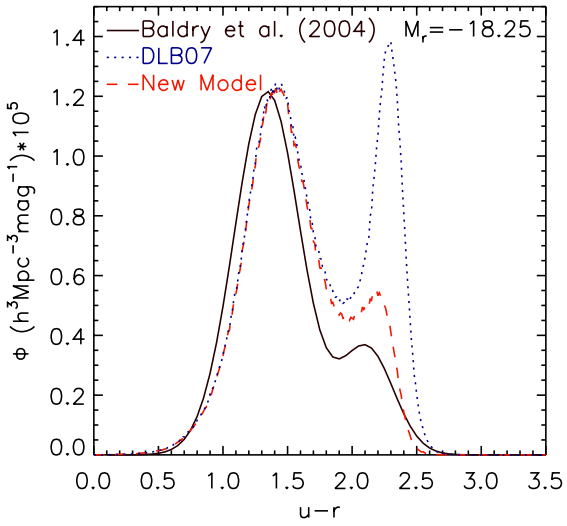

Figure 4.3: The u-r colour distribution for an absolute magnitude bin of width 0.5 centred at $M_{\rm r}$=-18.25. The predictions for the disruption and original models (red dashed and blue dotted lines respectively) are compared with observational data from Baldry et al. (2004) (black solid line).

The De Lucia & Blaizot (2007) model under predicts the fraction of red galaxies in low-density environments (see e.g. Baldry et al., 2006, figure 15). Our model preferentially disrupts red galaxies in clusters and so does not help to correct this deficiency: in fact, the predicted red fractions are reduced slightly from those shown in Baldry et al. (2006).

4.3.2 Luminosity and Stellar Mass functions

In this Section we investigate the effect of disruption on the abundance of galaxies, and in particular on the stellar mass function and on the $b_{\rm J}$-band luminosity function at $z = 0$. The top panel of Fig. 4.4 shows the stellar mass functions for the original and disruption models (dashed and solid lines respectively). The data points represent observations from Baldry et al. (2008) (blue open circles) and Bell et al. (2003)(green filled squares). The bottom panel shows the $b_{\rm J}$-band luminosity functions from the original and disruption models compared with data points from the 2 degree Field Galaxy Redshift Survey (2dFGRS, Norberg et al. 2002b) and of the 6 degree Field Galaxy Survey (6dFGS, Jones et al. 2006). In both panels, the disruption of satellite galaxies strongly affects the number density of dwarf galaxies, decreasing the slope of the low end in both functions, and giving a better agreement with the observations than the original model (for the stellar mass a slight decrease is noted in all ranges due to the fact that some of this type 2 satellites have

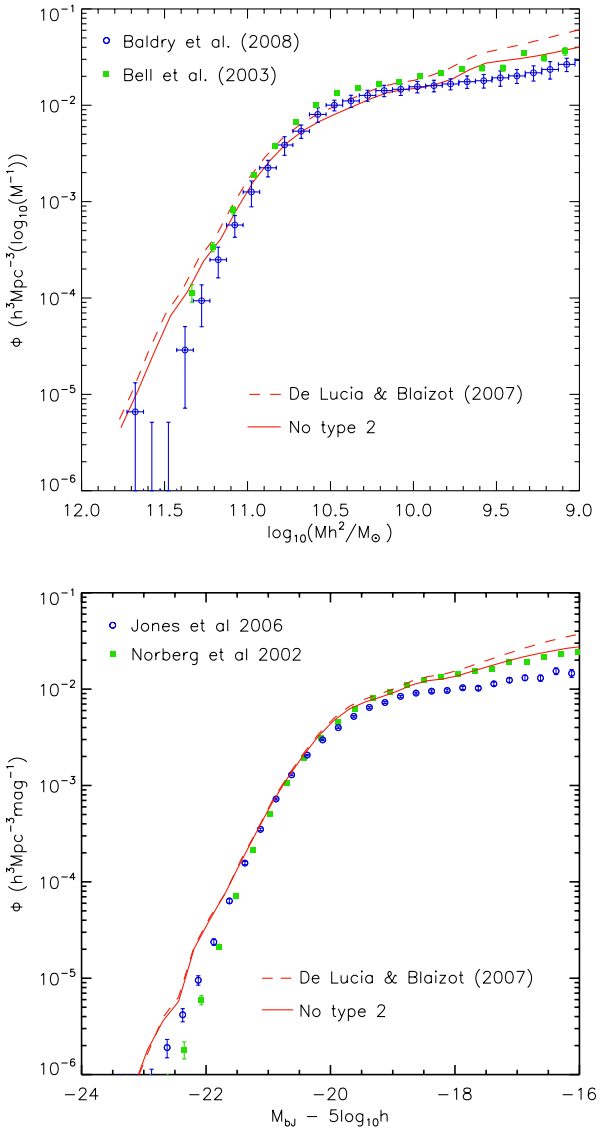

Figure 4.4: The galaxy stellar mass function and the b_J-band luminosity function at $z = 0$. In both plots, the dashed line represents the original and the solid line the disruption models. In the top panel, the predicted stellar mass function is compared with observations from Baldry et al. (2008) (blue open circles) and Bell et al. (2003)(green filled squares). Removing type 2 satellites has the effect of reducing the number density of galaxies for all masses across the plotted range. In the bottom panel the theoretical b_J band from both models is compared to the results of the 2dFGRS (Norberg et al., 2002b) and to those of the 6dFGS (Jones et al., 2006).

considerably large masses).

The disagreement between the model predictions for the number density of faint galaxies and observations has been identified in the past. Croton et al. (2006) showed that this is mainly due to an excess of early-type, red galaxies. The top panel of Fig. 4.5 illustrates this discordance. The long-dashed and the solid lines in both panels of Fig. 4.5 show the luminosity functions of late- and early-type galaxies respectively for the 2dFGRS data (Madgwick et al., 2002). The dotted and dashed lines show the predictions for late- and early-type galaxies respectively for the De Lucia & Blaizot (2007) model. The populations of late (blue) and early (red) galaxies are defined as a function of $B-V$ colour, late galaxies having $B-V<0.8$ and early galaxies $B-V>0.8$, respectively. This colour cut differs from the one used in Section 4.3.1 since in here we are not adjusting the model to fit a specific division between populations. Consequently, we need to draw an empirical line to select between red and blue theoretical galaxies. The lower panel of Fig. 4.5 shows the effect of disrupting type 2 galaxies. Whilst the luminosity function of late type galaxies is hardly affected, the reduction in the number density of faint early type galaxies is dramatic (more than an order of magnitude) and brings the model into much closer agreement with the observations. The luminosity function of early type galaxies shows a dip at $b_{\rm J}\sim-19$. However, this dip can also be seen in the luminosity function for the original model and is not caused by galaxy disruption.

4.3.3 Contribution to the ICL

Despite the uncertainty related to the difficulty in detecting very faint sources, observations suggest that diffuse intra-cluster stars contribute a substantial fraction of the optical light emitted by clusters and rich groups. In massive clusters, between 10 and 30 per cent of the optical luminosity is estimated to be diffuse ICL (Section 4.1). In Fig. 4.6 we show our results for the fraction of $B-$band luminosity contributed by type 2 galaxies, compared to the total luminosity of a cluster, which is the sum of the B luminosities of all the galaxies in the cluster, including type 2 galaxies. Results are presented for groups and clusters with $M_{\rm vir}>10^{13}h^{-1}\,{\rm M}_{\odot}$. Although there is considerable scatter in the distribution, our estimated fractions fall well within the observed range (Bernstein et al. 1995; Gonzalez et al. 2000; Feldmeier et al. 2002; Feldmeier et al. 2004b; Gonzalez et al. 2005; Zibetti et al. 2005), and agree with the predictions of other semi-analytic models where galaxy disruption is implemented self-consistently (Purcell et al., 2007). We find that the median B luminosity of type 2 galaxies accounts for about 20 per cent of the total

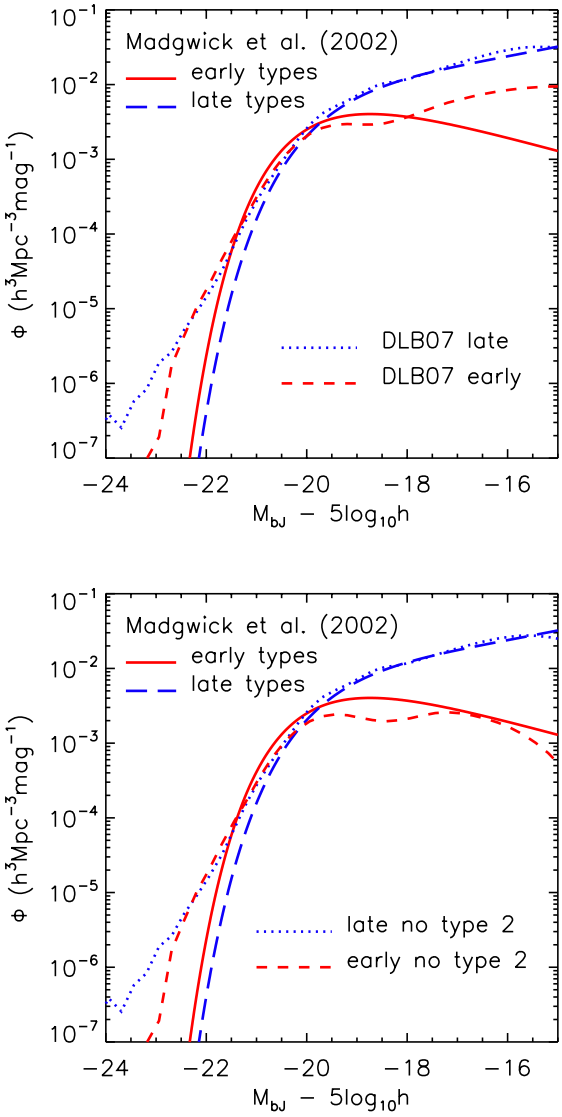

Figure 4.5: The galaxy luminosity function in b_J-band divided by colour. The upper panel shows results for the original model, the lower panel for the disruption model. In both panels the model predictions for the red and blue population (red dashed and blue dotted lines respectively) are compared with 2dFGRS data of Madgwick et al. (2002) for early- and late-type galaxies (red solid and blue long-dashed lines respectively). The relative poor fit to the bright end of this specific luminosity function is related to the new dust model implemented by De Lucia & Blaizot (2007). The blue bands are the most affected by reddening and in principle this agreement could be improved without significantly changing what is obtained for other bands.

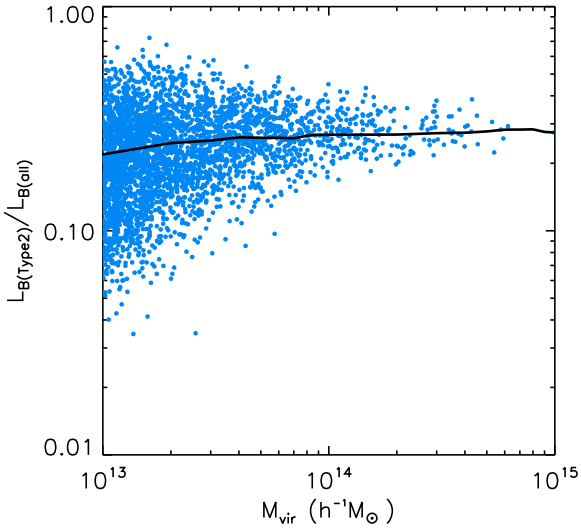

Figure 4.6: Fraction of the luminosity of type 2 galaxies over the total galaxy luminosity in the B-band as a function of virial mass for a representative sample of the total galaxy population in the disruption model. The solid line represents the median of the $L_{\mathrm{B(Type2)}}/L_{\mathrm{B(all)}}$ distribution for the full millennium volume.

luminosity for halos with $M_{\mathrm{vir}} \sim 10^{13} h^{-1}\,\mathrm{M}_{\odot}$, increasing to about 30 per cent in halos with $M_{\mathrm{vir}} = 10^{15} h^{-1}\,\mathrm{M}_{\odot}$. This is strong evidence that disruption of dwarf galaxies is not only helpful in reducing the number density of faint red galaxies but is actually required by the observations, as there is no other plausible mechanism for generating the ICL.

4.4 Discussion

In this chapter, we have considered the possibility that dwarf galaxies may become disrupted when subjected to gravitational tidal forces and repeated galaxy encounters within clusters and rich galaxy groups. For this purpose, we have introduced an *ad hoc* prescription for the disruption of galaxies in our analysis of galaxy catalogues produced by semi-analytic models of galaxy formation. Our simple prescription considers the stability of substructure within dark matter halos. The merger trees produced by the algorithm SUBFIND (Springel et al., 2001) can identify dark matter sub-halos within a larger structure until they are completely disrupted. We make the simple assumption that galaxies whose halos have been disrupted will themselves disperse, while their stars become part of the population of intra-cluster stars responsible for the observed intra-cluster light.

Despite the simplicity of this assumption, our results show a substantial improvement

over previous models and indicate that the inclusion of galaxy disruption might be indeed a necessary ingredient of galaxy formation models. Our main results can be summarised as follows:

- it suppresses the number of red dwarf galaxies, improving the model predictions for the low mass end of the galaxy stellar mass and $b_{\rm J}$-band luminosity functions;
- correspondingly, it suppresses the number density of the faint, reddest galaxies in colour-magnitude diagrams;
- it predicts values for the fraction and colour of intra-cluster light in good agreement with observational estimates for clusters and rich galaxy groups.

Our prescription to model the ICL, implemented *a posteriori* in the publicly available galaxy catalogue of De Lucia & Blaizot (2007), assumes that all type 2 galaxies that have survived merging until $z = 0$ are disrupted and contribute their stars to the population of intra-cluster stars. By doing this, the evolution of type 2 galaxies at $z > 0$ is not affected.

Although the simplicity of our model is to be valued, the assumption that halo disruption leads to galaxy disruption is very simplistic. Hydrodynamical simulations (Moore et al. 1996; Napolitano et al. 2003; Sommer-Larsen et al. 2005; Murante et al. 2007) suggest that tidal stripping of stars from the outer regions of a galaxy is a gradual process that takes several passages of the galaxy through the cluster core and that can be enhanced by previous galaxy encounters in groups. Furthermore, a galaxy infalling into a cluster might not be completely disrupted, but might conserve its densest core intact, as the existence of UCD galaxies seem to suggest.

A natural extension of the results presented here is to introduce the satellite disruption self-consistently within the semi-analytic model, as Monaco et al. (2006) and Somerville et al. (2008) have done. This would have several effects, the main ones being to limit the growth of central galaxies and to affect the abundance of dwarf galaxies. The next chapter describes how we implement this new physical recipe into De Lucia & Blaizot (2007) following the work done by Taylor & Babul (2001). Our newly developed MCMC statistical tools will allows us to gain insight on the importance of this new recipe and on the changes it introduces into the modelling of galaxy formation and evolution.

Chapter 5

Satellite Disruption

"Some men see things as they are and say why? I dream things that never were and say Why not?"

George Bernard Shaw

5.1 Introduction

In the previous chapter we introduced the motivation for including satellite disruption into semi-analytic models of galaxy formation. The present excess of dwarf galaxies in these models calls for an improvement on the physical processes that shape the distribution of these objects. The disruption of a satellite's stellar material by the tidal effects from the parent halo during mergers might indeed be part of the solution to this problem. In this chapter we describe the implementation of this new physical recipe and test it against observations using the MCMC statistical tools.

The new recipe is based on the work of Taylor & Babul (2001) and requires that we follow the radial position of satellites as they merge into central objects, computing the satellite radius at which the sum of the tidal force from the parent halo and the centrifugal force equal the self gravitational force of the satellite. Any material outside this radius at each time step is considered to be unbound and its moved from the satellite galaxy into the intra-cluster medium. Over time, this material will add up and as objects hierarchically merge together will become a significant component in massive groups and clusters, known as the intra-cluster light.

5.1.1 Dynamical Friction

As explained in section 2.6, the original model computes the merging time of satellites by setting up a "merging clock", whenever a satellite loses its dark matter halo. This is calculated using the Chandrasekhar (1943) formula for the dynamical friction force acting on the satellite. After that time the model simply assumes that the satellite and central galaxies have merged. For our implementation we use the same equation, but we now record the orbital radius of the satellite at each time step as it falls into the centre. In this way, at each time step, we can compute the forces acting on each satellite at that specific radius and determine the amount of stellar material that becomes unbound.

We note that the drag force acting on satellites and causing them to merge with central objects depends on their mass. Because of this, despite us using the same equation for the dynamical friction as the original De Lucia & Blaizot (2007), the implementation of satellite mass loss will change the predicted merging times. As satellites lose their stellar material, the drag force they experience will decrease, causing them to survive longer before being accreted by the central galaxy.

5.1.2 Tidal Disruption

The mass loss from satellites occurs through the action of tidal forces. Assuming a slowly varying system (a satellite in a circular orbit) with a spherically symmetric mass distribution, material outside the tidal radius will be stripped from the satellite. This radius can be identified as the distance from the satellite centre at which the radial forces acting on it cancel (King, 1962; Binney & Tremaine, 1987). These forces are the gravitational binding force of the satellite, the tidal force from the central halo and the centrifugal force and following King (1962) the disruption radius $R_{\rm t}$ will be given by:

$$R_t \approx \left(\frac{\mathrm{G}\, m_{\rm sat}}{\omega_{\rm sat}^2 - \mathrm{d}^2\phi/\mathrm{dr}^2} \right)^{1/3}, \tag{5.1}$$

where $m_{\rm sat}$ is the mass of the satellite, ω is its orbital angular velocity and ϕ represents the potential of the central object.

The second derivative of the potential from the central object, $\mathrm{d}^2\phi/\mathrm{dr}^2$, is given by

$$\frac{\mathrm{d}^2\phi}{\mathrm{dr}^2} = \frac{\mathrm{d}}{\mathrm{dr}} \left(\frac{\mathrm{G}M(<r)}{r^2} \right), \tag{5.2}$$

where r represents the radial distance from the central galaxy to the satellite and $M(<r)$ the mass distribution of the central object within that radius.

Equation 5.1 can then be rewritten as:

$$R_t \approx \left(\frac{\mathrm{G}\, m_{\mathrm{sat}}}{\omega_{\mathrm{sat}}^2 - 4\pi\rho G + \frac{2MG}{r^3}} \right)^{1/3}, \tag{5.3}$$

where ρ and M represent respectively the density and mass of the central halo. Taking the isothermal sphere approximation ($M = 2\sigma_{\mathrm{halo}}^2 r/\mathrm{G}$), the disruption radius becomes:

$$R_t \approx \left(\frac{\mathrm{G}\, m_{\mathrm{sat}}}{\omega_{\mathrm{sat}}^2 + \frac{2\sigma_{\mathrm{halo}}^2}{r^2}} \right)^{1/3}, \tag{5.4}$$

where σ_{halo} represents the velocity dispersion of the central halo. Using the same approximation for the distribution of mass in the satellite galaxy, R_t becomes,

$$R_t \approx \left(\frac{2\sigma_{\mathrm{sat}}^2 R_t}{\omega_{\mathrm{sat}}^2 + \frac{2\sigma_{\mathrm{halo}}^2}{r^2}} \right)^{1/3}, \tag{5.5}$$

where σ_{sat} is the velocity dispersion of the satellite galaxy, which we approximate by the velocity dispersion of the satellite halo just before it becomes stripped.

From the assumption that satellites follow circular orbits we get $\omega_{\mathrm{sat}}^2 = \mathrm{G}M/r^3$ and

$$R_t \approx \left(\frac{\sigma_{\mathrm{sat}}^2 r^2}{\frac{\mathrm{G}M}{2r} + \sigma_{\mathrm{halo}}^2} \right)^{1/2}. \tag{5.6}$$

The final expression for the disruption radius will therefore be:

$$R_t \approx \frac{1}{\sqrt{2}} \frac{\sigma_{\mathrm{sat}}}{\sigma_{\mathrm{halo}}} r \tag{5.7}$$

The material outside this radius is assumed to disrupted and becomes part of the intra-cluster medium component. We keep following the satellites until their orbital radius becomes smaller than the sum of the radii of the central and satellite galaxies, at which point we assume a merger has occurred.

The spherical symmetry approximation for the mass distribution of satellites is valid if the mass of the satellite is considerably smaller than the mass of the central object. We only apply disruption forces to galaxies that have already lost their halo and from Fig. 4.1 we can see that these objects, despite spanning a range of magnitudes (and consequently masses) are more concentrated towards the low mass bins, being in general considerably smaller than central objects. Nevertheless massive satellites do exist in the model and the rate of major mergers (where the mass ratio between the central and the satellite galaxy is close to 1) in the model is not negligible. The calculation of the tidal radius should be considered as an approximation for mergers of this type.

Satellite Mass Distribution

To compute the forces acting on satellite galaxies, we assume a spherically symmetric distribution for the mass of the galaxies in the model. However, to determine the amount of material outside the disruption radius that is lost at each time step, we need to adopt different distribution models for the stellar mass in the different galaxy components. The model naturally defines galaxies as a combination of a disc and a spheroid. Galaxies form only as discs, with mergers moving material into the bulge component. We now explain how these two components are modelled.

Mass Distribution in Disks

We model the disc component as an exponential mass distribution given by:

$$M_{\rm disk}(< R) = \int_0^R 2\pi R \Sigma_{d,0} \exp^{-R/R_d} dR = M_{\rm disk} \int_0^x x \exp^{-x} dx, \tag{5.8}$$

where $\Sigma_{d,0}$ gives the surface density of the disk and $M_{\rm disk} = 2\pi\Sigma_{d,0}R_D^2$ its total mass. The auxiliary variable $x = R/R_D$ and the disk scale-length is calculated using the formalism derived by Mo et al. (1998). Integrating equation 5.8, the disk mass inside a given radius R is given by:

$$M_{\rm disk}(< R) = M_{\rm disk}\left[1 - \left(1 + \frac{R}{R_D}\right)\exp^{-\frac{R}{R_D}}\right]. \tag{5.9}$$

Mass Distribution in Bulges

The mass in bulges is spherically symmetric distributed according to a $r^{1/4}$ law:

$$M_{\rm bulge}(< R) = \int_0^R 4\pi R^2 \Sigma_{b,0} \exp^{-7.67\left[\left(\frac{R}{R_b}\right)^{\frac{1}{4}}-1\right]} dx, \tag{5.10}$$

where $\Sigma_{b,0}$ gives the surface density of the bulge and R_b its scale-length, obtained from observational scaling relations. However, since this integral has no analytic solution, we use the Hernquist (1990) approximation instead:

$$M_{\rm bulge}(< R) = M_{\rm bulge} \int_0^x \frac{x^2}{x(1+x)^3} dx, \tag{5.11}$$

where $M_{\rm bulge}$ is the total stellar mass of the bulge. The auxiliary variable $x = R/a$ where $a = 0.56R_b$. Integrating equation 5.11, the bulge mass inside a given radius R is given by:

$$M_{\rm bulge}(< R) = M_{\rm bulge} \frac{\left(\frac{R}{a}\right)^2}{\left(1+\frac{R}{a}\right)^2}. \tag{5.12}$$

The disk and bulge scale lengths are crucial quantities to correctly predict the mass distribution in the two components. While for disks this can be determined by theoretical

arguments of angular momentum conservation, for the bulges formed during violent merger events there is no such possibility. The adopted value for R_b must be obtained from observational scaling relations for elliptical galaxies.

The pioneering work of Kormendy (1977) demonstrated that there is a correlation between the effective radius (R_b) and the effective surface brightness (I) of ellipticals galaxies. At the same time, Faber & Jackson (1976) showed that the luminosity of these galaxies is proportional to the velocity dispersion, with the derived relation $L \propto \sigma^4$ expressing the intuitive notion that more luminous galaxies have higher velocity dispersions (and hence higher masses). From these two correlations known respectively as the Kormendy and the Faber-Jackson relations and since $L = \pi R_b^2 \langle I \rangle$, it follows that the effective radius R_b should be correlated with the velocity dispersion σ. Since the velocity dispersion is an intrinsic quantity of theoretical galaxies derived from the properties of their host halos, we can use it to determine the effective radius and the mass distribution of bulges. To do so, we use the proportional law from Djorgovski & Davis (1987):

$$\log \sigma = 0.21 \log R_b + 2.58. \tag{5.13}$$

This law is a simplification of a more fundamental relation for ellipticals, which are better described by a fundamental plane built from the characteristic scaling length R_b, the velocity dispersion σ and the mean effective surface brightness $\langle I \rangle$. Quantitatively, the plane as determined by Binney & Tremaine (1987), is

$$\log R_b = 0.36(\langle I \rangle / \mu_B) + 1.4 \log \sigma, \tag{5.14}$$

where μ_B represents the galaxy surface brightness for the B-band. To determine the characteristic radius of bulges we use the simplified relation from equation 5.13 instead of this one, because the models have no direct way of predicting the surface brightness of galaxies.

Recent work has shown that small spheroidal objects might be slightly tilted in this fundamental plane. The range in question is below our resolution limit for dwarf galaxies, but recently formed bulges in the predicted spirals might be within these objects. This could in principle introduce some errors into the determination of the fraction of mass disrupted, however, these observations are still subjected to uncertainties and we choose to treat all bulges identically.

The amount of material disrupted is largely dependent on the mass distribution and size of the disk and bulge components described in this section. The adopted relations are

the ones currently favoured by data, but if this is changed by future observations we will adapt our model accordingly.

5.2 The New Semi-Analytic Model Predictions

In the previous chapter we introduced the motivation for implementing satellite disruption into the De Lucia & Blaizot (2007) semi-analytic model. We assumed that all the satellites without a dark matter halo at redshift zero would be entirely disrupted, with all their material being transferred into the intra-cluster medium. By correctly implementing the process into the model some changes are expected.

First of all, disruption is a continual process, so we would expect satellites to become partially disrupted as they follow their path into the central galaxy. In comparison to our simplified approach, where we assumed instantaneous and total disruption, this should make the effects of this phenomenon less dramatic at the low mass end of the stellar mass function, since more low mass galaxies will survive. The same should happen for the fraction of small red galaxies, with more low mass red galaxies surviving. On the other hand, the fact that the process is now assumed to be continuous over redshift, means that less material will merge into central galaxies, leading to noticeable changes at the high mass end (the behaviour of massive objects was not affected before, since we only removed satellite galaxies at redshift zero).

In this section, we show the predictions from the semi-analytic model with the new implementation of satellite disruption. In here we use the parameters from De Lucia & Blaizot (2007), which were never tuned to incorporate this recipe. The black hole-bulge mass relation is almost unaffected by the inclusion of disruption and we choose not to show it again. In section 5.3 we apply the MCMC parameter estimation techniques to sample the parameter space for the new model, finding a best fit for which we present predictions for a range of observable quantities.

The Luminosity Function

In Fig. 5.1 we plot the predictions for the K and $b_{\rm J}$ band luminosity functions for the disruption model. In the top panel, the K-band luminosity functions from the canonical and disruption models are compared with a combined data set from (Cole et al., 2001; Bell et al., 2003; Jones et al., 2006) as described in section 3.3.2. The introduction of satellite disruption into the model has a considerable effect on the bright end side of the K-band luminosity function. At redshift zero the brightest objects that determine this

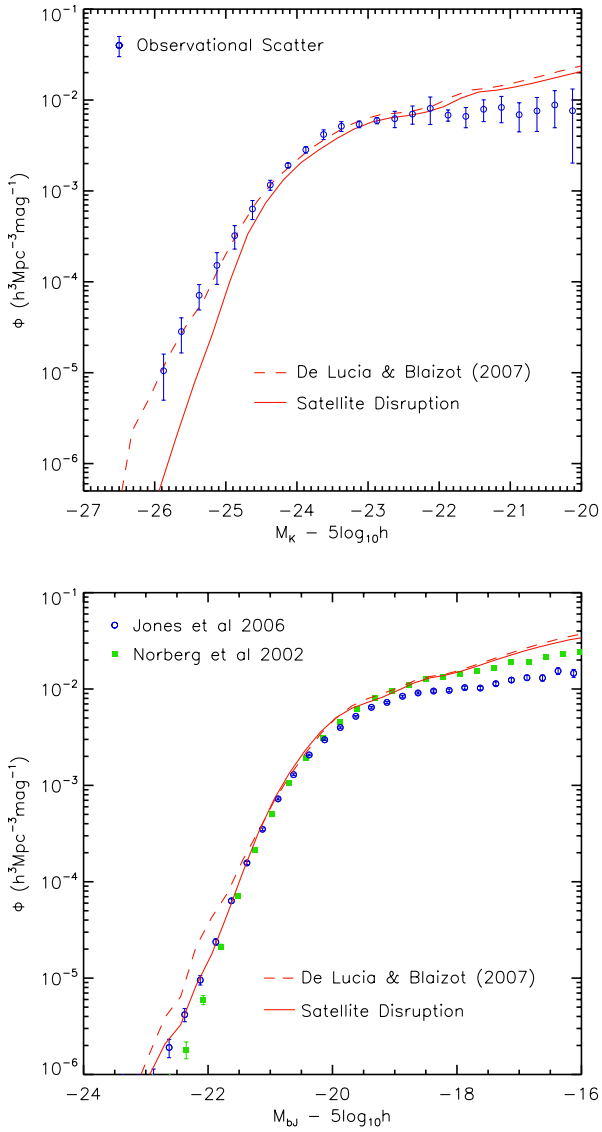

Figure 5.1: Comparison of the predicted K-band luminosity function (top panel) and the b_J-band luminosity function (bottom panel) at $z = 0$, from De Lucia & Blaizot (2007) (dashed red line) and the satellite disruption model (solid red line). On the top panel, the data points represent observations from (Cole et al., 2001; Bell et al., 2003; Jones et al., 2006) as described in section 3.3.2. In the bottom panel the theoretical b_J band from both models is compared to the results of the 2dFGRS (Norberg et al., 2002b) and to those of the 6dFGS (Jones et al., 2006).

modification are at the centre of the most massive clusters and groups of galaxies. In the framework of a hierarchically growing Universe, these objects grow from material received during numerous mergers over their lifetime. With the inclusion of satellite disruption, a large amount of material which would otherwise end up at the most bright objects at redshift zero is transferred from satellites into the intra-cluster medium. The result is an excessively low number density of bright objects in the K-band when compared to observations and the previous model. However, we emphasize that the results presented in this section were obtained without changing the parameter values from the original De Lucia & Blaizot (2007). In the next section, we will test if there is a region in parameter space where disruption can produce an overall better agreement between the predicted and observed luminosity functions.

The number density of dwarf galaxies is, in its turn, less affected than we inferred from our simplified approach. With the self-consistent implementation, disruption is no longer an instantaneous and dramatic process, instead galaxies lose material slowly as they follow their route into the central galaxy. Moreover, we now account for the increase on the merger time scale due to the fact that satellites become smaller and less affected by dynamical friction (this also helps explaining the smaller amount of material received by massive objects). Nevertheless, the decrease in the number density of dwarfs is still significant, due to the large numbers of these objects contained in the Universe.

In the bottom panel of Fig. 5.1 , the $b_{\rm J}$-band luminosity functions from the canonical and disruption models are compared to the results of the 2dFGRS (Norberg et al., 2002b) and to those of the 6dFGS (Jones et al., 2006). Since disruption acts on satellites that already lost their dark matter halos and are predominantly red, it comes at no surprise that the "blue" $b_{\rm J}$-band is less affected than the K-band luminosity function. Still, disruption has visible effects at both luminosity extremes, with the changes making predicted galaxies become closer to what is expected from observations.

The Stellar Mass Function

In the top panel of Fig. 5.1 we saw that galaxy disruption has a dramatic effect on the bright end side of the K-band luminosity function, significantly reducing the number density of these objects. This luminosity band is known as a good tracer of galaxy mass and indeed the same effect is seen on the stellar mass function. However, unlike in the K-band, this reduction in the number density of massive objects brings the model into a much better agreement with the latest observational data set. The predicted stellar masses

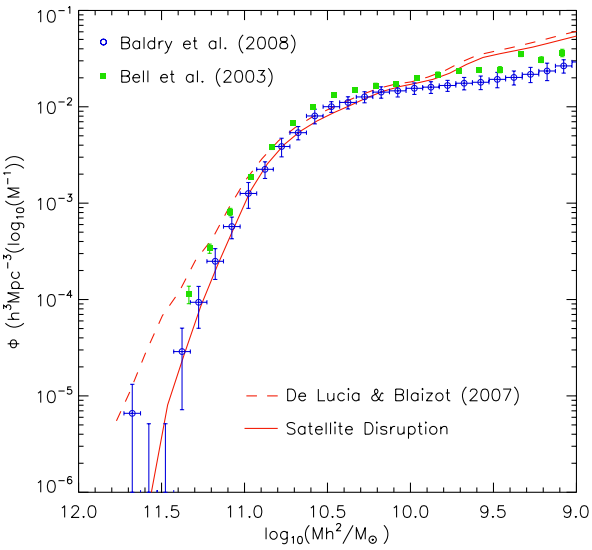

Figure 5.2: The galaxy stellar mass function at $z = 0$, for the canonical model (dashed red line) and the disruption model (solid red). The data points represent observations from Baldry et al. (2008) (blue open circles) and Bell et al. (2003)(green filled squares).

from De Lucia & Blaizot (2007) (dashed red line) and the satellite disruption model (solid red line) at $z = 0$ are compared with observations from Bell et al. (2003) (green filled squares) and Baldry et al. (2008)(blue open circles) in Fig. 5.2. The discrepancy between different conversions from observational luminosities to masses, which we believe is related to the stellar population synthesis models adopted, was already discussed in section 3.4.3.

The low mass end of the mass function, again follows the behaviour of the K-band luminosity function, with a less dramatic effect from disruption than previously inferred. Despite that, it again helps in reducing the known excess of dwarf galaxies in semi-analytic models.

Galaxy Colours

In the top panel of Fig. 5.3 we show the B-V colour-stellar mass relation for the galaxies in the satellite disruption model. As expected from the analysis of the predicted luminosity functions, the self consistent implementation of satellite disruption has a less dramatic effect on dwarf galaxies than our previous approximation. The number density of red dwarfs is still reduced in comparison to the original De Lucia & Blaizot (2007) model, but a peak in the low mass end of the red population persists, unlike in Fig. 4.2.

The changes introduced can be better analysed by looking at the fraction of galaxies in each population in this plot. This is shown on the bottom panel where the fraction

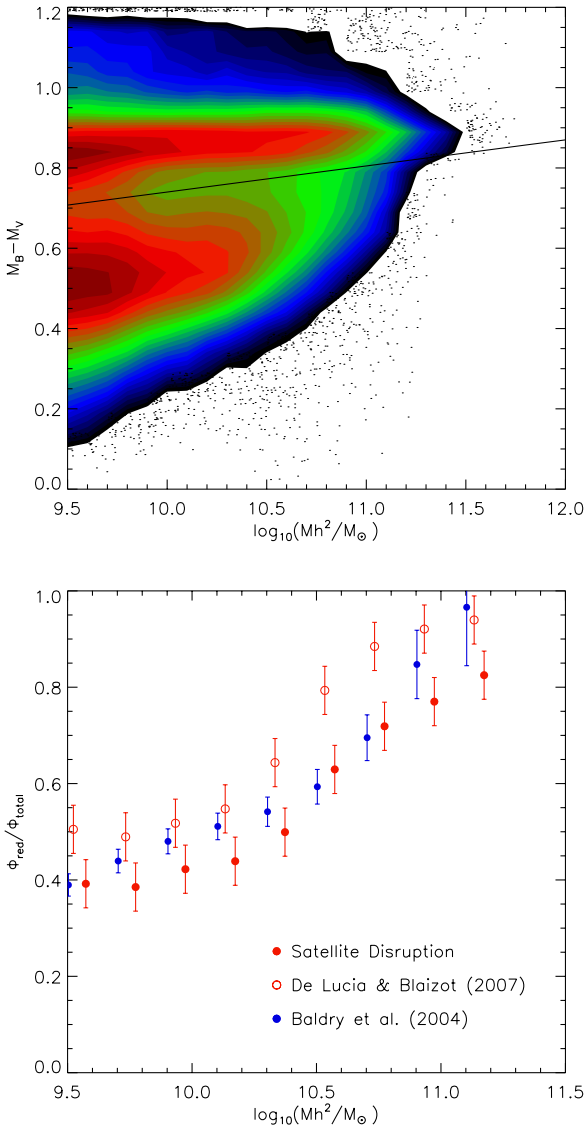

Figure 5.3: The top panel shows the B-V colour-stellar mass relation for the galaxies in the satellite disruption model. The solid line represents the division between the red and blue populations in Weinmann et al. (2006a). The predicted fraction of red galaxies as a function of stellar mass is showed in the bottom panel. The original De Lucia & Blaizot (2007) model (open red circles) is compared with our best fit model (filled red circles) and observational data from Baldry et al. (2004) (filled blue circles).

of red galaxies from the De Lucia & Blaizot (2007) model (open red circles) is compared with our best fit model (filled red circles) and observational data from Baldry et al. (2004) (filled blue circles). The fraction of red galaxies is reduced over the entire plotted range. The behaviour at the low/intermediate mass end is expected, since these objects are the satellites from which material is disrupted and that continuously move to even lower mass bins.

Perhaps less intuitive is the decrease in the fraction of massive red galaxies since these are expected to be the central objects of massive groups and clusters. More of these galaxies are now blue since they receive less red material from satellites (which is moved into the intra-halo light), but will still have large star formation bursts during massive mergers. This happens since the intensity of bursts only depends on the amount of cold gas available which is unaffected by disruption. In principle, one could assume some profile for the distribution of gas and disrupt it partially with the stellar material. However, type 2 satellites have already lost their dark matter halo, and with it most of their gas. The remaining cold gas is normally consumed by star formation in a short time scale (starvation). Therefore, gas disruption should have a negligible effect in our model.

For comparison with the simplified model of chapter 4, in Fig. 5.4 we plot the $u - r$ colour distribution of galaxies of different types as a function of $M_{\rm r}$, for the disruption model. In comparison with the previous model (Fig. 4.1), where we assumed that all type 2 galaxies would be disrupted, we see that with the self-consistent implementation of disruption a large fraction of these objects survives. Nevertheless, in comparison to the original De Lucia & Blaizot (2007) model, the number of satellites without a halo is significantly reduced.

Intra Cluster Light

In Fig. 4.6 we plotted the predicted intra-cluster light from our simplified disruption model. Fig. 5.5 represents the results for the self-consistent implementation of satellite disruption. The solid line gives the mean fraction of mass in the ICL compared to the total mass of the group or cluster at each virial mass bin. Here we extend the predictions to a range that goes from the most massive clusters, $M_{\rm vir} = 10^{15}\,{\rm M}_{\odot}$, to relatively small groups, $M_{\rm vir} = 10^{12}\,{\rm M}_{\odot}$. In agreement with the previous results and with cluster observations (Bernstein et al. 1995; Gonzalez et al. 2000; Feldmeier et al. 2002; Feldmeier et al. 2004b; Gonzalez et al. 2005; Zibetti et al. 2005), the predicted ICL fraction for groups with $M_{\rm vir} > 10^{13}\,{\rm M}_{\odot}$ has a mean of $\approx 20\%$. This amount falls down systematically has

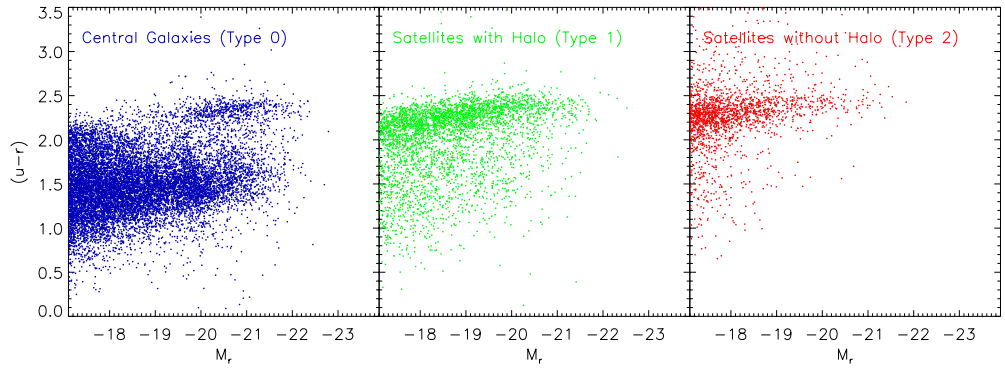

Figure 5.4: The $u-r$ colour distribution of galaxies as a function of $M_{\rm r}$ for the disruption model. Galaxies have been colour-coded by type: central galaxies (blue, left panel), type 1 galaxies (green, central panel) and type 2 galaxies (red, right panel).

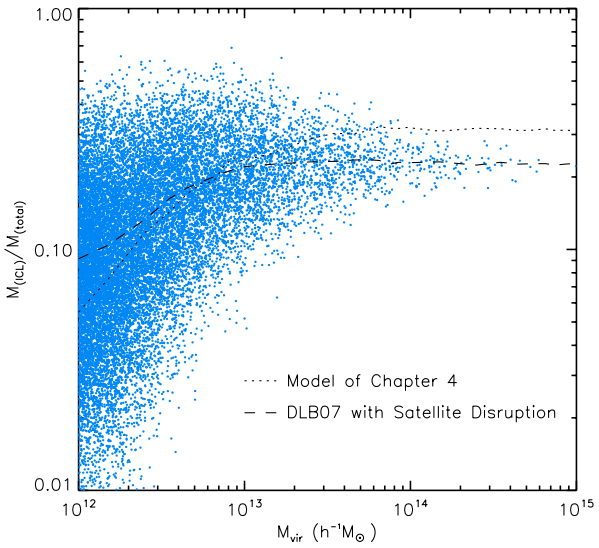

Figure 5.5: Fraction of the mass in the intra-cluster medium over the total stellar mass as a function of virial mass. The blue dots are a representative sample of the total galaxy population in the model with satellite disruption. The solid line represents the median of the $M_{\rm ICL}/\ M_{\rm total}$ distribution for the full millennium volume and the dotted line shows the predictions from the *a posteriori* model of chapter 4.

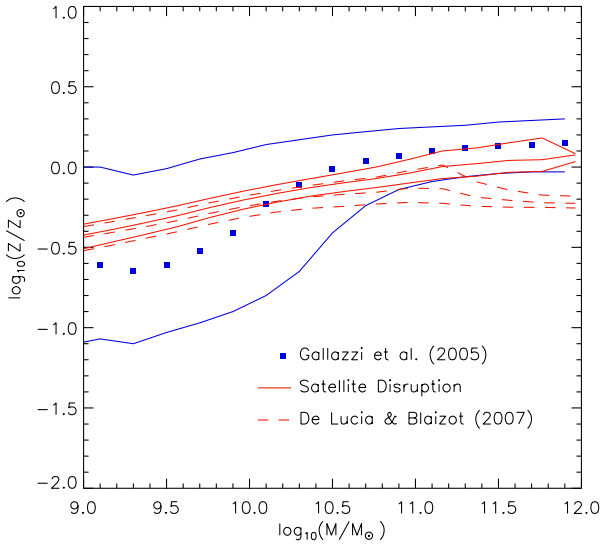

Figure 5.6: Comparison between the metallicity of stars in the satellite disruption model (solid red lines), in De Lucia & Blaizot (2007) (dashed red lines) and in observations from Gallazzi et al. (2005) (blue squares and lines). For all the data sets, the central line represents the median value of metallicity in each mass bin (the blue squares for the observational data), while the upper and lower lines represent the 16th and 86th percentiles of the distribution.

we move to smaller virial masses reaching a mean of $\approx 10\%$ for $M_{\rm vir} = 10^{12}\,{\rm M}_{\odot}$.

As showed by the dotted line in Fig. 4.6 , in comparison to our previous predictions, the total and instantaneous disruption assumed before gives similar fractions of ICL than a less effective self-consistent implementation that acts over redshift. Nevertheless, for the most massive groups ($M_{\rm vir} > 10^{13}\,{\rm M}_{\odot}$) the self-consistent implementation gives $\approx$ less 10% of the ICL to total mass fraction.

The Metallicity of Stars

Apart from the galaxy quantities that originally motivated the introduction of a new recipe into the semi-analytic model, there is another predicted property that is significantly improved by the disruption of satellite galaxies. In Fig. 5.6 we show the metallicity of stars as a function of the galaxy stellar mass. The new disruption model (solid red lines) is compared with the original De Lucia & Blaizot (2007) (dashed red lines) and with observations from Gallazzi et al. (2005) (blue squares and lines). As in Fig. 3.15 the central line represents the median value of metallicity in each mass bin (the blue squares for the observational data), while the upper and lower lines represent the 16th and

86th percentiles of the distribution. From the figure it is clear that satellite disruption improves the agreement between semi-analytic predictions and observations, by increasing the metallicity of intermediate/high mass galaxies, $M_\star > 10^{10}\,M_\odot$. The explanation for this effect is related to the decrease of the number density of the most massive galaxies. With the implementation of disruption a considerable amount of material that would otherwise end up in these objects is now transferred into the intra-cluster light. In terms of the metallicity of stars, this results in massive objects receiving less low metallicity material from satellites, hence increasing their metallicity.

5.3 MCMC Sampling with Individual Constraints

In the previous section we presented the predictions for the semi-analytic model with a self-consistent treatment of the disruption of satellite galaxies. These were obtained using the parameters from the original model (De Lucia & Blaizot, 2007), not adjusted to incorporate this new physical recipe. In this and the next section, we will use the MCMC sampling techniques introduced in chapter 3 to search for the combination of parameters that give the best fit for the satellite disruption model. The comparison will be done using the same observational data sets and statistical tests as before and since we have not introduced any additional parameter, the relative goodness of the original and the satellite disruption model can be assessed directly. The ability or not of the MCMC to find a best fit model with a likelihood higher than before will tell us if the introduction of the new physical recipe is justified.

The parameters sampled here are the same as in chapter 3 and are shown in table 3.1. A similar chain size is obtained ($\approx 30\,000$ steps) and the MCMC output is again analyzed using the COSMOMC software package.

As in section 3.3, we will start by analysing the MCMC sampling when the model is constrained with separate observational data sets. This will allow us to understand if the introduction of the new physics significantly changes the way in which other recipes affect each galaxy property. We will restrict the study to the K-band luminosity function and the black hole-bulge mass relation, since no significant changes are seen in the MCMC sampling for the colour constraint.

5.3.1 The Luminosity Function

As shown in the previous section, the K-band luminosity function for the semi-analytic model with satellite disruption shows a considerable decrease in the number density of

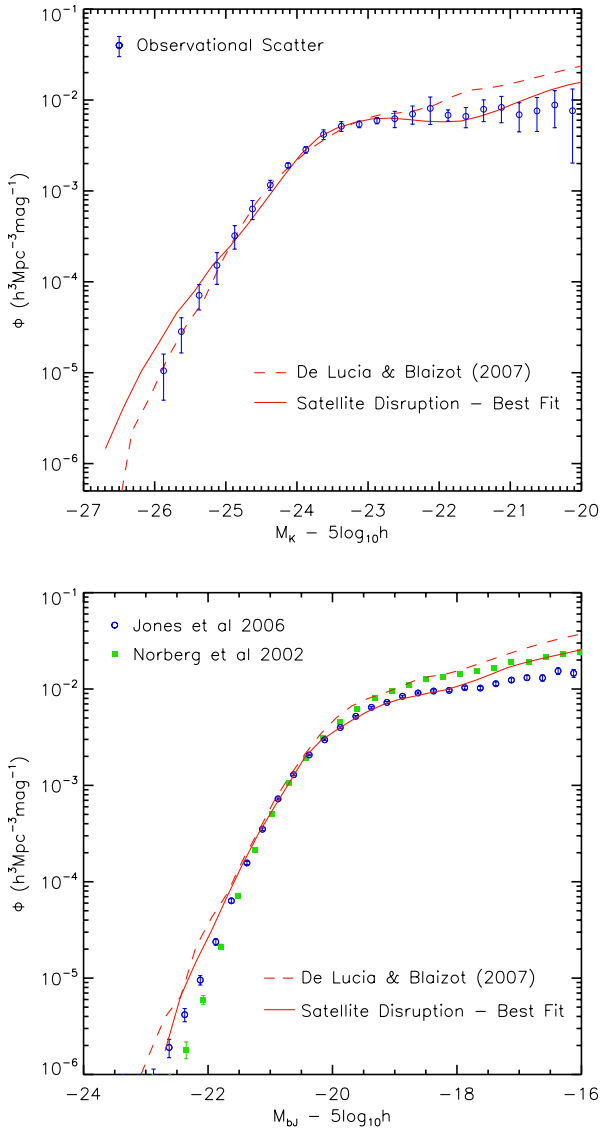

Figure 5.7: The galaxy K-band and b_J-band luminosity functions at z=0 for the De Lucia & Blaizot (2007) model (dashed red line) and our best fit model with satellite disruption (solid red line). On the top panel the model predictions are compared with observations from (Cole et al., 2001; Bell et al., 2003; Jones et al., 2006), combined to form a single data set as described in section 3.3.2. On the bottom panel, the b_J-band luminosity functions are compared with observations from 2DFGRS (green filled squares) and 6DFGS (blue open circles), respectively Norberg et al. (2002b) and Jones et al. (2006).

bright objects and a less significant, but still noticeable, reduction in the number of dwarf galaxies. We now analyze the effects that these changes have on the physics of star formation, AGN and supernova feedback. We start by performing an MCMC sampling only requiring the model to fit the observational luminosity function and look at the correlations shown between the physical parameters. At each MCMC step, the likelihood between the model predictions and observations is computed using the same chi-square probability function described in section 3.3.2 (equation 3.8).

In Fig 5.7 we show the predictions for the K-band and $b_{\rm J}$-band luminosity functions for the best fit model, when only the K-band constraint is used in the MCMC sampling. Apart from the three brightest bins in the K-band luminosity function (not constrained in the sampling due to the small volume used), the model shows good agreement with both observational quantities over the entire luminosity range.

In comparison with the best fit for the K-band luminosity function obtained for the model without disruption (Fig. 3.1), the likelihood is now slightly lower, with the chi-square probability changing from 0.96 to 0.90. However, looking at the overall shape of this function, it seems now in much better agreement with what is expected from observations.

In Fig. 5.8 we plot the 1σ and 2σ preferred values from the MCMC (solid lines) and the maximum likelihood value sampled in each bin (colour contours), for the subset of the original parameters (with values plotted in log space) constrained only by the observational K-band luminosity function. As in our previous analysis the colour contours are scaled by the maximum likelihood obtained in each sampling, 0.90 in this case.

In comparison to the model without satellite disruption (Fig. 3.2) the parameters controlling supernova feedback show similar correlations, although the more likely regions now correspond to an overall lower efficiency from this form of feedback. This means that a lower fraction of hot gas is now ejected from small galaxies ($\epsilon_{\rm halo}$), with an accordingly lower reincorporation from the external reservoir required ($\gamma_{\rm ej}$), as can be seen in the right bottom panel of Fig. 5.8. The position of the line corresponding to the correlation between the reheating ($\epsilon_{\rm disk}$) and ejection parameters in the bottom left panel, is unchanged from the previous study. As explained in section 3.3.2 using equation 3.10, this means that the virial velocity above which supernova feedback stops being effective is similar to what was required without satellite disruption. In fact, the supernova feedback is still very efficient and can only be effective in small galaxies. However, satellite disruption reduces the excess of dwarfs in the original model, so its overall strength can be reduced.

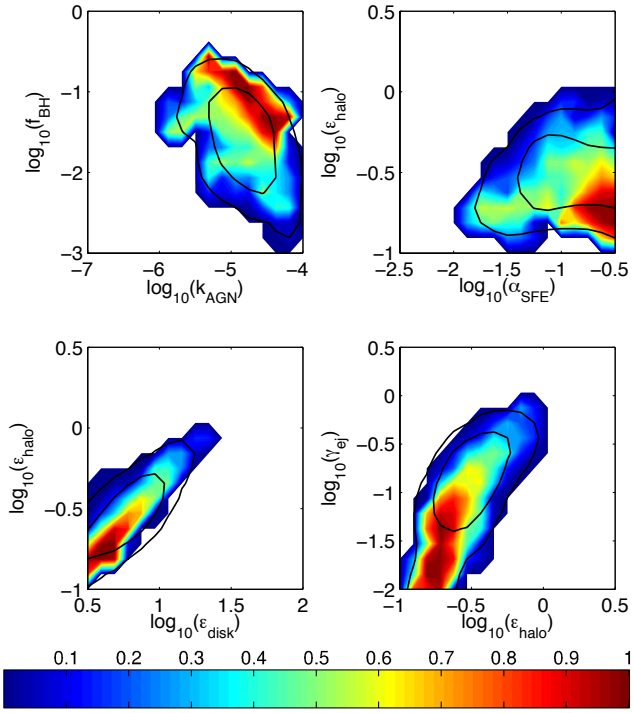

Figure 5.8: Correlations between the 6 parameters analysed in the study for the semi-analytic model with satellite disruption, only constrained by the χ^2 test on the K-band luminosity function. As in chapter 3, the values of the parameters are plotted in log space, with the solid contours representing the 68% and 95% preferred regions from the MCMC (the posterior distribution) and the colours the maximum likelihood value sampled in each bin (the profile distribution). The colour scale is normalized by the maximum likelihood value of 0.90.

The upper left panel shows the allowed range for the AGN feedback parameters ($f_{\rm BH}$ and $k_{\rm AGN}$). As before, a correlation exists, corresponding to a unique value of mechanical heating and hence a fixed amount of cooling being suppressed by this form of feedback. This value is slightly higher than before, which seems contradictory, since the disruption of satellites reduces the number density of massive objects. However, as shown in the upper right panel, a considerably higher star formation efficiency ($\alpha_{\rm SF}$) compensates for it, increasing the number of objects on and above $\rm L_\star$ in comparison with the predictions for the satellite disruption model with the original parameters. This increase in the star formation efficiency is less noted in the faint end side. From equation 2.15 we see that an increase in the amount of stars formed will correspond to a proportional increase in the amount of energy released by supernovae, hence having a smaller effect on the luminosity of dwarf galaxies. Moreover, the increase in star formation efficiency is also balanced by an increase in the gas reincorporation time scale.

5.3.2 The Black Hole-Bulge Mass Relation

In this section we discuss the results of the MCMC parameter estimation when the semi-analytic model is only tuned to fit the black hole-bulge mass relation and the K-band luminosity of the brightest objects. As explained in section 3.3.4, running the sampling only requiring an agreement between theoretical and observational black hole and bulge masses leaves the parameters unconstrained. For this reason we run the MCMC calculating the model likelihood as a product of two tests: the chi-square probability of the luminosity function for galaxies brighter than $M_k = -23$ (equation 3.8) and the binomial probability of the black hole-bulge mass relation (equation 3.14).

Once more, the black hole-bulge mass relation is almost unchanged in relation to the original De Lucia & Blaizot (2007) predictions and we do not repeat it here. However, despite the predictions being identical, the parameter values are not and in comparison to our previous MCMC analysis significant changes are seen in their correlations and allowed regions.

In Fig. 5.9 we plot the posterior and profile likelihood distributions of the parameters constrained only by the black hole-bulge mass and the K-band luminosity function of galaxies brighter than $M_k = -23$. In order to understand the changes introduced by satellite disruption we include two additional plots (two top panels), the correlations between the AGN quasar mode parameter and the star formation efficiency and the AGN radio mode and the disk reheating efficiency.

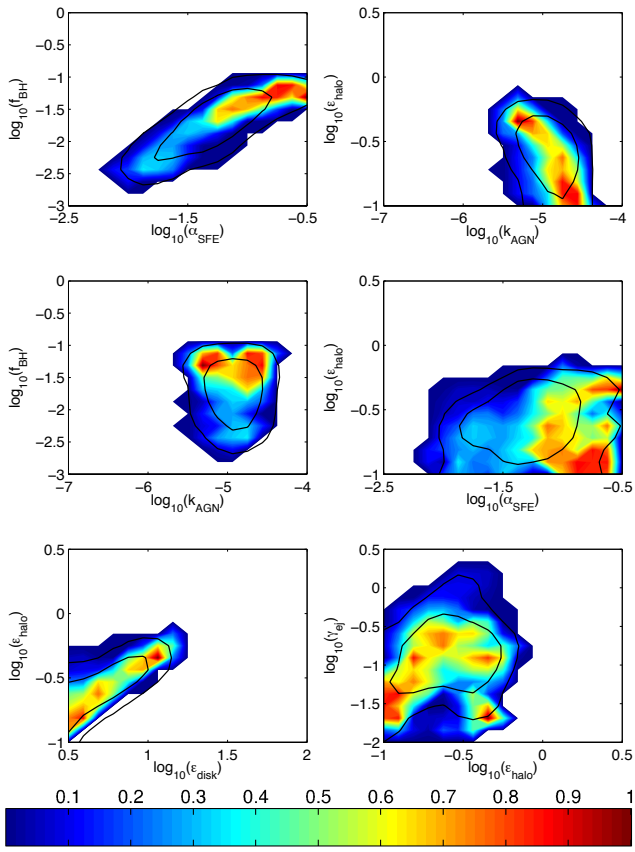

Figure 5.9: As for Fig. 5.8, but constrained only by the binomial test on the black hole-bulge mass relation and by the K-band luminosity function of galaxies brighter than $M_k = -23$. The colour scale is normalized by the maximum likelihood value of 0.80.

A somewhat expected correlation, but not present before, is shown in the upper left panel. A positive correlation is now evident between the quasar mode, responsible for the black hole growth, and the star formation efficiency, responsible for the bulge growth. Considering the physics governed by them, it comes as no surprise that an increase in one requires an increase in the other in order to maintain the black hole-bulge mass fraction of galaxies.

The fact that this correlation was not present in the previous study (with the two parameters unconstrained against each other), is explained by the considerably smaller regions with acceptable likelihood that we found before. For the same reason, the correlation between the supernova reheating and ejection parameters, seen in the sampling for the K-band luminosity constraint, is now clear in the lower left corner. This correlation is driven by the test on the K-band luminosity for objects around $L_\star$. Despite not suffering directly from this form of feedback, their number density is affected by the amount of stars formed and gas available in smaller objects. Accordingly, the lower and middle right panels show an identical behaviour for the parameters as in the K-band sampling.

In the middle left panel we see that there are two regions with high likelihood for the combination of parameters controlling the black hole physics. Since both correspond to the same $f_{\rm BH}$ value, they will produce similar black hole masses, but different AGN feedback efficiencies. For this reason, the two different regions only affect significantly the K-band luminosity constraint and represent two distinct ways of getting a good agreement between the predicted and observed abundance of objects on and above $L_\star$. Looking at the upper right panel, this fact is reflected in a correlation between $\epsilon_{\rm disk}$ and $k_{\rm AGN}$. A large reheating efficiency will reheat the cold gas in massive objects and since their cooling time scales are relatively large, will effectively reduce their star formation. This reduces the efficiency of AGN feedback needed. Conversely, less reheating from supernova will require more AGN feedback to decrease the number density of massive objects. This correlation is not seen when the K-band constraint is studied in isolation since in that case we consider the full luminosity range, while in here only the most bright objects. In fact, the lower reheating values are ruled out by the faint end of the luminosity function, since they over-produce the number of dwarf galaxies.

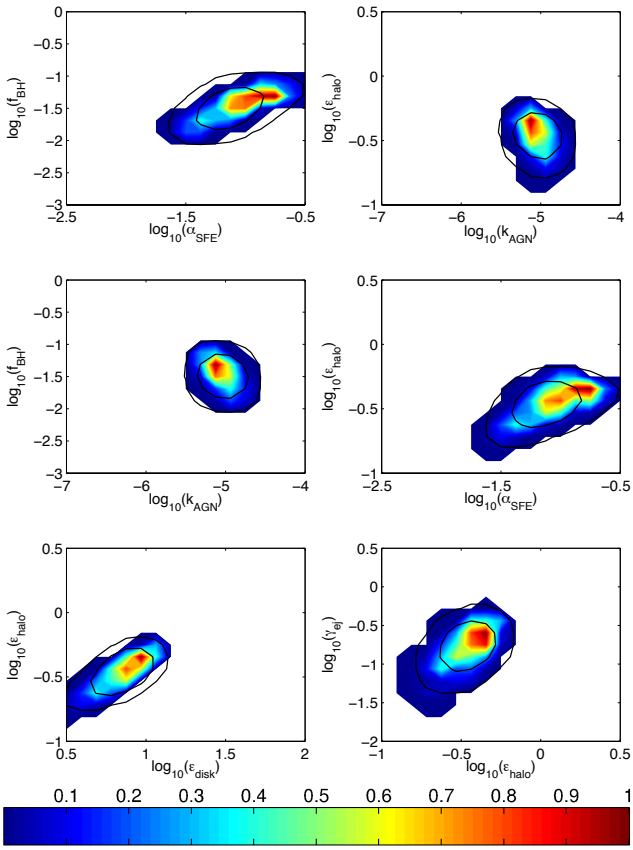

Figure 5.10: As for Fig. 5.8, but constrained by all three observational properties: the K-band luminosity function, the fraction of red galaxies, and the black hole-bulge mass relation. The colour scale is normalized by the maximum likelihood value of 0.15.

5.4 The Best Fit Semi-Analytic Model with Satellite Disruption

As in section 3.4 we now present the results for the MCMC sampling when the semi-analytic model with satellite disruption is constrained by the three observational data sets combined. The likelihood for the best fit model is once more given by the product of the likelihood from the three statistical tests:

$$\pi(x_i) = \mathcal{L}_{(\mathrm{K-band})} \times \mathcal{L}_{(\mathrm{Colour})} \times \mathcal{L}_{(\mathrm{BH-Bulge})}. \tag{5.15}$$

Fig. 5.10 shows the allowed ranges and correlations between the parameters sampled. As before, the use of combined observations to produce one comprehensive data set in terms of galaxy formation properties, restricts the parameters to one small region with acceptable likelihood.

The original model had a maximum likelihood value of just 0.037 when compared with

Table 5.1: Statistics from the MCMC parameter estimation for the parameters in the satellite disruption model. The best fit and confidence limits (derived from the colour contours in Fig. 5.10) are compared with the published values from De Lucia & Blaizot (2007) and with the best fit values obtained without the inclusion of satellite disruption.

	DLB07	No Disruption	Mean	-2σ	-1σ	+1σ	+2σ
$\alpha_{\rm SF}$	0.03	0.039	0.16	0.023	0.025	0.28	0.29
$k_{\rm AGN}$	7.5×10^{-6}	5.0×10^{-6}	6.9×10^{-6}	4.7×10^{-6}	5.0×10^{-6}	1.6×10^{-5}	1.7×10^{-5}
$f_{\rm BH}$	0.03	0.032	0.057	0.013	0.013	0.082	0.086
$\epsilon_{\rm disk}$	3.5	10.28	9.06	2.78	3.06	12.00	12.00
$\epsilon_{\rm halo}$	0.35	0.53	0.44	0.15	0.16	0.54	0.54
$\gamma_{\rm ej}$	0.5	0.42	0.24	0.035	0.042	0.41	0.51

the chosen set of observational constraints, meaning it was ruled out at a 2-σ level. However, the new satellite disruption recipe brings the model likelihood up to 0.15, meaning it is now fully compatible with observations. Since we introduced no additional parameters, this means that the inclusion of the new physical process seems to be required by data.

Despite having a significantly higher likelihood than before, the new best fit model is still far from exactly reproducing observations. To improve its predictions, we again refer to the points about the black hole growth, dust and stellar population synthesis models raised in sections 3.4 and 3.5.

5.4.1 Best Fit Parameters and Confidence Limits

The best fit and confidence limits for the 6 free parameters in the model with satellite disruption, together with the published values from De Lucia & Blaizot (2007) and the best fit for the model without satellite disruption are shown in table 5.1. Despite a different model being used, all the parameters from both the original De Lucia & Blaizot (2007) and the previous MCMC analysis fall within the new 2σ confidence limits.

In comparison to the best fit obtained for the model without satellite disruption, the most dramatic effect is the increase in the star formation efficiency. It represents a change in the fraction of cold gas transformed into stars in a disk dynamical time from 4% to 16%. Such an increase is required to repopulate the bright end side of the K-band luminosity function, largely affected by disruption. This effect is somewhat balanced by an increase in the mechanical heating from AGN, given by the product of $k_{\rm AGN}$ and $f_{\rm BH}$.

The virial velocity cutoff, above which supernova stops being effective (which is given

by $\epsilon_{\rm halo}/\epsilon_{\rm disk}$), is similar to that found for the model without disruption. This means that the new model still requires a large supernova feedback that is effective only for small objects. However, the lower 2σ limits for both the parameters controlling this form of feedback now extend into smaller values, which seem more likely from an observational point of view. Looking at the ejection and reincorporation parameters, we see that despite the ejection being slightly reduced, the reincorporation is now half of the best fit value for the model without disrupted. This means that the disruption model requires more gas to be moved from the hot into the external reservoir in order to reduce the amount of cooling. This should be seen in conjunction with the high star formation efficiency required by the bright end side of the K-band luminosity function. Considering this, satellite disruption indeed reduces the number density of dwarfs and requires less suppression of star formation in these objects.

5.4.2 Predictions for the Best Fit Satellite Disruption Model

In this section we analyze the predictions from the best fit model with satellite disruption. Contrary to the MCMC sampling, done in a single volume due to computational power issues, the following predictions were obtained using the full millennium dynamic range.

Galaxy Luminosity Functions

In the top panel of Fig. 5.11 the K-band luminosity functions from De Lucia & Blaizot (2007) and the best fit for the satellite disruption model are plotted against the observational data set used to constrain the sampling. The predictions for this galaxy property are identical to what was obtained for the best fit model without disruption. The new model still requires a strong supernova feedback to suppress faint objects that can only be effective in a limited low mass range, so that enough $L_\star$ galaxies still form. Despite that, the overall supernova feedback efficiency is now lower than before, in better agreement with observations.

In the bottom panel of Fig. 5.11 we show the predictions for the $b_{\rm J}$-band luminosity function. The best fit satellite disruption model is compared with the original De Lucia & Blaizot (2007) and two observational data sets. The predictions are once more identical to what was obtained for the optimized model without disruption. As seen in section 5.3.1, the model can, at the same time, reproduce the luminosity function for K and $b_{\rm J}$-band. The excess of galaxies around $L_\star$ seems to be caused by the observational colours constraint, which require a considerable fraction of galaxies in this range to be

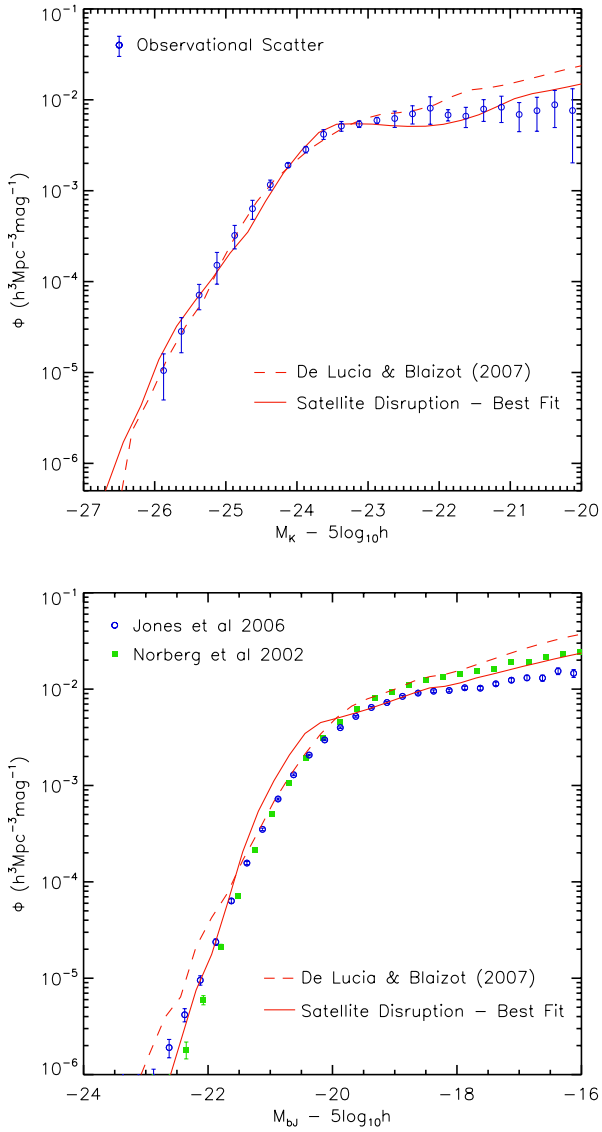

Figure 5.11: Comparison of the predicted K-band (top panel) and $b_{\rm J}$-band (bottom panel) luminosity functions at $z = 0$ from De Lucia & Blaizot (2007) (dashed red line) and the best fit satellite disruption model (solid red line). On the top panel, the data points represent the observations used to constrain the luminosities of galaxies in the MCMC parameter estimation (Cole et al., 2001; Bell et al., 2003; Jones et al., 2006). On the bottom panel, the $b_{\rm J}$-band luminosity function is compared with observations from 2DFGRS (green filled squares) and 6DFGS (blue open circles), respectively Norberg et al. (2002b) and Jones et al. (2006).

blue.

Galaxy Colours

Fig. 5.12 shows the predictions for the galaxy colours in the best fit model with satellite disruption. The top panel gives the *B-V* colour-stellar mass relation, while the bottom panel shows the fraction of red over the total number of galaxies as a function of stellar mass. The introduction of disruption without changing the original De Lucia & Blaizot (2007) parameter values decreases the overall fraction of red galaxies, causing the model to under-predict the number of these objects except for $L_\star$ galaxies (Fig. 5.3). As seen in the bottom panel of the figure, the MCMC optimization brings the model into agreement with observations for the entire plotted range.

More interesting is that the model now starts to produce an isolated population of massive red galaxies, as required by observations (top panel). Despite reducing the number of dwarf red galaxies, the disruption model still has an excessive fraction of these objects when compared to observations. This problem was addressed in section 3.5 and will be revisited in the end of this chapter (section 5.5), in the context of the new physics introduced.

The Black Hole-Bulge Mass Relation

In Fig. 5.13 we show the black hole-bulge mass relation for the satellite disruption model with the best fit parameters. Despite the changes in the parameters, the relation between black hole and bulge masses is almost unchanged from both the original De Lucia & Blaizot (2007) (Fig. 3.5) and the best fit model without disruption (Fig. 3.13).

Looking at the three relations just mentioned, the predictions for these galaxy properties seem to be quite robust and characteristic of the star formation and black hole growth recipes built in this semi-analytic model. It remains to be seen in the future, when statistics for black hole properties will be available, if the shape of the contours is matched by observations.

The Intra-Cluster Light

In Fig. 5.14 we plot the predicted intra-cluster light from our best fit model with satellite disruption. The solid line represents the median of the $M_{\rm ICL}/\ M_{\rm total}$ distribution in each bin while the dashed line gives the same relation for the disruption model with the original

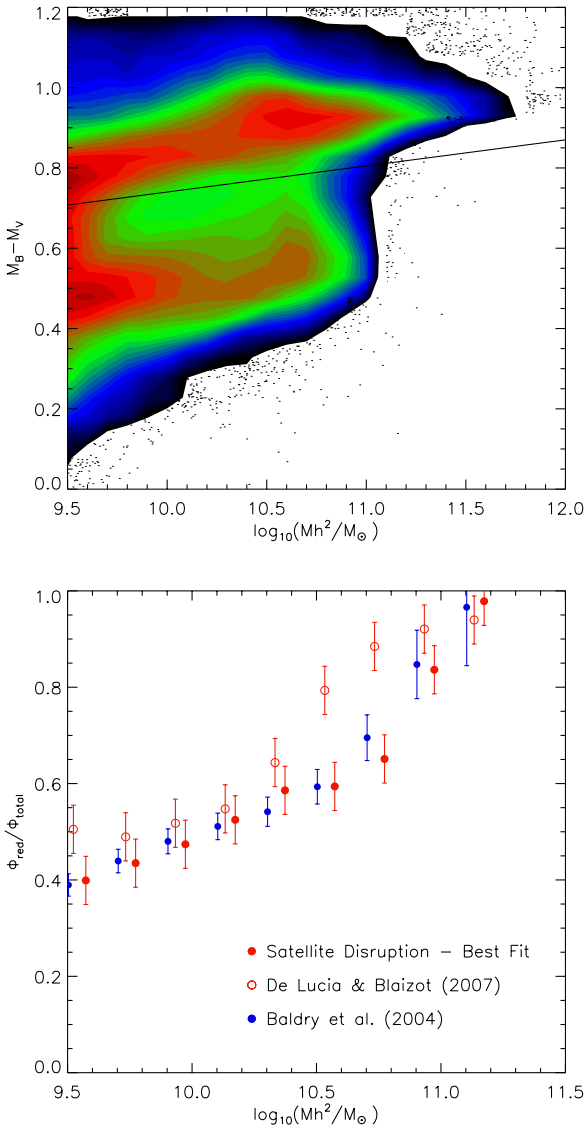

Figure 5.12: The top panel shows the B-V colour-stellar mass relation for the galaxies in the best fit satellite disruption model. The solid line represents the division between the red and blue populations in Weinmann et al. (2006a). The predicted fraction of red galaxies as a function of stellar mass is showed in the bottom panel. The original De Lucia & Blaizot (2007) model (open red circles) is compared with our best fit model (filled red circles) and observational data from Baldry et al. (2004) (filled blue circles).

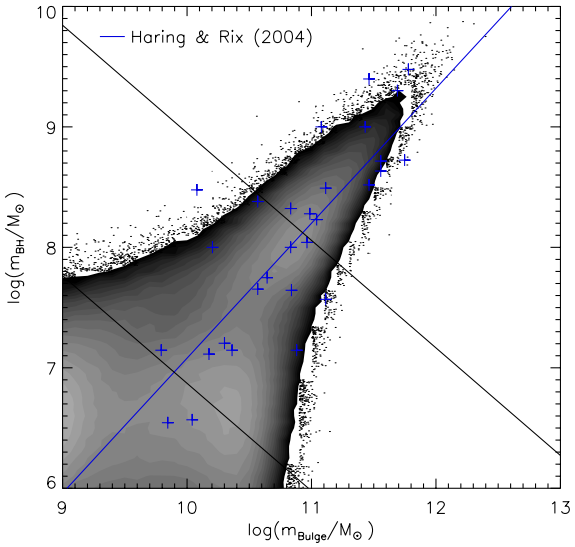

Figure 5.13: The black hole-bulge mass relation for the best fit satellite disruption model (solid contours). The blue crosses represent observations from Häring & Rix (2004) with the best fit to the data points given by the blue line.

set of parameters (Fig. 5.5). In comparison to the original parameters, the best fit lowers the fraction of light in the intra-cluster medium, which is justified by the increase in the number density of massive objects. This increase in the mass of the brightest cluster objects (BCGs), means that the relative amount of intra-cluster light when compared to the galaxies will be lower.

The predicted ICL fraction for groups with $M_{\rm vir} > 10^{13}\,{\rm M}_{\odot}$ has now a mean of $\approx$ 17%, decreasing to $\approx$ 7% for $M_{\rm vir} = 10^{12}\,{\rm M}_{\odot}$. These values are still compatible with observations, which present large error bars in the determination of this property, due to the difficulty in distinguishing between the light from the intra-cluster medium and the BCGs.

The Metallicity of Stars

In Fig. 5.15 we show the metallicity of stars as a function of the galaxy stellar mass. The best fit disruption model (solid red lines) is compared with the original De Lucia & Blaizot (2007) (dashed red lines) and with observations from Gallazzi et al. (2005) (blue squares and lines). As in Fig. 3.15, the central line represents the median value of metallicity in each mass bin (the blue squares for the observational data), while the upper and lower lines represent the 16th and 86th percentiles of the distribution.

Similarly to the best fit model without disruption, the increase in supernova feedback

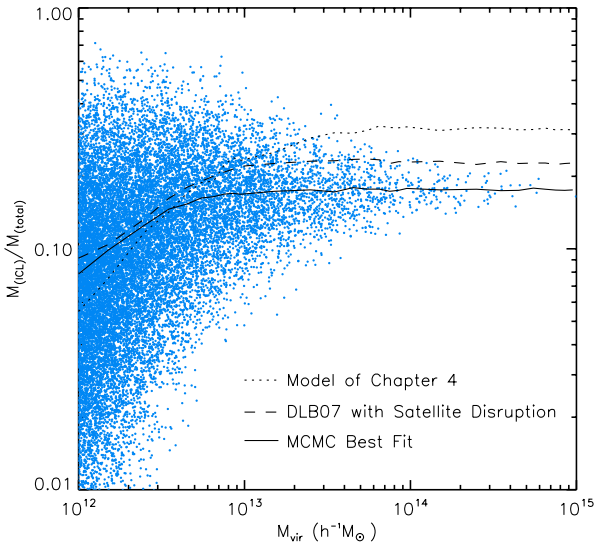

Figure 5.14: Fraction of the mass in the intra-cluster medium over the total stellar mass as a function of virial mass. The blue dots are a representative sample of the total galaxy population in the best fit model with satellite disruption. The solid, dashed and dotted lines represent the median of the $M_{\rm ICL}/\ M_{\rm total}$ distribution respectively for the satellite disruption model with the best fit parameters, the original De Lucia & Blaizot (2007) parameters and for the *a posteriori* model of chapter 4.

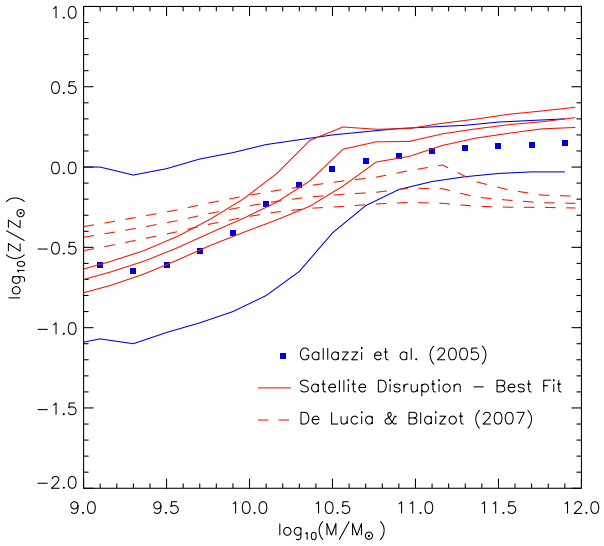

Figure 5.15: Comparison between the metallicity stars in the best fit satellite disruption model (solid red lines), in De Lucia & Blaizot (2007) (dashed red lines) and in observations from Gallazzi et al. (2005) (blue squares and lines). For all the data sets, the central line represents the median value of metallicity in each mass bin (the blue squares for the observational data), while the upper and lower lines represent the 16th and 86th percentiles of the distribution.

required by the MCMC lowers the metallicity of stars in our disruption model. As explained in section 5.2, the introduction of disruption increases the metallicity of massive objects, by reducing the amount of low metallicity material that they receive from mergers. This, combined with the higher metallicity of the gas in the external reservoirs that cools down in massive galaxies, means that our best fit model slightly over-predicts the metallicity of these objects. However, the agreement with observations is significantly better than in the original De Lucia & Blaizot (2007) model and could in principle be improved by including this property as a constraint on the MCMC sampling.

5.5 Discussion

In chapter 3, we introduced a new approach to galaxy formation modelling. Combining the MCMC sampling techniques with semi-analytic models, allowed us to gain insight into the relative importance of the different physics present in these models in shaping the galaxy population. Furthermore, these techniques made it straightforward to understand how well the model can fit a set of observations and what regions in parameter space correspond to a model with an acceptable likelihood. For this reason, the MCMC tools

can be of crucial importance when new physics are introduced in the model, since they will clearly show the impact of new recipes on the ones already present in the model and on the likelihood distribution in parameter space.

In this chapter we implement a new physical ingredient in the semi-analytic recipe: the disruption of satellite galaxies by tidal forces, during merging events. The concept had already been introduced in chapter 4, but only has an *a posteriori* study. That approach, despite enabling us to gain insight on the impact that this process would have in the population of dwarfs, did not allow us to study its effects on galaxies with higher masses and on the other semi-analytic physics.

The self-consistent implementation that we describe in this chapter makes it possible to study the impact of disruption on the properties of galaxies of all types and the MCMC sampling allows us to understand if the new process is required or not by observations.

In order to compute the forces acting on satellites and hence the amount of material disrupted, it is first necessary to track their positions. We decide to only apply disruption on type two satellites, the ones that have already been orbiting central galaxies for long enough to have their dark matter halo disrupted and that experience sufficiently large forces to get their material disrupted. However, this means that their positional information from the dark matter simulation is no longer available.

We compute satellite positions by assuming that they follow circular orbits, decaying into the centre due to the effects of dynamical friction. Having their position in relation to the mass distribution of the central object, we can then calculate the point inside the satellite's radius at which its own gravitational binding force equals the tidal force that it experiences from the central galaxy. Any material outside this radius is considered to be unbound and transferred into the intra-cluster medium.

The implementation of disruption allows us to study the loss in mass by satellite galaxies, the slower build up of central galaxies (since they receive less material from satellites) and the growth of the intra-cluster medium component, previously neglected. Without tuning the parameters we present the semi-analytic predictions for the model with the original parameters from De Lucia & Blaizot (2007), but with disruption included. As expected there is a decrease on the number density of galaxies at all luminosity ranges, being more significant at the bright end. In a hierarchical growing Universe, the properties of massive objects at the centre of large groups and clusters are dominated by the material received from highly frequent mergers. The decrease in material received from satellite galaxies also means that central galaxies have larger metallicities, matching observations

without any tuning of parameters needed. Finally, we present predictions for the intra-cluster light, which for this first parameter set correspond to a fraction of ≈20% in clusters.

5.5.1 MCMC Sampling with Satellite Disruption

After implementing satellite disruption self-consistently into the semi-analytic model we perform an identical MCMC sampling to the new model as in chapter 3 for the original De Lucia & Blaizot (2007). The same 30 000 steps are taken and the model compared to the same observational data sets, first separately and then combined to get a final best fit model.

The study with individual constraints allows us to better understand the impact of disruption on each galaxy property and on the other physics present in the model. Significant changes are seen in the individual study of the K-band luminosity function and black hole-bulge mass relation, while the sampling with the colour constraint gives similar results to our previous study.

When the model is only required to fit the observational K-band luminosity function, the best parameters from the MCMC give a predicted luminosity function that correctly reproduces not only the observational number density on each bin, but also its shape over most of the range studied. This is a significant improvement in comparison to the previous model. When the sampling is only constrained by the black hole-bulge mass relation a new correlation appears. The black hole quasar mode ($f_{\rm BH}$) and the star formation efficiency ($\alpha_{\rm SF}$) are now positively correlated, since the first controls the masses of black holes and the second the masses of bulges. The reduced size of the allowed parameter space we got in our previous analysis hid this correlation.

The combination of the three observational tests once more reduces the allowed region in parameters space. The new best fit parameter set and respective 2σ confidence limits are given by: $\alpha_{\rm SF} = 0.16^{+0.13}_{-0.14}$, $k_{\rm AGN} = (6.9^{+4.8}_{-2.2}) \times 10^{-6}$, $f_{\rm BH} = 0.057^{+0.029}_{-0.044}$, $\epsilon_{\rm disk} = 9.06^{+2.94}_{-6.28}$, $\epsilon_{\rm halo} = 0.44^{+0.1}_{-0.29}$ and $\gamma_{\rm ej} = 0.24^{+0.27}_{-0.21}$). Despite the introduction of a new physical recipe, all the parameter values in the original De Lucia & Blaizot (2007) fall within the new confidence regions. We interpret this as an indication of the physical meaning of the parameters, very well constrained by comprehensive observational data sets.

The new best fit has a considerably higher star formation efficiency in order to correct the reduction in the number density of massive objects caused by disruption. This is, however, slightly balanced in massive galaxies by an increase in the AGN feedback efficiency. At low masses, a less effective supernova feedback is now required, with the higher star

formation efficiency being balanced by a higher reincorporation time-scale. Nevertheless, this form of feedback is still strong and the MCMC requires the same virial velocity cutoff as before, so that it is only effective in dwarf galaxies.

The likelihood for the best fit has more than quadrupled, from the previous value of 0.037 to: $\pi(x_i) = L_{(\mathrm{Mass})} \times L_{(\mathrm{Colour})} \times L_{(\mathrm{BH-Bulge})} = 0.15$. Firstly, this means that the new model is now fully consistent with the combined observational data set we used. Secondly, since we did not introduce any additional parameter to model disruption, it means that the inclusion of the new physical recipe seems to be required by observations.

From the likelihood value of the best fit, it follows that the model predictions show a good agreement with all the observational data sets used as constraints: the K-band luminosity function, the fraction of red galaxies versus stellar mass and the black hole-bulge mass relation. Apart from these, the model reproduces the b_{J}-band luminosity and the stellar mass functions reasonably well. Also, the metallicity of stars is now in better agreement with what is expected from observations. Finally, the introduction of disruption allows us to follow the build up of the intra-cluster medium, which represents 17% of the total light in clusters, as expected from observational studies (between 10% and 30%).

5.5.2 Challenges

Despite the higher likelihood found for the best fit model, semi-analytic predictions are still far from exactly reproducing observations. We analyzed possible improvements in section 3.5.1 and revisit them in the light of the new model.

The biggest challenge for the semi-analytic model is still to reproduce the properties of dwarf galaxies. With the introduction of satellite disruption, the model is able to reproduce the number density of these objects with a less efficient supernova feedback, which is in better agreement with observational studies (Martin, 1999). However, despite decreasing the number of red dwarfs, when compared to observations the model still overproduces the number of these objects in the colour-stellar mass diagram. In observations, the population of passive, red galaxies is dominated by massive objects. Theoretically, despite the peak of massive red galaxies now starting to emerge, red dwarfs are still dominant. As we pointed out in section 3.5.1 stellar disruption is only part of the solution to this problem. An improved treatment of the stripping of gas in satellites might play an even bigger role. As shown by Font et al. (2008), if the gas in these objects is continuously, instead of instantaneously disrupted, they will be able to form stars and remain on the blue sequence for longer.

The higher likelihood found for the best fit model seems to be directly related to a better agreement between the black hole-bulge mass and the other two constraints. This fact is apparently related to the slower build up of bulges in large galaxies, due to the material being transferred into the intra-cluster medium. However, we emphasize the points raised before about the simplicity of the black hole growth model, which still appears to neglect important features, such as the impact of the quasar mode feedback on galaxy properties. In addition, from an observational point of view, larger and more robust data sets of black hole properties are needed to fully constrain theory.

The predictions obtained for the intra-cluster light are in good agreement with observations. However, the available data is still subjected to large error bars, due to the difficulties in distinguish between the light from the brightest cluster galaxies and the intra-cluster medium itself. Also, this component is still only detectable in large groups and clusters due to its low surface brightness. Ideally, to fully constrain the model with satellite disruption, this property should be used. If future improvements in observations make it possible, we will include it in our sampling.

Chapter 6

Conclusion

"In a given day, at given circumstances, you think you have a limit. You then go until that limit, you touch it and you think that is the limit. However, as soon as you touch that limit, something happens and you suddenly can go a little bit further. With your mind power, determination, instinct and the experience as well, you can fly very high."

Ayrton Senna

The main objective of the work presented in this thesis, is to include MCMC sampling techniques in a semi-analytic model of galaxy formation in order to better understand the physics that shape a galaxy population. This was initially done using the last version of the Munich semi-analytic model (De Lucia & Blaizot, 2007) and then with an updated version to include the treatment of satellite disruption.

Over the years, this theoretical model has grown in complexity including more physical recipes and predicting a wide range of observational properties. Presently, it follows the evolution of the gas from when it collapses into a hot phase and as it cools into a disk where stars can form. As the most massive stars die, they eject energy into the surrounding medium, reheating the cold gas back into the hot phase or even ejecting it into the external reservoir. Black hole evolution is modeled and in massive galaxies the mechanical heating from its quiescent growth suppresses the cooling. Mergers generate star formation bursts and depending on the mass ratio between the galaxies, disks are destroyed to form bulges. Finally dust and stellar population synthesis models transform the predicted quantities into galaxy properties that can be compared with observations. With all the recipes in place, the model is able to reasonably predict the shape of the luminosity function in different bands, the stellar mass function, the galaxy colours, the black hole-bulge mass

relation, the metallicity of stars, the Tully-Fisher relation, etc.

However, the growing complexity comes at a cost. The large number of observational properties predicted by the model requires a large number of parameters, some of which are strongly correlated. This creates considerable difficulties in determining how to improve the agreement with new observations without destroying the match with existing data sets. In addition, whenever reasonable agreement proves to be impossible, it is hard to know whether there is a failure in determining the right parameter configuration, whether there is a fundamental problem with the underlying model, or whether the introduction of new physics is required. Another drawback of semi-analytic modelling is that, until now, the level of agreement with observations and the relative weight of different observations in the final choice of the parameters in the model have never been studied in a statistically-consistent way.

The level of agreement with observations achieved in recent versions of the code makes it possible to overcome these difficulties, using statistical tools that have been developed and optimized in theoretical cosmology. In this work, we combine the constraining power of multiple observations with proper sampling of high-dimensional parameter spaces, by means of MCMC parameter estimation. This allows us to understand how each physical process in the model affects each observational property, to quantify the level of agreement between theory and observations, and to identify the need for extra ingredients to be added into semi-analytic modelling.

6.1 MCMC Sampling in the Original Model

In chapter 3 we describe the first application of MCMC techniques done in the original semi-analytic model of De Lucia & Blaizot (2007), using only one of the 512 millennium sub-volumes due to the computational power required. Instead of studying all the free parameters in the model, we decide to restrict the analysis to the 6 parameters controlling star formation and supernova and AGN feedback. This approach makes it easier to learn about the basic physics of the model.

Observational Constraints

After selecting the parameters it is necessary to choose the experimental data that will constrain the sampling. This is of crucial importance and ultimately determines the results. A narrow data set with large error bars will leave the parameters unconstrained, giving large acceptable likelihood regions, producing poor discriminating power. On the

other hand, if the model is required to fit a wide range of observational properties, we might be left without any region with acceptable likelihood. These concerns led us to extensively analyze observational data sets. First to identify what observations uniquely define a galaxy population, and then to understand what level of agreement should be required from a theoretical model, by looking at the scatter between different data sets of the same galaxy observables.

For our analysis we choose to combine three different data sets. The K-band luminosity function, the fraction of red galaxies versus stellar mass and the black hole-bulge mass relation. The statistical tests chosen to compute the model likelihood reflect the characteristics of each property. The agreement between luminosity functions is computed using a chi-square test, with observational error bars given by the scatter between three observational data sets. For the fraction of red galaxies a maximum likelihood method is applied, with theoretical errors bars given by the variance on this quantity between different sub-volumes. Finally, the probability from the black hole-bulge mass relation is obtained by dividing the data into only two bins and performing a binomial test on each.

MCMC Output

Both in this sampling on the original model, and later on the new model with satellite disruption, we start by constraining the parameters with each observational property at a time and then combining them. This allows us to understand how each galaxy quantity is affected by each physical recipe in the model and what changes and correlations are created in parameter space by each test.

When all the observations are combined, we obtain the confidence limits for the parameters and the likelihood for the best fit model. The maximum likelihood for the original De Lucia & Blaizot (2007) is 0.037, which despite being a low value, still means that the model is able to match the three quantities together reasonably well.

The best fit represents a combination of changes in parameter space. The significant decrease in the faint end side of the luminosity function requires a considerably more effective supernova feedback, with more gas being ejected into the external reservoir and being reincorporated in a longer time-scale, in order to decrease the amount of star formation in these objects. To ensure that enough stars will still form in $L_\star$ galaxies, this form of feedback can only be effective for dwarfs, which is achieved by decreasing the virial velocity cutoff above which gas can no longer be ejected. This also makes $L_\star$ galaxies bluer than before, in agreement with the colour constraint. This cutoff is highly constrained

in our sampling and is given by the ratio between $\epsilon_{\rm halo}$ and $\epsilon_{\rm disk}$ (equation 3.10), shown as a positive correlation between the two parameters. When only the luminosity function and colour constraints are considered, the two black hole parameters show a negative correlation. These quantities only require a fixed amount of AGN feedback (and hence of mechanical heating) that can be achieved by varying both parameters in opposite directions (equation 3.11). The black hole-bulge mass relation breaks the degeneracy by fixing the quasar mode, the main responsible for the black hole growth.

Remaining Challenges

We interpret the difference between the acceptable likelihood regions required by the black hole-bulge mass constraint and the other two tests as the main cause for the low likelihood of the best fit model. The discrepancy can either be caused by an inadequate modelling of black hole physics (for example not including the feedback from the quasar mode), or by wider problems in the conversions between theoretical and observable quantities using stellar population synthesis and dust models. Recent studies (Maraston, 2005; Conroy et al., 2008) showed that the assumptions used in these models can significantly affect the comparison between theory and observations and make it premature to assume that more fundamental properties of semi-analytic models are ruled out.

Additional problems arise from this first study. The change in parameters from the original model to the best fit allows the model to correctly predict the number density of dwarfs. Nevertheless, this is achieved by assuming an extremely effective supernova feedback, which seems to be exaggerated in comparison to what observations require (Martin, 1999). Moreover, the colour-stellar mass plot shows that the predicted dwarf galaxies are predominately red, in contradiction with observations (Fig. 3.12). These two aspects seem to indicate an inadequate treatment of the physics of dwarfs in semi-analytic models.

The population of excessive dwarfs is dominated by satellite galaxies that have lost their dark matter halo and gas content and have therefore stopped forming stars. The delayed stripping of gas from satellite proposed by Font et al. (2008) could be one of the solutions, causing a shift of the red dwarfs back into the blue population. Since they can retain their gas for longer, they will form stars and stay bluer until later times. However, this process can only change the colour of dwarf galaxies and cannot help to reduce their excessive number.

Another process that can in principle reduce the excessive number of dwarfs and dir-

ectly make blue dwarfs predominant, is the disruption of stellar material from satellites by tidal forces. This could in principle move dwarf satellites to lower mass bins (below the resolution limit), where an upturn in the stellar mass and luminosity functions is seen. At the same time, since almost all satellites are red, this would increase the relative fraction of blue versus red dwarfs in our low mass bins.

6.2 The Population of Dwarf Galaxies

In chapter 4 we introduce the concept of satellite galaxy disruption in the Munich semi-analytic model. We do so, by assuming that at redshift zero all the satellites that have already lost their dark matter halo (type 2 galaxies) will also have all their stellar material disrupted and transferred into the intra-cluster medium.

The disruption of satellites material due to tidal forces is a continuous and partial process. Since in this chapter, we do not follow disruption effects over redshift we cannot predict the changes on central galaxies. In particular, their slower growth due to the smaller fraction of material they would receive from satellites. Nevertheless, it does give us an idea of the upper limit of the effects that this process would have on dwarf galaxies.

The simplified approach we follow in this chapter generates three main improvements in the model. First, it does reduce the number density of dwarfs, bringing the faint end of the luminosity functions and the low mass end of the stellar mass functions into a better agreement with observations. Secondly, it suppresses the number density of red dwarfs in the colour-magnitude diagrams, making blue galaxies predominant around our resolution limit. Finally, it predicts the relative fraction of light in the intra-cluster medium (30%) and its colour (red), both in agreement with observations.

The study done in this chapter emphasizes the conclusion of chapter 3, that satellite disruption might play a crucial role in bringing the properties of dwarf galaxies into agreement with observations. For this reason, we implement it self-consistently into the model in the last chapter of this thesis and use MCMC statistical techniques to verify if the changes introduced are indeed required by observations.

6.3 MCMC Sampling in the Satellite Disruption Model

Implementing Satellite Disruption

In chapter 5 we introduce satellite disruption self-consistently into the semi-analytic model. In order to compute the forces acting on satellite galaxies we first have to follow their

positions. Since these galaxies have already lost their dark matter halo, we need to assume that they follow circular orbits, decaying to centre of the potential due to dynamical friction. After calculating their position, we compute the distance from the satellite centre at which the sum of the tidal force from the parent halo and the centrifugal force equal the self gravitational force of the satellite. Any material outside this radius is assumed to be disrupted and added to the intra-cluster component.

The self-consistent treatment of disruption introduces significant changes when compared to our simplified approach. Since the process is now less dramatic, the changes seen in satellite galaxies, despite following the previous predictions, are less significant. On the other hand, we can now follow the effects on massive galaxies, which are now strongly affected. With the disruption of material from satellites, the most massive galaxies (that reside in the centre of large groups and clusters) have a much weaker growth, leading to a strong suppression of the bright end side of the K-band luminosity function at redshift zero. For the same reason, these massive objects receive less low metallicity material and their stars have higher metallicities in agreement with observations. Finally, the predicted fraction of intra-cluster material remains the same as in our simplified approach, with a value corresponding to $\approx$30% of the mass in clusters.

After introducing the new physical recipe, we apply the MCMC techniques developed in chapter 3 to the new model, in order to understand how the new ingredient affects existing physics and if it can raise the model likelihood when compared to the same observational data sets.

As in chapter 3, we start by performing the study with separate constraints. The sampling with the colour constraint shows similar results to that of the original model, while the best fit for the K-band luminosity function reproduces not only the number density, but also the observational shape considerably better than before. The black hole-bulge mass relation is once more combined with the K-band test for the most massive objects to avoid an excessive freedom of the parameters, in this case showing substantial changes from the previous sampling. The acceptable likelihood region in parameter space becomes wider and the correlations seen in the test for the luminosity function show up. More important a correlation between the black hole quasar mode and the star formation rate is now apparent. This previously hidden correlation, shows that the quasar mode is indeed responsible for the black hole mass growth and the star formation efficiency determinant for the growth of bulges.

MCMC Output

After performing the analysis with individual constraints we run the MCMC with the three data sets combined to obtain a best fit for the satellite disruption model. The results from our implementation of disruption without any parameter optimization do not show any improvement in model predictions. However, that is not the case once the MCMC sampling is performed, with the best fit model with disruption having a likelihood of 0.15. This likelihood value is three times higher than what was found for the original model, meaning that the theoretical predictions are now consistent with the data. Furthermore, since no additional parameter was introduced it also means that satellite disruption seems indeed to be required by observations.

Qualitatively, the final predictions for the observable properties used to constrain the sampling are similar to those from the original model, with both matching observations reasonably well. However, the disruption model does help to reduce the amount of red dwarfs in the low mass end of the colour-stellar mass plot. Moreover, despite not being constrained to fit the metallicity of galaxies, it produces an almost perfect match with observations of this property. Finally it has predictions for the intra-cluster material, which for the best fit represents 20% of the mass in clusters, also in agreement with observations (between 10% and 30%).

In terms of the parameter values, a considerably larger star formation rate is now needed to repopulate the bright end side of the K-band luminosity function. This is balanced at the faint end by a longer reincorporation time-scale. Despite still requiring a large supernova feedback efficiency to reduce the number density of dwarfs, the contribution of disruption means that the overall energy required from this process is now smaller.

6.4 Pathways to a Better Understanding of Galaxy Formation

Model Physics

Despite the higher likelihood achieved with the introduction of satellite disruption in the semi-analytic model, a number of questions remain to be solved. Most notably, the model is still unable to reproduce the properties of dwarf galaxies. With the disruption of satellites in place, the model correctly predicts the number density of these objects. However, it still overproduces the number of small passive objects in the colour-stellar mass diagram. As we pointed out throughout this work, stellar disruption is only part of the solution to

this problem. An improved treatment of the stripping of gas in satellites might play an even bigger role. As shown by Font et al. (2008), if the gas in these objects is continuously, instead of instantaneously disrupted, they will be able to form stars and remain in the blue sequence for longer.

Another open question concerns the treatment of black holes. In the final model, the black hole-bulge mass relation becomes consistent with the observational constraints. Even so, the black hole model still seems too simplistic, namely by disregarding the impact of quasar mode feedback on the galaxy properties. As shown by Bower et al. (2008); Short & Thomas (2008), this form of feedback might be necessary in massive galaxies, in order to reproduce the X-ray luminosity function of halos.

On top of the specific physics adopted for galaxy formation, another crucial aspect that needs further study is the impact of the adopted cosmology on the predicted galaxy properties. From an observational point of view, the values for the cosmological parameters (like σ_8 or $\Omega_{\rm matter}$) are systematically updated. To accordingly update the dark matter simulations, in which semi-analytic models are built, is computationally unfeasible. It is then necessary to understand the impact that changing the cosmological paradigm has on galaxies, without re-simulating them.

Conversion to Observables

A crucial part of galaxy formation theory is the conversion between predicted and observable quantities. The models predict fundamental quantities such as masses and star formation rates, which are not obtained directly from observations and need to be converted into luminosities. Whenever a fraction of cold gas is turned into stars, stellar population synthesis models are used to predict the corresponding change in the galaxy luminosities, knowing the age and metallicity of the population and assuming a certain initial mass function. For many years, these conversions have been treated as flawless and their impact on the final predictions remained untested. Recently, some groups showed that the different treatment of the post main sequence evolution of stars can result in dramatic changes in the mass-to-light ratios (Maraston, 2005; Conroy et al., 2008). Stellar population synthesis models are part of semi-analytics and have a great impact on their predictions. For this reason, in the future they should be subjected to scrutiny from observational tests and improved accordingly, as any other semi-analytic ingredient.

Another related component of semi-analytic models is dust extinction. Dust models are used compute the fraction of optical light absorbed, giving the corresponding

corrections in the predicted optical/near infra-red luminosities. Different studies have been done in recent years, either by including corrections from different dust components De Lucia & Blaizot (2007), or even by including self-consistent dust models to predicted the amount of light re-emitted in the infrared by dust Baugh et al. (2005). However, the physics of dust are complex and large uncertainties remain on the effects that absorption and re-emission have on galaxy properties.

Higher, Further, Faster

Over the years, semi-analytic models have mostly been focused on predicting galaxy properties at redshift zero. Recent improvements, have enabled theory to achieve a reasonable level of agreement with observations in this specific area. However, as new observations plan to go higher and deeper, unveiling galaxy properties in the full spectra with high quality statistics, the models need to evolve accordingly.

In the near future, it will be possible to determine the evolution of the luminosity and stellar mass functions from the local Universe to high redshift with uncertainties given only by the statistics of large number counts. It remains to be seen if semi-analytic models, which reproduce the number density of objects at redshift zero fairly well, are also capable of correctly predicting the history of mass assembly of galaxies. For the most massive galaxies, for example, hierarchical merging models predict a large growth at latter times. These objects are located at the centre of the largest groups and clusters and are constantly accreting material from merger events. Recent observational studies apparently contradict these predictions, showing a very weak growth of the most massive objects since redshift 2 (Fontana et al., 2006). Future work will tell if more robust observations and improved semi-analytic predictions (for example for the merging processes) can be reconciled.

Another crucial area for future studies of galaxy formation theory is the infra-red emission of galaxies. Star formation occurs in dusty environments and almost half the light emitted in the optical/near UV by stars is absorbed and re-emitted in the infra-red. As this thesis was being finished, the largest ever telescope was sent to orbit, having as one of the main goals, to study the peak of star formation in the Universe. This will be done, by looking at luminous infra-red galaxies at redshift around two. In order to understand the data obtained, a large effort is required from a theoretical point of view. The principle introduced by Baugh et al. (2005) needs to be followed, in order to build semi-analytic models that self-consistently predict both the optical and infra-red emission of galaxies, from the local Universe to high redshift.

Theoretical models of galaxy formation have reached a reasonable level of complexity and their predictive power makes them crucial to understand the ever growing range of physical processes and environments unveiled by observations. However, most of our knowledge relies on approximations of the complex and highly non-linear physics that govern galaxy formation and evolution and a large amount of work remains to be done until we can fully understand them.

Bibliography

Arnaboldi, M., Freeman, K. C., Mendez, R. H., Capaccioli, M., Ciardullo, R., Ford, H., Gerhard, O., Hui, X., Jacoby, G. H., Kudritzki, R. P., & Quinn, P. J. (1996). The Kinematics of the Planetary Nebulae in the Outer Regions of NGC 4406. *ApJ*, 472, 145–+. Cited on 65

Arnaboldi, M., Gerhard, O., Aguerri, J. A. L., Freeman, K. C., Napolitano, N. R., Okamura, S., & Yasuda, N. (2004). The Line-of-Sight Velocity Distributions of Intracluster Planetary Nebulae in the Virgo Cluster Core. *ApJ*, 614, 33–36. Cited on 65

Baldry, I. K., Balogh, M. L., Bower, R. G., Glazebrook, K., Nichol, R. C., Bamford, S. P., & Budavari, T. (2006). Galaxy bimodality versus stellar mass and environment. *MNRAS*, 373, 469–483. Cited on 4, 43, 56, 62, 69, 71

Baldry, I. K. & Glazebrook, K. (2003). Constraints on a Universal Stellar Initial Mass Function from Ultraviolet to Near-Infrared Galaxy Luminosity Densities. *ApJ*, 593, 258–271. Cited on 27, 28

Baldry, I. K., Glazebrook, K., Brinkmann, J., Ivezić, Ž., Lupton, R. H., Nichol, R. C., & Szalay, A. S. (2004). Quantifying the Bimodal Color-Magnitude Distribution of Galaxies. *ApJ*, 600, 681–694. Cited on 4, 43, 44, 45, 55, 60, 69, 70, 71, 86, 87, 102

Baldry, I. K., Glazebrook, K., & Driver, S. P. (2008). On the galaxy stellar mass function, the mass-metallicity relation and the implied baryonic mass function. *MNRAS*, 388, 945–959. Cited on 4, 56, 57, 58, 71, 72, 85

Baugh, C. M. (2006). A primer on hierarchical galaxy formation: the semi-analytical approach. *Reports on Progress in Physics*, 69, 3101–3156. Cited on 1

Baugh, C. M., Cole, S., & Frenk, C. S. (1996a). Evolution of the Hubble sequence in hierarchical models for galaxy formation. *MNRAS*, 283, 1361–1378. Cited on 7

Baugh, C. M., Cole, S., & Frenk, C. S. (1996b). Faint galaxy counts as a function of morphological type in a hierarchical merger model. *MNRAS*, 282, L27–L32. Cited on 7

Baugh, C. M., Lacey, C. G., Frenk, C. S., Granato, G. L., Silva, L., Bressan, A., Benson, A. J., & Cole, S. (2005). Can the faint submillimetre galaxies be explained in the Λ cold dark matter model? *MNRAS*, 356, 1191–1200. Cited on 118

Bell, E. F., McIntosh, D. H., Katz, N., & Weinberg, M. D. (2003). The Optical and Near-Infrared Properties of Galaxies. I. Luminosity and Stellar Mass Functions. *ApJ Supp.*, 149, 289–312. Cited on 4, 39, 40, 45, 54, 56, 57, 58, 60, 71, 72, 82, 83, 85, 91, 100

Benson, A. J., Bower, R. G., Frenk, C. S., Lacey, C. G., Baugh, C. M., & Cole, S. (2003). What Shapes the Luminosity Function of Galaxies? *ApJ*, 599, 38–49. Cited on 8

Benson, A. J., Frenk, C. S., Lacey, C. G., Baugh, C. M., & Cole, S. (2002a). The effects of photoionization on galaxy formation - II. Satellite galaxies in the Local Group. *MNRAS*, 333, 177–190. Cited on 8

Benson, A. J., Lacey, C. G., Baugh, C. M., Cole, S., & Frenk, C. S. (2002b). The effects of photoionization on galaxy formation - I. Model and results at z=0. *MNRAS*, 333, 156–176. Cited on 8, 20, 62, 66, 68

Bernstein, G. M., Nichol, R. C., Tyson, J. A., Ulmer, M. P., & Wittman, D. (1995). The Luminosity Function of the Coma Cluster Core for $-25 < M/R < -9.4$. *AJ*, 110, 1507–+. Cited on 65, 73, 87

Bertone, S., De Lucia, G., & Thomas, P. A. (2007). The recycling of gas and metals in galaxy formation: predictions of a dynamical feedback model. *MNRAS*, 379, 1143–1154. Cited on 10, 62, 69

Binney, J. & Tremaine, S. (1987). *Galactic dynamics*. Princeton, NJ, Princeton University Press, 1987, 747 p. Cited on 25, 78, 81

Blanton, M. R., Lupton, R. H., Schlegel, D. J., Strauss, M. A., Brinkmann, J., Fukugita, M., & Loveday, J. (2005). The Properties and Luminosity Function of Extremely Low Luminosity Galaxies. *ApJ*, 631, 208–230. Cited on 4

Bower, R. G., Benson, A. J., Malbon, R., Helly, J. C., Frenk, C. S., Baugh, C. M., Cole, S., & Lacey, C. G. (2006). Breaking the hierarchy of galaxy formation. *MNRAS*, 370, 645–655. Cited on xii, 9, 52, 53, 69

Bower, R. G., McCarthy, I. G., & Benson, A. J. (2008). The flip side of galaxy formation: a combined model of galaxy formation and cluster heating. *MNRAS*, 390, 1399–1410. Cited on 10, 23, 61, 117

Brinchmann, J., Charlot, S., White, S. D. M., Tremonti, C., Kauffmann, G., Heckman, T., & Brinkmann, J. (2004). The physical properties of star-forming galaxies in the low-redshift Universe. *MNRAS*, 351, 1151–1179. Cited on 43

Bruzual, G. & Charlot, S. (2003). Stellar population synthesis at the resolution of 2003. *MNRAS*, 344, 1000–1028. Cited on 28, 29

Budavári, T., Connolly, A. J., Szalay, A. S., et al. (2003). Angular Clustering with Photometric Redshifts in the Sloan Digital Sky Survey: Bimodality in the Clustering Properties of Galaxies. *ApJ*, 595, 59–70. Cited on 4

Bullock, J. S., Kravtsov, A. V., & Weinberg, D. H. (2000). Reionization and the Abundance of Galactic Satellites. *ApJ*, 539, 517–521. Cited on 8, 20

Bullock, J. S., Kravtsov, A. V., & Weinberg, D. H. (2001). Hierarchical Galaxy Formation and Substructure in the Galaxy's Stellar Halo. *ApJ*, 548, 33–46. Cited on 62, 66, 68

Calcáneo-Roldán, C., Moore, B., Bland-Hawthorn, J., Malin, D., & Sadler, E. M. (2000). Galaxy destruction and diffuse light in clusters. *MNRAS*, 314, 324–333. Cited on 65

Cattaneo, A., Dekel, A., Devriendt, J., Guiderdoni, B., & Blaizot, J. (2006). Modelling the galaxy bimodality: shutdown above a critical halo mass. *MNRAS*, 370, 1651–1665. Cited on 9

Chabrier, G. (2003). Galactic Stellar and Substellar Initial Mass Function. *PASP*, 115, 763–795. Cited on 27, 28, 45, 58

Chandrasekhar, S. (1943). Dynamical Friction. I. General Considerations: the Coefficient of Dynamical Friction. *ApJ*, 97, 255–+. Cited on 78

Charlot, S. & Fall, S. M. (2000). A Simple Model for the Absorption of Starlight by Dust in Galaxies. *ApJ*, 539, 718–731. Cited on 29, 30

Coil, A. L., Newman, J. A., Cooper, M. C., Davis, M., Faber, S. M., Koo, D. C., & Willmer, C. N. A. (2006). The DEEP2 Galaxy Redshift Survey: Clustering of Galaxies as a Function of Luminosity at z = 1. *ApJ*, 644, 671–677. Cited on 4

Cole, S. (1991). Modeling galaxy formation in evolving dark matter halos. *ApJ*, 367, 45–53. Cited on 6, 60

Cole, S., Aragon-Salamanca, A., Frenk, C. S., Navarro, J. F., & Zepf, S. E. (1994). A Recipe for Galaxy Formation. *MNRAS*, 271, 781–+. Cited on 6

Cole, S., Lacey, C. G., Baugh, C. M., & Frenk, C. S. (2000). Hierarchical galaxy formation. *MNRAS*, 319, 168–204. Cited on 7

Cole, S., Norberg, P., Baugh, C. M., et al. (2001). The 2dF galaxy redshift survey: near-infrared galaxy luminosity functions. *MNRAS*, 326, 255–273. Cited on 4, 39, 40, 54, 60, 82, 83, 91, 100

Cole, S., Percival, W. J., Peacock, J. A., et al. (2005). The 2dF Galaxy Redshift Survey: power-spectrum analysis of the final data set and cosmological implications. *MNRAS*, 362, 505–534. Cited on 2

Colless, M., Dalton, G., Maddox, S., et al. (2001). The 2dF Galaxy Redshift Survey: spectra and redshifts. *MNRAS*, 328, 1039–1063. Cited on 2

Conroy, C., Gunn, J. E., & White, M. (2008). The propagation of uncertainties in stellar population synthesis modeling I: The relevance of uncertain aspects of stellar evolution and the IMF to the derived physical properties of galaxies. *ArXiv e-prints*. Cited on 29, 58, 113, 117

Conroy, C., Wechsler, R. H., & Kravtsov, A. V. (2007). The Hierarchical Build-Up of Massive Galaxies and the Intracluster Light since z = 1. *ApJ*, 668, 826–838. Cited on 66

Crenshaw, D. M., Kraemer, S. B., & George, I. M. (2003). Mass Loss from the Nuclei of Active Galaxies. *ARA&A*, 41, 117–167. Cited on 23

Croton, D. J., Springel, V., White, S. D. M., De Lucia, G., Frenk, C. S., Gao, L., Jenkins, A., Kauffmann, G., Navarro, J. F., & Yoshida, N. (2006). The many lives of active galactic nuclei: cooling flows, black holes and the luminosities and colours of galaxies. *MNRAS*, 365, 11–28. Cited on xii, 9, 11, 16, 32, 38, 45, 52, 53, 62, 66, 69, 73

Daigne, F., Olive, K. A., Vangioni-Flam, E., Silk, J., & Audouze, J. (2004). Cosmic Star Formation, Reionization, and Constraints on Global Chemical Evolution. *ApJ*, 617, 693–706. Cited on 8, 33

De Lucia, G. & Blaizot, J. (2007). The hierarchical formation of the brightest cluster galaxies. *MNRAS*, 375, 2–14. Cited on xi, xii, 9, 11, 13, 16, 17, 24, 32, 33, 38, 39, 40, 42, 43, 44, 45, 47, 50, 51, 53, 54, 55, 56, 57, 59, 60, 61, 62, 63, 66, 67, 69, 71, 73, 74, 76, 78, 82, 83, 84, 85, 86, 87, 89, 90, 91, 94, 98, 99, 100, 101, 102, 103, 104, 105, 106, 107, 110, 111, 112, 118

De Lucia, G., Kauffmann, G., & White, S. D. M. (2004). Chemical enrichment of the intracluster and intergalactic medium in a hierarchical galaxy formation model. *MNRAS*, 349, 1101–1116. Cited on 8, 11, 16, 18, 21, 22, 32

Devriendt, J. E. G., Guiderdoni, B., & Sadat, R. (1999). Galaxy modelling. I. Spectral energy distributions from far-UV to sub-mm wavelengths. *Astronomy and Astrophysics Supplement Series*, 350, 381–398. Cited on 29

Djorgovski, S. & Davis, M. (1987). Fundamental properties of elliptical galaxies. *ApJ*, 313, 59–68. Cited on 81

Drinkwater, M. J., Jones, J. B., Gregg, M. D., & Phillipps, S. (2000). Compact stellar systems in the Fornax Cluster: Super-massive star clusters or extremely compact dwarf galaxies? *Publications of the Astronomical Society of Australia*, 17, 227–233. Cited on 66

Durrell, P. R., Ciardullo, R., Feldmeier, J. J., Jacoby, G. H., & Sigurdsson, S. (2002). Intracluster Red Giant Stars in the Virgo Cluster. *ApJ*, 570, 119–131. Cited on 65

Efstathiou, G. (1992). Suppressing the formation of dwarf galaxies via photoionization. *MNRAS*, 256, 43P–47P. Cited on 20

Eisenstein, D. J., Zehavi, I., Hogg, D. W., et al. (2005). Detection of the Baryon Acoustic Peak in the Large-Scale Correlation Function of SDSS Luminous Red Galaxies. *ApJ*, 633, 560–574. Cited on 2

Faber, S. M. & Jackson, R. E. (1976). Velocity dispersions and mass-to-light ratios for elliptical galaxies. *ApJ*, 204, 668–683. Cited on 81

Fabian, A. C., Sanders, J. S., Allen, S. W., Crawford, C. S., Iwasawa, K., Johnstone, R. M., Schmidt, R. W., & Taylor, G. B. (2003). A deep Chandra observation of the Perseus cluster: shocks and ripples. *MNRAS*, 344, L43–L47. Cited on 4

Faltenbacher, A. & Mathews, W. G. (2005). On the dynamics of the satellite galaxies in NGC 5044. *MNRAS*, 362, 498–504. Cited on 66

Feldmeier, J. J., Ciardullo, R., Jacoby, G. H., & Durrell, P. R. (2003). Intracluster Planetary Nebulae in the Virgo Cluster. II. Imaging Catalog. *ApJ Supp.*, 145, 65–81. Cited on 65

Feldmeier, J. J., Ciardullo, R., Jacoby, G. H., & Durrell, P. R. (2004a). Intracluster Planetary Nebulae in the Virgo Cluster. III. Luminosity of the Intracluster Light and Tests of the Spatial Distribution. *ApJ*, 615, 196–208. Cited on 65

Feldmeier, J. J., Mihos, J. C., Morrison, H. L., Harding, P., Kaib, N., & Dubinski, J. (2004b). Deep CCD Surface Photometry of Galaxy Clusters. II. Searching for Intracluster Starlight in Non-cD clusters. *ApJ*, 609, 617–637. Cited on 65, 73, 87

Feldmeier, J. J., Mihos, J. C., Morrison, H. L., Rodney, S. A., & Harding, P. (2002). Deep CCD Surface Photometry of Galaxy Clusters. I. Methods and Initial Studies of Intracluster Starlight. *ApJ*, 575, 779–800. Cited on 65, 73, 87

Ferreras, I., Charlot, S., & Silk, J. (1999). The Age and Metallicity Range of Early-Type Galaxies in Clusters. *ApJ*, 521, 81–89. Cited on 58

Font, A. S., Bower, R. G., McCarthy, I. G., Benson, A. J., Frenk, C. S., Helly, J. C., Lacey, C. G., Baugh, C. M., & Cole, S. (2008). The colours of satellite galaxies in groups and clusters. *MNRAS*, 389, 1619–1629. Cited on 10, 63, 108, 113, 117

Fontana, A., Salimbeni, S., Grazian, A., et al. (2006). The Galaxy mass function up to z =4 in the GOODS-MUSIC sample: into the epoch of formation of massive galaxies. *Astronomy and Astrophysics Supplement Series*, 459, 745–757. Cited on 118

Fukugita, M., Ichikawa, T., Gunn, J. E., Doi, M., Shimasaku, K., & Schneider, D. P. (1996). The Sloan Digital Sky Survey Photometric System. *AJ*, 111, 1748–+. Cited on 43

Gal-Yam, A., Maoz, D., Guhathakurta, P., & Filippenko, A. V. (2003). A Population of Intergalactic Supernovae in Galaxy Clusters. *AJ*, 125, 1087–1094. Cited on 65

Gallazzi, A., Charlot, S., Brinchmann, J., White, S. D. M., & Tremonti, C. A. (2005). The ages and metallicities of galaxies in the local universe. *MNRAS*, 362, 41–58. Cited on 59, 89, 103, 105

Gelman, A. & Rubin, D. B. (1992). Inference from iterative simulation using multiple sequences. *Statistical Science*, 7, 457–472. Cited on 35

Gnedin, N. Y. (2000). Effect of Reionization on Structure Formation in the Universe. *ApJ*, 542, 535–541. Cited on 20, 21

Gnedin, O. Y. (2003). Dynamical Evolution of Galaxies in Clusters. *ApJ*, 589, 752–769. Cited on 65

Gonzalez, A. H., Zabludoff, A. I., & Zaritsky, D. (2005). Intracluster Light in Nearby Galaxy Clusters: Relationship to the Halos of Brightest Cluster Galaxies. *ApJ*, 618, 195–213. Cited on 65, 73, 87

Gonzalez, A. H., Zabludoff, A. I., Zaritsky, D., & Dalcanton, J. J. (2000). Measuring the Diffuse Optical Light in Abell 1651. *ApJ*, 536, 561–570. Cited on 65, 73, 87

Granato, G. L., De Zotti, G., Silva, L., Bressan, A., & Danese, L. (2004). A Physical Model for the Coevolution of QSOs and Their Spheroidal Hosts. *ApJ*, 600, 580–594. Cited on 9

Gregg, M. D. & West, M. J. (1998). Galaxy disruption as the origin of intracluster light in the Coma cluster of galaxies. *Nat.*, 396, 549–552. Cited on 65

Guiderdoni, B. & Rocca-Volmerange, B. (1987). A model of spectrophotometric evolution for high-redshift galaxies. *Astronomy and Astrophysics Supplement Series*, 186, 1–2. Cited on 30

Häring, N. & Rix, H.-W. (2004). On the Black Hole Mass-Bulge Mass Relation. *ApJ*, 604, L89–L92. Cited on 4, 23, 46, 47, 57, 60, 103

Hastings, W. K. (1970). Monte Carlo Sampling Methods Using Markov Chains and their Applications. *Biometrika*, 57, 97–109. Cited on 34

Hatton, S., Devriendt, J. E. G., Ninin, S., Bouchet, F. R., Guiderdoni, B., & Vibert, D. (2003). GALICS- I. A hybrid N-body/semi-analytic model of hierarchical galaxy formation. *MNRAS*, 343, 75–106. Cited on 8

Henriques, B. M., Bertone, S., & Thomas, P. A. (2008). The effect of dwarf galaxy disruption in semi-analytic models. *MNRAS*, 383, 1649–1654. Cited on 62, 63, 67

Henriques, B. M. B., Thomas, P. A., Oliver, S., & Roseboom, I. (2009). Monte Carlo Markov Chain parameter estimation in semi-analytic models of galaxy formation. *MNRAS*, 396, 535–547. Cited on 33

Hernquist, L. (1990). An analytical model for spherical galaxies and bulges. *ApJ*, 356, 359–364. Cited on 80

Hilker, M., Baumgardt, H., Infante, L., Drinkwater, M., Evstigneeva, E., & Gregg, M. (2007). Dynamical masses of ultra-compact dwarf galaxies in Fornax. *Astronomy and Astrophysics Supplement Series*, 463, 119–130. Cited on 66

Hilker, M., Infante, L., Vieira, G., Kissler-Patig, M., & Richtler, T. (1999). The central region of the Fornax cluster. II. Spectroscopy and radial velocities of member and background galaxies. *Astronomy and Astrophysics Supplement Series*, 134, 75–86. Cited on 66

Huang, J.-S., Glazebrook, K., Cowie, L. L., & Tinney, C. (2003). The Hawaii+Anglo-Australian Observatory K-Band Galaxy Redshift Survey. I. The Local K-Band Luminosity Function. *ApJ*, 584, 203–209. Cited on 52, 53

Ikeuchi, S. (1986). The baryon clump within an extended dark matter region. *Ap. & Sp. Sci.*, 118, 509–514. Cited on 20

Jones, D. H., Peterson, B. A., Colless, M., & Saunders, W. (2006). Near-infrared and optical luminosity functions from the 6dF Galaxy Survey. *MNRAS*, 369, 25–42. Cited on 4, 39, 40, 54, 60, 71, 72, 82, 83, 84, 91, 100

Kampakoglou, M., Trotta, R., & Silk, J. (2008). Monolithic or hierarchical star formation? A new statistical analysis. *MNRAS*, 384, 1414–1426. Cited on 33

Kang, X., Jing, Y. P., Mo, H. J., & Börner, G. (2005). Semianalytical Model of Galaxy Formation with High-Resolution N-Body Simulations. *ApJ*, 631, 21–40. Cited on 8

Kauffmann, G. (1995a). Hierarchical clustering and the Butcher-Oemler effect. *MNRAS*, 274, 153–160. Cited on 7

Kauffmann, G. (1995b). The observed properties of high-redshift cluster galaxies. *MNRAS*, 274, 161–170. Cited on 7

Kauffmann, G. (1996a). Disc galaxies at z=0 and at high redshift: an explanation of the observed evolution of damped Lyalpha absorption systems. *MNRAS*, 281, 475–486. Cited on 7

Kauffmann, G. (1996b). The age of elliptical galaxies and bulges in a merger model. *MNRAS*, 281, 487–492. Cited on 7, 19

Kauffmann, G., Colberg, J., Diaferio, A., & White, S. (1999). Clustering of galaxies in a hierarchical universe - I. Methods and results at z=0. *MNRAS*, 303, 188–206. Cited on 7, 8, 9, 16

Kauffmann, G., Guiderdoni, B., & White, S. D. M. (1994). Faint Galaxy Counts in a Hierarchical Universe. *MNRAS*, 267, 981–+. Cited on 7

Kauffmann, G. & Haehnelt, M. (2000). A unified model for the evolution of galaxies and quasars. *MNRAS*, 311, 576–588. Cited on 7, 23, 32

Kauffmann, G., Heckman, T. M., White, S. D. M., et al. (2003). Stellar masses and star formation histories for 10^5 galaxies from the SDSS. *MNRAS*, 341, 33–53. Cited on 43

Kauffmann, G., White, S. D. M., & Guiderdoni, B. (1993). The Formation and Evolution of Galaxies Within Merging Dark Matter Haloes. *MNRAS*, 264, 201–+. Cited on 6

Kennicutt, Jr., R. C. (1983). The rate of star formation in normal disk galaxies. *ApJ*, 272, 54–67. Cited on 28

Kennicutt, Jr., R. C. (1998). The Global Schmidt Law in Star-forming Galaxies. *ApJ*, 498, 541–+. Cited on 19

King, I. (1962). The structure of star clusters. I. an empirical density law. *AJ*, 67, 471–+. Cited on 78

Kormendy, J. (1977). Brightness distributions in compact and normal galaxies. II - Structure parameters of the spheroidal component. *ApJ*, 218, 333–346. Cited on 81

Kravtsov, A. V., Gnedin, O. Y., & Klypin, A. A. (2004). The Tumultuous Lives of Galactic Dwarfs and the Missing Satellites Problem. *ApJ*, 609, 482–497. Cited on 20, 21, 38

Krick, J. E., Bernstein, R. A., & Pimbblet, K. A. (2006). Diffuse Optical Light in Galaxy Clusters. I. Abell 3888. *ApJ*, 131, 168–184. Cited on 65

Kroupa, P. (2001). On the variation of the initial mass function. *MNRAS*, 322, 231–246. Cited on 27, 28

Kroupa, P., Tout, C. A., & Gilmore, G. (1993). The distribution of low-mass stars in the Galactic disc. *MNRAS*, 262, 545–587. Cited on 28

Lacey, C., Guiderdoni, B., Rocca-Volmerange, B., & Silk, J. (1993). Tidally triggered galaxy formation. II - Galaxy number counts. *ApJ*, 402, 15–41. Cited on 6

Lacey, C. & Silk, J. (1991). Tidally triggered galaxy formation. I - Evolution of the galaxy luminosity function. *ApJ*, 381, 14–32. Cited on 6, 60

Lagos, C. D. P., Cora, S. A., & Padilla, N. D. (2008). Effects of AGN feedback on ΛCDM galaxies. *MNRAS*, 388, 587–602. Cited on 9

Lewis, A. & Bridle, S. (2002). Cosmological parameters from CMB and other data: A Monte Carlo approach. *Phys. Rev.*, 66(10), 103511–+. Cited on 39

Madau, P., Ferguson, H. C., Dickinson, M. E., Giavalisco, M., Steidel, C. C., & Fruchter, A. (1996). High-redshift galaxies in the Hubble Deep Field: colour selection and star formation history to z˜4. *MNRAS*, 283, 1388–1404. Cited on 4

Madgwick, D. S., Lahav, O., Baldry, I. K., , et al. (2002). The 2dF Galaxy Redshift Survey: galaxy luminosity functions per spectral type. *MNRAS*, 333, 133–144. Cited on 73, 74

Maraston, C. (2005). Evolutionary population synthesis: models, analysis of the ingredients and application to high-z galaxies. *MNRAS*, 362, 799–825. Cited on 29, 58, 113, 117

Martin, C. L. (1996). Kinematic Evidence for Superbubbles in I ZW 18: Constraints on the Star Formation History and Chemical Evolution. *ApJ*, 465, 680–+. Cited on 21

Martin, C. L. (1999). Properties of Galactic Outflows: Measurements of the Feedback from Star Formation. *ApJ*, 513, 156–160. Cited on 21, 62, 64, 108, 113

Mathis, J. S., Mezger, P. G., & Panagia, N. (1983). Interstellar radiation field and dust temperatures in the diffuse interstellar matter and in giant molecular clouds. *Astronomy and Astrophysics Supplement Series*, 128, 212–229. Cited on 30

McCracken, H. J., Peacock, J. A., Guzzo, L., et al. (2007). The Angular Correlations of Galaxies in the COSMOS Field. *ApJ Supp.*, 172, 314–319. Cited on 4

McNamara, B. R., Nulsen, P. E. J., Wise, M. W., Rafferty, D. A., Carilli, C., Sarazin, C. L., & Blanton, E. L. (2005). The heating of gas in a galaxy cluster by X-ray cavities and large-scale shock fronts. *Nat.*, 433, 45–47. Cited on 4

Menci, N., Cavaliere, A., Fontana, A., Giallongo, E., & Poli, F. (2002). Binary Aggregations in Hierarchical Galaxy Formation: The Evolution of the Galaxy Luminosity Function. *ApJ*, 575, 18–32. Cited on 8

Menci, N., Fontana, A., Giallongo, E., Grazian, A., & Salimbeni, S. (2006). The Abundance of Distant and Extremely Red Galaxies: The Role of AGN Feedback in Hierarchical Models. *ApJ*, 647, 753–762. Cited on 9

Merritt, D. (1984). Relaxation and tidal stripping in rich clusters of galaxies. II - Evolution of the luminosity distribution. *ApJ*, 276, 26–37. Cited on 65

Metropolis, N., Rosenbluth, A., Rosenbluth, M., Teller, A., & Teller, E. (1953). Equation of State Calculaions by Fast Computing Machines. *J. Chem. Phys.*, 21, 1087–1092. Cited on 34

Mihos, J. C. (2004). The Evolution of Tidal Debris. In P.-A. Duc, J. Braine, & E. Brinks (Eds.), *Recycling Intergalactic and Interstellar Matter*, volume 217 of *IAU Symposium* (pp. 390–+). Cited on 65

Mihos, J. C. & Hernquist, L. (1996). Gasdynamics and Starbursts in Major Mergers. *ApJ*, 464, 641–+. Cited on 19

Miller, G. E. & Scalo, J. M. (1979). The initial mass function and stellar birthrate in the solar neighborhood. *ApJ Supp.*, 41, 513–547. Cited on 28

Mo, H. J., Mao, S., & White, S. D. M. (1998). The formation of galactic discs. *MNRAS*, 295, 319–336. Cited on 7, 19, 30, 80

Monaco, P. (2004). Physical regimes for feedback in galaxy formation. *MNRAS*, 352, 181–204. Cited on 8

Monaco, P., Fontanot, F., & Taffoni, G. (2007). The MORGANA model for the rise of galaxies and active nuclei. *MNRAS*, 375, 1189–1219. Cited on 9

Monaco, P., Murante, G., Borgani, S., & Fontanot, F. (2006). Diffuse Stellar Component in Galaxy Clusters and the Evolution of the Most Massive Galaxies at z$<\sim$ 1. *ApJ*, 652, L89–L92. Cited on 62, 65, 66, 68, 76

Moore, B., Katz, N., Lake, G., Dressler, A., & Oemler, A. (1996). Galaxy harassment and the evolution of clusters of galaxies. *Nat.*, 379, 613–616. Cited on 65, 76

Murante, G., Arnaboldi, M., Gerhard, O., Borgani, S., Cheng, L. M., Diaferio, A., Dolag, K., Moscardini, L., Tormen, G., Tornatore, L., & Tozzi, P. (2004). The Diffuse Light in Simulations of Galaxy Clusters. *ApJ*, 607, L83–L86. Cited on 65

Murante, G., Giovalli, M., Gerhard, O., Arnaboldi, M., Borgani, S., & Dolag, K. (2007). The importance of mergers for the origin of intracluster stars in cosmological simulations of galaxy clusters. *MNRAS*, 377, 2–16. Cited on 62, 65, 66, 76

Napolitano, N. R., Pannella, M., Arnaboldi, M., Gerhard, O., Aguerri, J. A. L., Freeman, K. C., Capaccioli, M., Ghigna, S., Governato, F., Quinn, T., & Stadel, J. (2003). Intracluster Stellar Population Properties from N-Body Cosmological Simulations. I. Constraints at z = 0. *ApJ*, 594, 172–185. Cited on 65, 76

Navarro, J. F. & Steinmetz, M. (1997). The Effects of a Photoionizing Ultraviolet Background on the Formation of Disk Galaxies. *ApJ*, 478, 13–+. Cited on 20

Neill, J. D., Shara, M. M., & Oegerle, W. R. (2005). Tramp Novae between Galaxies in the Fornax Cluster: Tracers of Intracluster Light. *ApJ*, 618, 692–704. Cited on 65

Norberg, P., Baugh, C. M., Hawkins, E., et al. (2002a). The 2dF Galaxy Redshift Survey: the dependence of galaxy clustering on luminosity and spectral type. *MNRAS*, 332, 827–838. Cited on 4

Norberg, P., Cole, S., Baugh, C. M., et al. (2002b). The 2dF Galaxy Redshift Survey: the b_J -band galaxy luminosity function and survey selection function. *MNRAS*, 336, 907–931. Cited on 4, 54, 71, 72, 83, 84, 91, 100

Peebles, P. J. E. (1980). *The large-scale structure of the universe*. Cited on 15

Percival, W. J., Baugh, C. M., Bland-Hawthorn, J., et al. (2001). The 2dF Galaxy Redshift Survey: the power spectrum and the matter content of the Universe. *MNRAS*, 327, 1297–1306. Cited on 2

Perlmutter, S., Aldering, G., Goldhaber, G., et al. (1999). Measurements of Omega and Lambda from 42 High-Redshift Supernovae. *ApJ*, 517, 565–586. Cited on 3

Pollo, A., Guzzo, L., Le Fèvre, O., et al. (2006). The VIMOS-VLT Deep Survey. Luminosity dependence of clustering at z$\simeq$1. *Astronomy and Astrophysics Supplement Series*, 451, 409–416. Cited on 4

Pounds, K. A., Reeves, J. N., King, A. R., Page, K. L., O'Brien, P. T., & Turner, M. J. L. (2003). A high-velocity ionized outflow and XUV photosphere in the narrow emission line quasar PG1211+143. *MNRAS*, 345, 705–713. Cited on 23

Press, W. H. & Schechter, P. (1974). Formation of Galaxies and Clusters of Galaxies by Self-Similar Gravitational Condensation. *ApJ*, 187, 425–438. Cited on 5

Press, W. H., Teukolsky, A. A., Vetterling, W. T., & Flannery, B. P. (2007). *Numerical Recipes, The Art of Scientific Computing - Third Edition*. ambridge University Press. Cited on 34, 47

Purcell, C. W., Bullock, J. S., & Zentner, A. R. (2007). Shredded Galaxies as the Source of Diffuse Intrahalo Light on Varying Scales. *ApJ*, 666, 20–33. Cited on 73

Rees, M. J. (1986). Lyman absorption lines in quasar spectra - Evidence for gravitationally-confined gas in dark minihaloes. *MNRAS*, 218, 25P–30P. Cited on 20

Richstone, D. O. (1976). Collisions of galaxies in dense clusters. II - Dynamical evolution of cluster galaxies. *ApJ*, 204, 642–648. Cited on 65

Rudick, C. S., Mihos, J. C., & McBride, C. (2006). The Formation and Evolution of Intracluster Light. *ApJ*, 648, 936–946. Cited on 65

Salpeter, E. E. (1955). The Luminosity Function and Stellar Evolution. *ApJ*, 121, 161–+. Cited on 27, 28

Scalo, J. M. (1986). The stellar initial mass function. *Fundamentals of Cosmic Physics*, 11, 1–278. Cited on 28

Seljak, U., Makarov, A., McDonald, P., et al. (2005). Cosmological parameter analysis including SDSS Lyα forest and galaxy bias: Constraints on the primordial spectrum of fluctuations, neutrino mass, and dark energy. *Phys. Rev.*, 71(10), 103515–+. Cited on 2

Seljak, U. & Zaldarriaga, M. (1996). A Line-of-Sight Integration Approach to Cosmic Microwave Background Anisotropies. *ApJ*, 469, 437–+. Cited on 15

Short, C. J. & Thomas, P. A. (2008). Combining semi-analytic models with simulations of galaxy clusters: the need for AGN heating. *ArXiv e-prints*. Cited on 23, 61, 117

Smail, I., Ivison, R. J., & Blain, A. W. (1997). A Deep Sub-millimeter Survey of Lensing Clusters: A New Window on Galaxy Formation and Evolution. *ApJ*, 490, L5+. Cited on 4

Smoot, G. F., Bennett, C. L., Kogut, A., et al. (1992). Structure in the COBE differential microwave radiometer first-year maps. *ApJ*, 396, L1–L5. Cited on 2

Somerville, R. S., Hopkins, P. F., Cox, T. J., Robertson, B. E., & Hernquist, L. (2008). A semi-analytic model for the co-evolution of galaxies, black holes and active galactic nuclei. *MNRAS*, 391, 481–506. Cited on 9, 62, 63, 66, 76

Somerville, R. S. & Primack, J. R. (1999). Semi-analytic modelling of galaxy formation: the local Universe. *MNRAS*, 310, 1087–1110. Cited on 8

Somerville, R. S., Primack, J. R., & Faber, S. M. (2001). The nature of high-redshift galaxies. *MNRAS*, 320, 504–528. Cited on 19

Sommer-Larsen, J., Romeo, A. D., & Portinari, L. (2005). Simulating galaxy clusters - III. Properties of the intracluster stars. *MNRAS*, 357, 478–488. Cited on 65, 76

Spergel, D. N., Bean, R., Doré, O., et al. (2007). Three-Year Wilkinson Microwave Anisotropy Probe (WMAP) Observations: Implications for Cosmology. *ApJ Supp.*, 170, 377–408. Cited on 2

Spergel, D. N., Verde, L., Peiris, H. V., et al. (2003). First-Year Wilkinson Microwave Anisotropy Probe (WMAP) Observations: Determination of Cosmological Parameters. *ApJ Supp.*, 148, 175–194. Cited on 2, 3

Springel, V., White, S. D. M., Jenkins, A., et al. (2005a). Simulations of the formation, evolution and clustering of galaxies and quasars. *Nat.*, 435, 629–636. Cited on 5, 8, 9, 13, 16

Springel, V., White, S. D. M., Jenkins, A., et al. (2005b). Simulations of the formation, evolution and clustering of galaxies and quasars. *Nat.*, 435, 629–636. Cited on 16

Springel, V., White, S. D. M., Tormen, G., & Kauffmann, G. (2001). Populating a cluster of galaxies - I. Results at z=0. *MNRAS*, 328, 726–750. Cited on 9, 15, 16, 18, 26, 67, 75

Strateva, I., Ivezić, Ž., Knapp, G. R., et al. (2001). Color Separation of Galaxy Types in the Sloan Digital Sky Survey Imaging Data. *AJ*, 122, 1861–1874. Cited on 4

Taylor, J. E. & Babul, A. (2001). The Dynamics of Sinking Satellites around Disk Galaxies: A Poor Man's Alternative to High-Resolution Numerical Simulations. *ApJ*, 559, 716–735. Cited on 62, 66, 68, 76, 77

Tegmark, M., Blanton, M. R., Strauss, M. A., et al. (2004). The Three-Dimensional Power Spectrum of Galaxies from the Sloan Digital Sky Survey. *ApJ*, 606, 702–740. Cited on 2

Thomas, D., Maraston, C., Bender, R., & Mendes de Oliveira, C. (2005). The Epochs of Early-Type Galaxy Formation as a Function of Environment. *ApJ*, 621, 673–694. Cited on 4

Thoul, A. A. & Weinberg, D. H. (1996). Hydrodynamic Simulations of Galaxy Formation. II. Photoionization and the Formation of Low-Mass Galaxies. *ApJ*, 465, 608–+. Cited on 20

Trentham, N. & Mobasher, B. (1998). The discovery of a giant debris arc in the Coma cluster. *MNRAS*, 293, 53–+. Cited on 65

Trotta, R. (2008). Bayes in the sky: Bayesian inference and model selection in cosmology. *Contemporary Physics*, 49, 71–104. Cited on 10

Weinmann, S. M., van den Bosch, F. C., Yang, X., & Mo, H. J. (2006a). Properties of galaxy groups in the Sloan Digital Sky Survey - I. The dependence of colour, star formation and morphology on halo mass. *MNRAS*, 366, 2–28. Cited on 4, 43, 44, 55, 86, 102

Weinmann, S. M., van den Bosch, F. C., Yang, X., Mo, H. J., Croton, D. J., & Moore, B. (2006b). Properties of galaxy groups in the Sloan Digital Sky Survey - II. Active galactic nucleus feedback and star formation truncation. *MNRAS*, 372, 1161–1174. Cited on 62, 63

White, S. D. M. & Frenk, C. S. (1991). Galaxy formation through hierarchical clustering. *ApJ*, 379, 52–79. Cited on 6, 60

White, S. D. M. & Rees, M. J. (1978). Core condensation in heavy halos - A two-stage theory for galaxy formation and clustering. *MNRAS*, 183, 341–358. Cited on 5, 17, 60

Willman, B., Governato, F., Wadsley, J., & Quinn, T. (2004). The origin and properties of intracluster stars in a rich cluster. *MNRAS*, 355, 159–168. Cited on 65

Worthey, G., Faber, S. M., Gonzalez, J. J., & Burstein, D. (1994). Old stellar populations. 5: Absorption feature indices for the complete LICK/IDS sample of stars. *ApJ Supp.*, 94, 687–722. Cited on 58

York, D. G., Adelman, J., Anderson, J. E., et al. (2000). The Sloan Digital Sky Survey: Technical Summary. *AJ*, 120, 1579–1587. Cited on 2

Zehavi, I., Blanton, M. R., Frieman, J. A., et al. (2002). Galaxy Clustering in Early Sloan Digital Sky Survey Redshift Data. *ApJ*, 571, 172–190. Cited on 4

Zibetti, S. & White, S. D. M. (2004). Intracluster light at z $\sim$ 0.25 from SDSS imaging data. In A. Diaferio (Ed.), *IAU Colloq. 195: Outskirts of Galaxy Clusters: Intense Life in the Suburbs* (pp. 226–230). Cited on 66

Zibetti, S., White, S. D. M., Schneider, D. P., & Brinkmann, J. (2005). Intergalactic stars in z $\sim$ 0.25 galaxy clusters: systematic properties from stacking of Sloan Digital Sky Survey imaging data. *MNRAS*, 358, 949–967. Cited on 65, 66, 73, 87

Zwicky, F. (1951). The Coma Cluster of Galaxies. *PASP*, 63, 61–+. Cited on 65